Geophysics Open-File Report 49
Geoscience Department and
Geophysical Research Center
New Mexico Tech, Socorro, NM 87801

AN ANALYSIS OF THE MAY AND JULY, 1983, SOCORRO MOUNTAIN MICROEARTHQUAKE SWARMS

by

Jon P. Ake

Submitted in partial fulfillment

of the requirement for

Geophysics 590

and the

Master's Degree Program

at

New Mexico Institute of
Mining and Technology

May, 1984

ABSTRACT

During May and July, 1983 two distinct microearthquake swarms occurred near Socorro, New Mexico. More than 700 events, all with magnitudes less than two, were recorded at the closest station. The temporal characteristics of the swarms were similar to those often associated with contemporary magma movement.

Good quality hypocentral locations were obtained for 60 events. No significant difference in earthquake locations existed between the two swarms. Average focal depth for both was 8.8 km, and the hypocenters were confined to a small volume of crust (~4 km^3) by a constant S-P time interval at the closest station.

Analysis of composite fault plane solutions obtained for the strongest events in the May and July swarms indicated normal faulting with nearly pure dip slip motion on a plane dipping steeply (~70°) to the west and striking N15°E. No correlation with mapped surface faults was found.

Spectral analysis indicated peak frequencies between 9 and 13 Hz with very little energy above 25 Hz. On the basis of spectral peaks, a rather low value of apparent whole path Q_β (~80) was found.

From high quality digital data at a station 2.2 km from the epicentral region, waveforms were found to be quite similar, except for amplitude, up to a magnitude of 1.2. This duplication was especially pronounced for the P-

phase. The period of the first half cycle of the P-phase ($\tau_{1/2}$) was measured from the digital data and found to be the same ($\overline{\tau}_{1/2}$=0.0360±0.0026 seconds) for earthquakes with magnitudes below 1.2 . This implies the waveforms of the smaller events are the path and instrument response to very short duration pulses at the source. Utilizing the source independence of the smaller events, source characteristics of the larger events were studied using an empirical deconvolution procedure. Assuming a circular fault model (Brune, 1970), the largest events had computed source radii between 30 and 150 m and stress drops between 2 and 75 bars.

ACKNOWLEDGEMENTS

I am indebted to Dr. Allan Sanford for his extensive technical discussions and manuscript critiques during this study. I would also like to thank some of my fellow students for their valuable assistance, in particular, Steve Jarpe, Phil Carpenter and Scott Phelps. Finally I would like to thank my family for their understanding, patience and encouragement during the course of this study.

TABLE OF CONTENTS

INTRODUCTION

This study will focus upon a fairly detailed examination and comparison of a pair of microearthquake swarms that occurred during May and July, 1983, near Socorro, New Mexico.

Socorro is within the central portion of the Rio Grande rift (Figure 1). The Rio Grande rift is a roughly north-south trending series of en-echelon grabens that extend from near Leadville, Colorado on the north into northern Mexico on the south (Chapin, 1971). The rift has been undergoing east-west crustal extension for approximately 30 million years (Chapin and Seager, 1975). Details on large scale aspects of the Rio Grande rift may be found in Chapin (1971), Chapin and Seager (1975), Sanford et al. (1977), Cordell (1978), and the volume Rio Grande Rift:Tectonics and Magmatism edited by Riecker (1979).

The area of interest for this study is the region immediately to the west of Socorro (~130 km south of Albuquerque). The character of the Rio Grande rift in the vicinity of Socorro changes somewhat from that to the north (Figure 2). The rift begins to become a series of parallel basins with intergraben horsts. The Socorro-Lemitar Mountains are horst blocks which separate the Socorro and La Jencia basins. Important geological and geophysical characteristics of the rift in the Socorro area include high heat flow (Reiter and Smith, 1977), deep alluvial basins

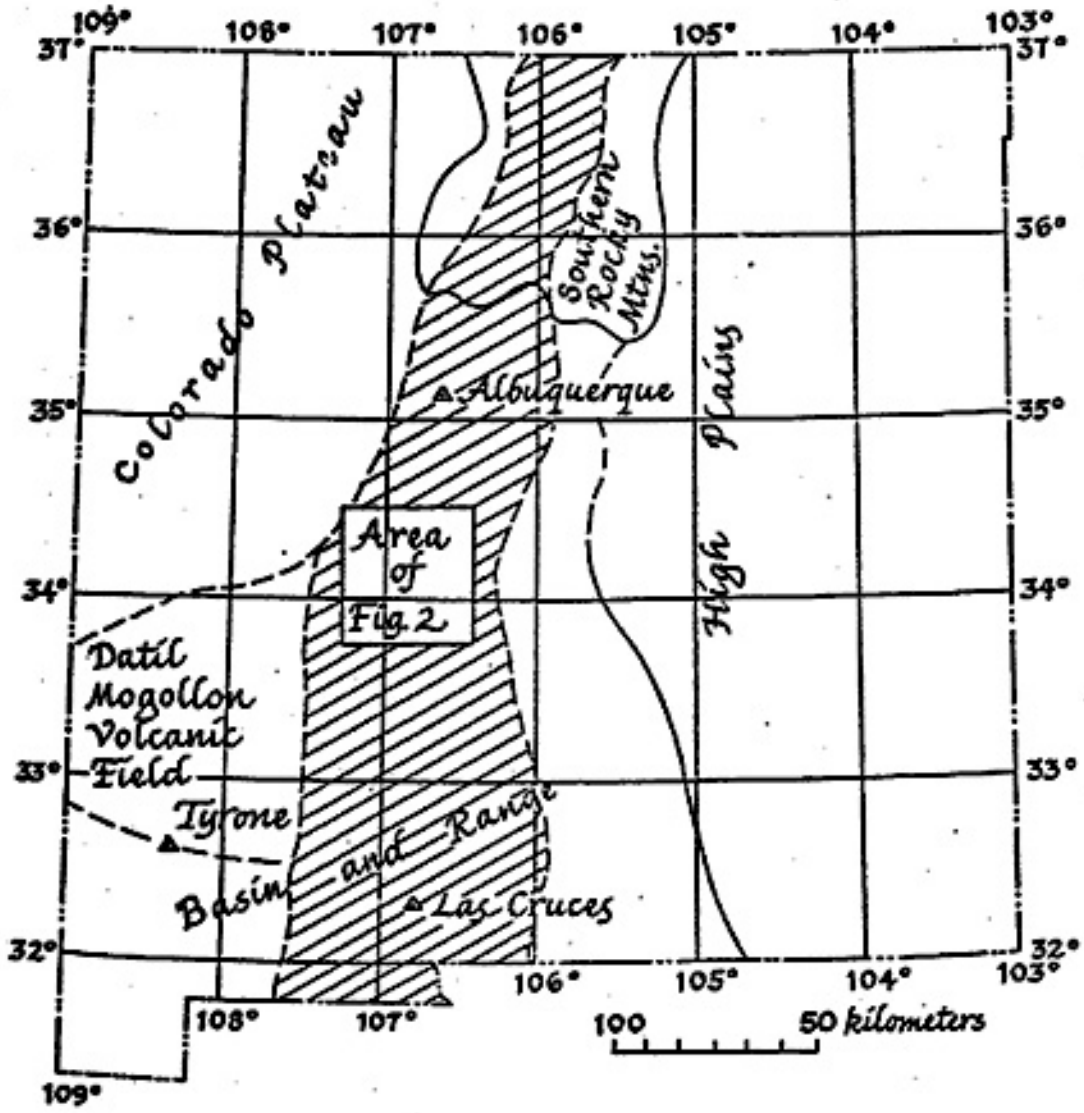

Figure 1. Physiographic provinces and the Rio Grande rift in New Mexico (after Chapin, 1971).

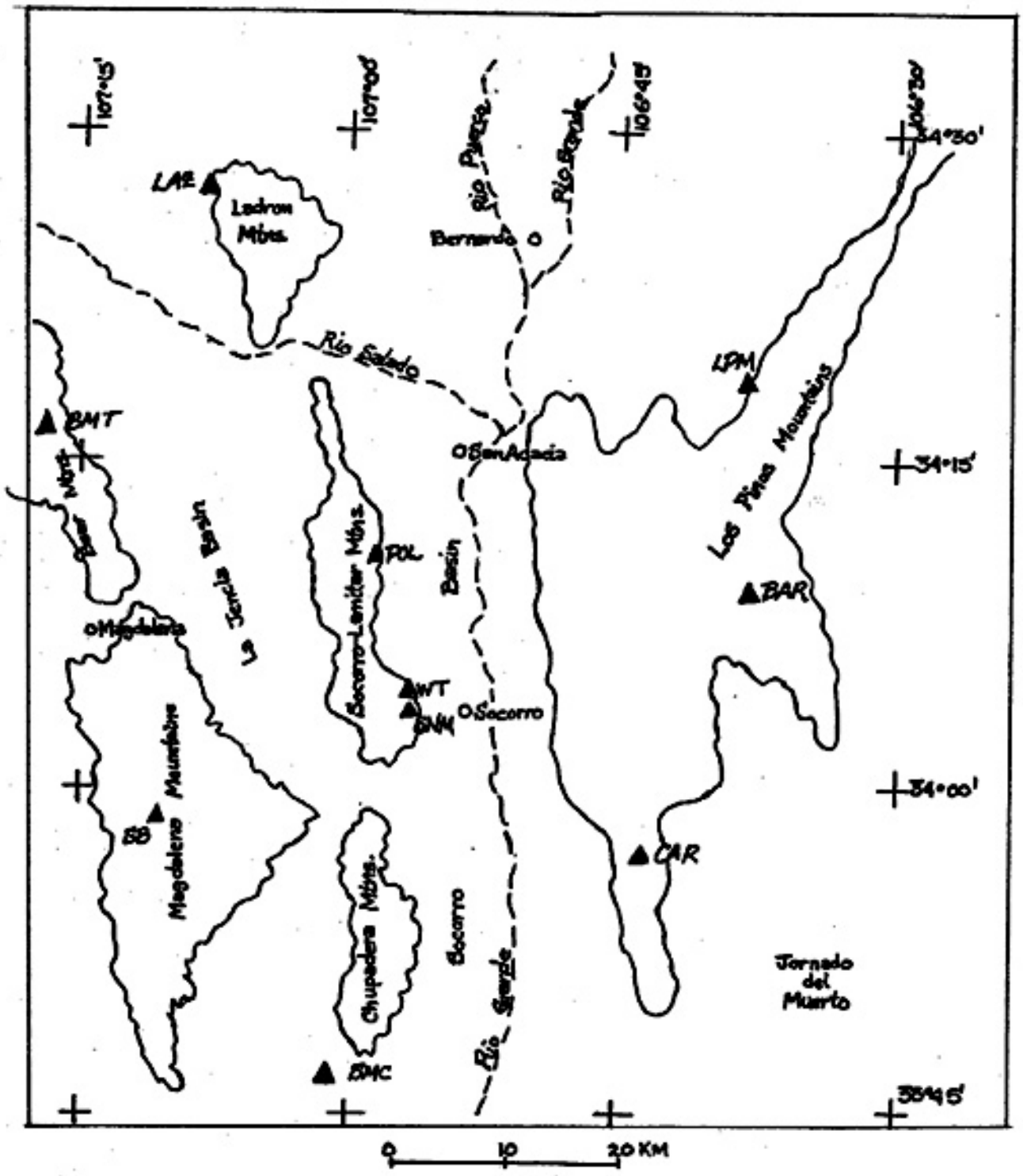

Figure 2. Major physiographic features near Socorro. Also shown are the locations of the NMT-USGS seismograph stations as of mid-1983.

(Sanford, 1968), roughly north-south trending Quaternary boundary faults (Sanford et al., 1972), the intersection of two volcanic lineaments (Chapin et al., 1978), the presence of an extensive mid-crustal magma body (Rinehart et al., 1979), an area of positive surface uplift north of Socorro (Reilinger et al., 1978) and a high level of seismicity, frequently in swarms (Sanford et al., 1983a). The major physiographic features of the central Rio Grande rift and the location of the seismograph stations of the United States Geological Survey-New Mexico Tech seismic network at the time of the swarms are shown in Figure 2.

West of Socorro, within the Socorro-Lemitar Mountains, is the specific region of interest in this study. Results of detailed geological investigations in this area are contained in Chamberlin (1980). The generalized, but still complex, geology of the Socorro Peak area is shown in Figures 3 and 4. From detailed mapping in the area, Chamberlin (1981) concludes that the primary control of intrusion, volcanism and subsequent hydrothermal activity in this area is the "leaky" Morenci lineament, a shear zone approximately normal to the rift.

The area immediately to the south and west of Socorro has historically been seismically active (Sanford and Holmes, 1962; Sanford et al., 1983a). The seismicity of the Socorro region for the period 1975 to 1983 is shown in Figure 5. For this period the most seismically active region appears to be the southern La Jencia Basin (southwest

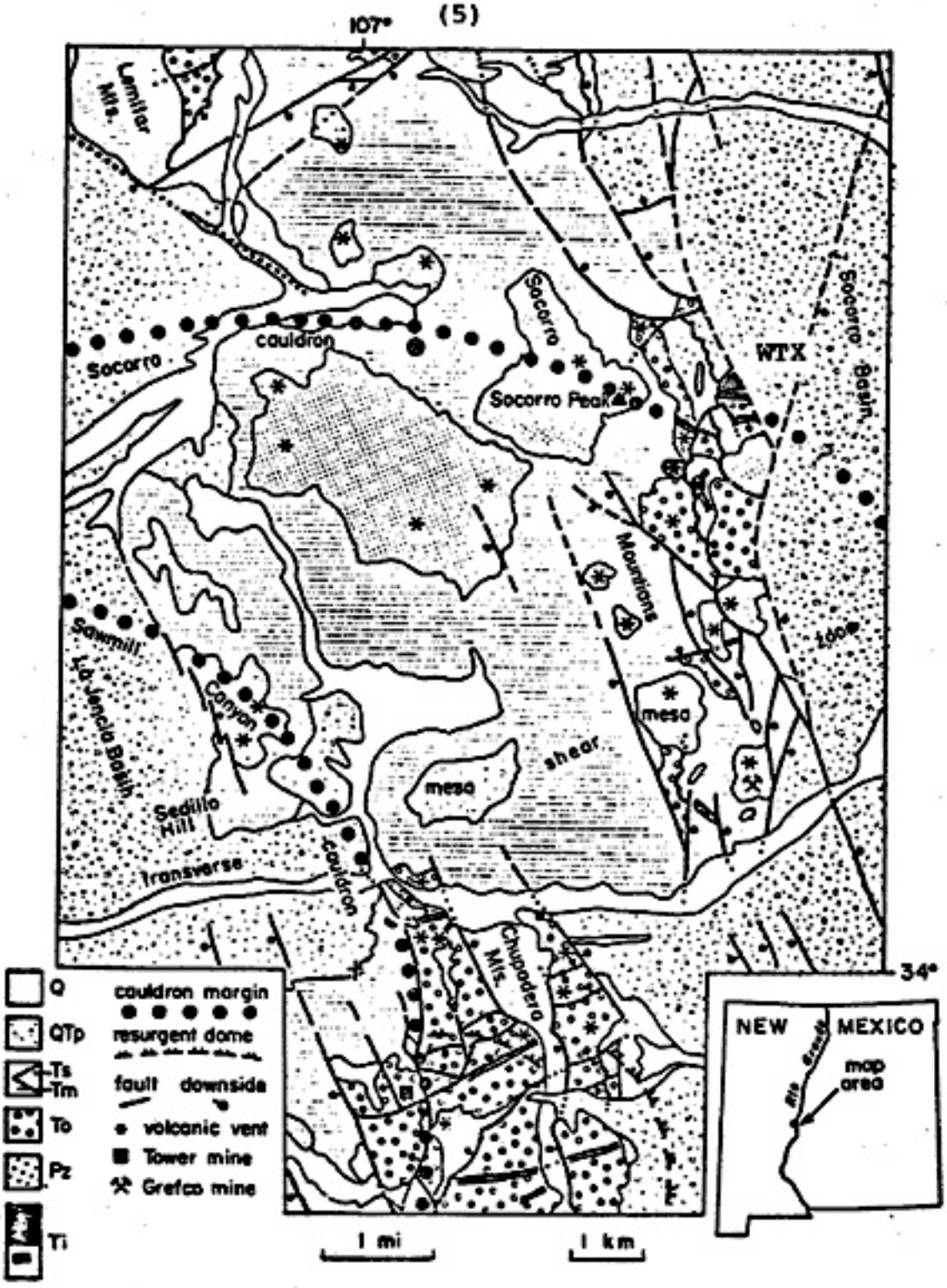

Figure 3. Generalized geologic map of the Socorro Peak volcanic center; Paleozoic and Precambrian rocks (Pz), Oligocene volcanic rocks (To), Miocene Popotosa Formation (Tm), late Miocene Socorro Peak Rhyolite (Ts), Oligocene and Miocene intrusive rocks (Ti), Pliocene to Pleistocene Sierra Ladrones Formation and older piedmont gravels (QTp), and late Quaternary alluvium (Q) (from Chamberlin, 1980).

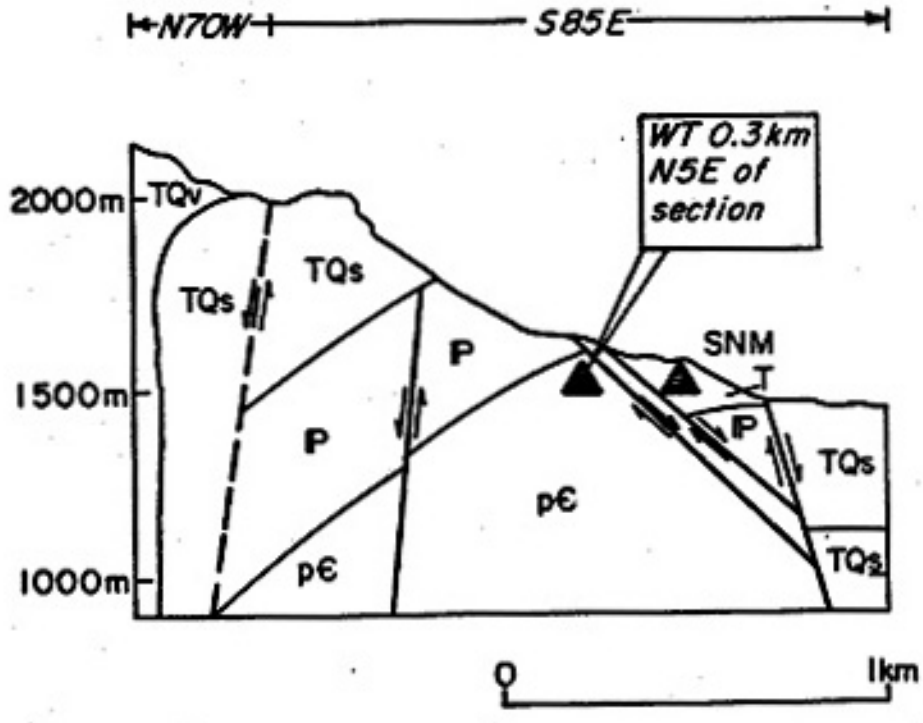

Figure 4. Cross section through station SNM and the summit of Socorro Peak illustrating the structural complexity in the area. Units are broadly lumped; Tertiary or Quaternary sediments (TQs), Tertiary or Quaternary volcanics (TQ), Pennsylvanian sediments (P), Precambrian undifferentiated (pC) (modified from Chamberlin, 1980 and Carpenter, 1984).

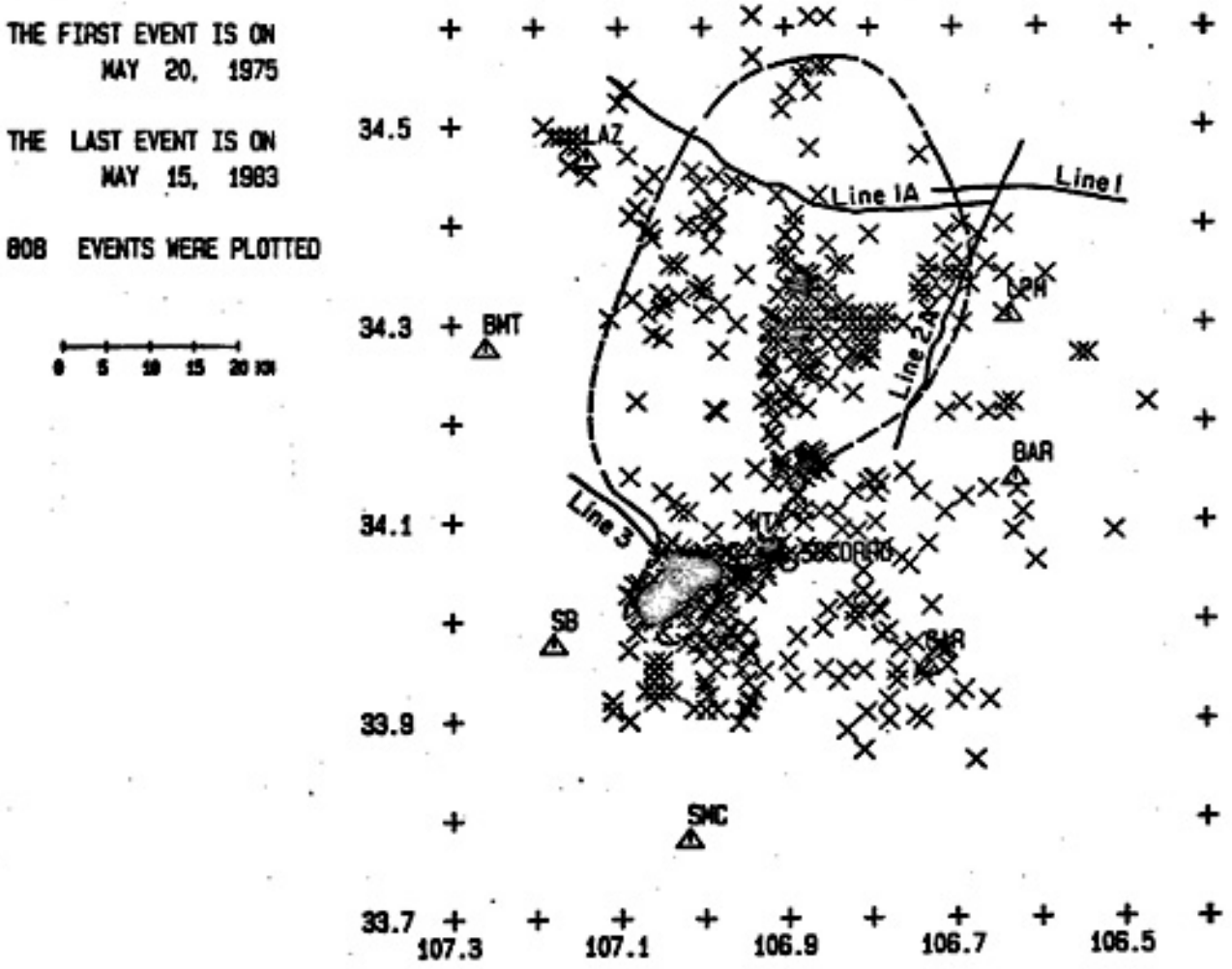

Figure 5. Seismicity of the Socorro area for the period 1975-1983. Locations of the NMT-USGS seismograph stations are shown by triangles. Outline of the mid-crustal magma body and COCORP reflection lines are also shown.

of Socorro). Previous studies (Shuleski, 1976; Johnston, 1978; Sanford and Schlue, 1980) have interpreted this activity to be related to the upward intrusion of small magma bodies in a complex network of dikes and sills.

INSTRUMENTATION

The principal source of data for all microearthquakes studied in this report were recordings from the eight permanent stations of the New Mexico Tech (NMT)-United States Geological Survey (USGS) seismograph network (see Figure 2). In addition, temporary stations MLM, POL and SNM were operational on an intermittent basis. The station locations and elevations are summarized in Appendix 1. A summary of the operational times for each station is also presented in Appendix 1.

Contained in Appendix 2 is a summary of the gain and response characteristics of most of the NMT-USGS systems as of mid-1983. The seismometers used in the permanent systems are either the Teledyne Geotech Model JM (natural frequency of 1 Hz) or the Teledyne Geotech Model 18300 (also a natural frequency of 1 Hz). The signal from the stations is radio telemetered to the New Mexico Tech campus and is recorded on helical drum recorders at a speed of 60 mm/minute using a hot-wire stylus. These analog records can usually be read to within ± 0.05 seconds using a hand lens.

In addition, beginning at 2030 hours U.T. on May 13,1983, a Sprengnether DR-100A digital event recorder was operated in Wood's Tunnel adjacent to station WTX. The DR-100 system continously samples the incoming signals and is triggered when the ratio of a short-term average signal to a long-term average signal exceeds a prescribed value. The

geophone used with the DR-100 in this study was a Marks Products L4-C (natural frequency of 1 Hz). The sampling rate was a constant 100 samples per second throughout the study. The response characteristics of the digital system are also contained in Appendix 2. In an attempt to record unsaturated events over as wide a range of magnitudes as possible, the gain on the DR-100 was changed at various times during the swarms (summarized in Table 1). Amplitudes of digital data in this study were corrected for the change in gain when neccessary.

Table 1. Summary of DR-100 Digital Unit Operation During 1983 Socorro Mountain Swarms

Date	Gain (dB)	Location	Filters Low-High (Hz)
2030,May 13- 1645,May 20	84	Concrete Pad, WTX	00,30
1630,July 14- 1612,July 18	78	Concrete Pad, WTX	00,30
1700,July 18- 1620,July 19	78	Wood's tunnel about 75m E of prev. location	00,30
1645,July 19- 1600,July 20	72	Concrete Pad, WTX	00,30
1615,July 20- 1545,July 21	66	Concrete Pad, WTX	00,30
1600,July 21-	72	Concrete Pad, WTX	00,30

EARTHQUAKE SWARM STATISTICS

At the NMT-USGS Seismological Observatory, the normal routine is to calculate the magnitude of an event at the same time as its location using a duration-based magnitude scale derived by Los Alamos National Labratory (LANL) for northern New Mexico (Newton et al., 1976). The LANL formula

$$M_\tau = 2.79 \log \tau - 3.63 \ , \qquad (1)$$

where τ is the measured signal duration in seconds, was found to be applicable to earthquake data from central New Mexico as well (Ake et al., 1983). However, this duration based magnitude scale was derived using data between magnitudes one and four. Hence it is uncertain how accurately the equation determines the magnitudes of very small events ($M_\tau < 0.0$).

A comparison between the amplitude-based and duration-based magnitudes was made. The amplitudes of the 19 strongest events in the two swarms (nine in May, ten in July) were measured on seven of the local network records. Corrections were made for station magnification and attenuator setting in each case. Magnitudes were then calculated using the relation

$$M_L = \log A - \log A_0 - 0.0014\Delta \qquad (2)$$

(see Richter, 1958 and Ake et al., 1983). These results were then compared to the duration based magnitude, calculated by the HYPO71 program using the LANL formula. The results are summarized in Table 2 and Figure 6. For all

Table 2. Summary of Comparison Between Amplitude-Based and Duration-Based Magnitudes

No.	Event	M_L (±std. dev.)		M_τ (±std. dev.)	
1	May 10,0627	1.00	0.30	0.46	0.30
2	May 10,0838	1.49	0.36	1.36	0.41
3	May 10,1105	1.30	0.34	1.00	0.40
4	May 11,0616	1.04	0.45	0.37	0.23
5	May 11,1359	0.99	0.50*	0.53	0.32
6	May 11,1430	1.27	0.42	0.64	0.31
7	May 11,1433	0.94	0.25*	0.34	0.32
8	May 11,1452	0.80	0.19	0.34	0.21
9	May 11,1525	1.36	0.42	1.03	0.26
10	July 16,0310	0.71	0.26*	0.57	0.22
11	July 16,0859	1.07	0.34	0.79	0.30
12	July 16,2206	1.56	0.48	1.77	0.30
13	July 16,2248	0.78	0.31	0.20	0.29
14	July 17,1132	1.24	0.34	1.27	0.42
15	July 19,0340	1.43	0.34	1.79	0.36
16	July 19,0440	0.62	0.28	0.44	0.42
17	July 19,0912	0.68	0.27	0.52	0.54
18	July 20,0041	0.87	0.32	0.60	0.30
19	July 20,1657	0.83	0.34	0.49	0.36*

*Indicates at least one station value was rejected because it was >2σ from the mean.

M_L was calculated using all local stations except LAZ.

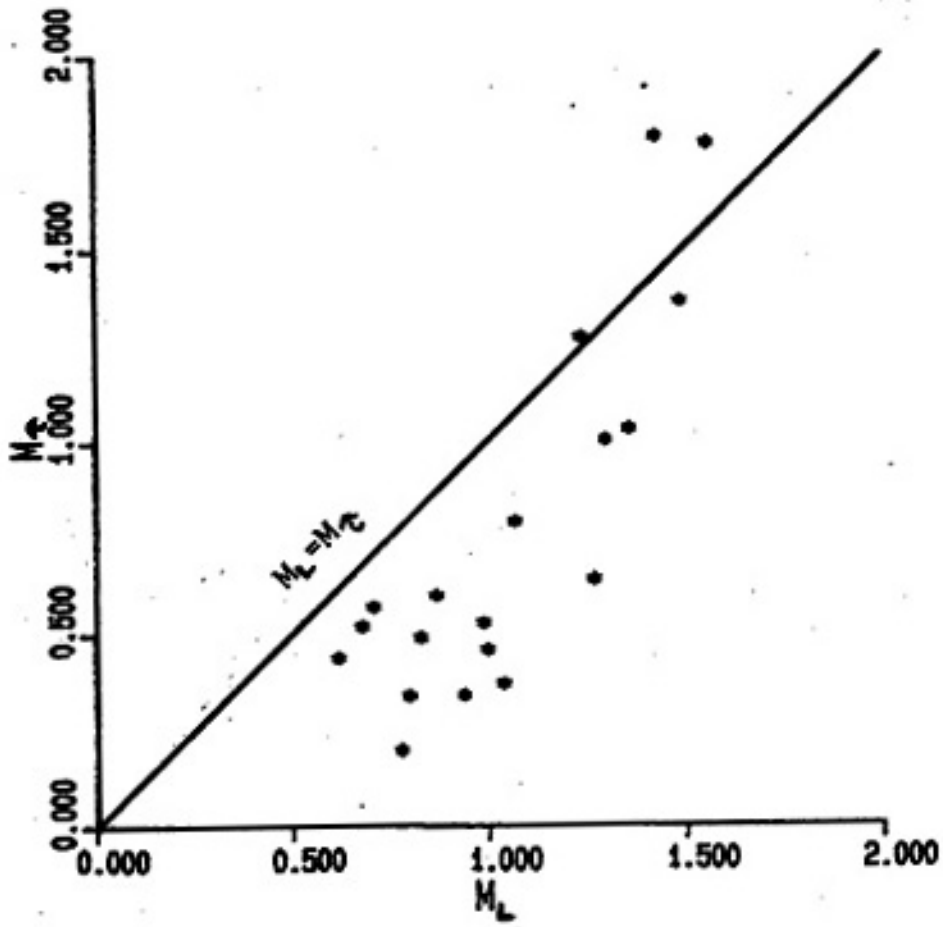

Figure 6. Comparison of duration-based and amplitude-based magnitudes for the 19 strongest events in the May and July, 1983, Socorro mountain swarms.

but two of these events the LANL formula underestimates the magnitude relative to the amplitude formula (Figure 6). However, in almost all cases there is no overall statistical significance to the difference (Table 2).

A count of the total number of events that occurred during the two swarms was conducted using the analog record of the closest station, WTX. The only count criteria was that the event amplitude on the record equal or exceed 1.5 mm, peak to peak. This amplitude corresponds to a local (amplitude-based) magnitude of -0.80. Using this criteria, 446 events were recorded at station WTX between 0400 hours on May 10 and 1200 hours on May 14, 1983. A total of 296 events with M_L>-0.8 were recorded at WTX between 1100 hours on July 14 and 1200 hours on July 21, 1983. The majority of the over 700 events recorded in these two swarms were quite weak.

The temporal distribution of events in the two swarms is illustrated in Figure 7. A comparison with lunar/solar tides produced no obvious correlation between tidal effects and swarm activity.

Figure 8 is a plot of cumulative number of events versus magnitude for the two Socorro Mountain swarms. To be consistent with other recent studies in the Socorro area (and greatly expedite obtaining results) the LANL duration based formula was used to compute the magnitudes. The linearity of both the May and July data to magnitudes as small as M_t=-1.0 would indicate that all events have been

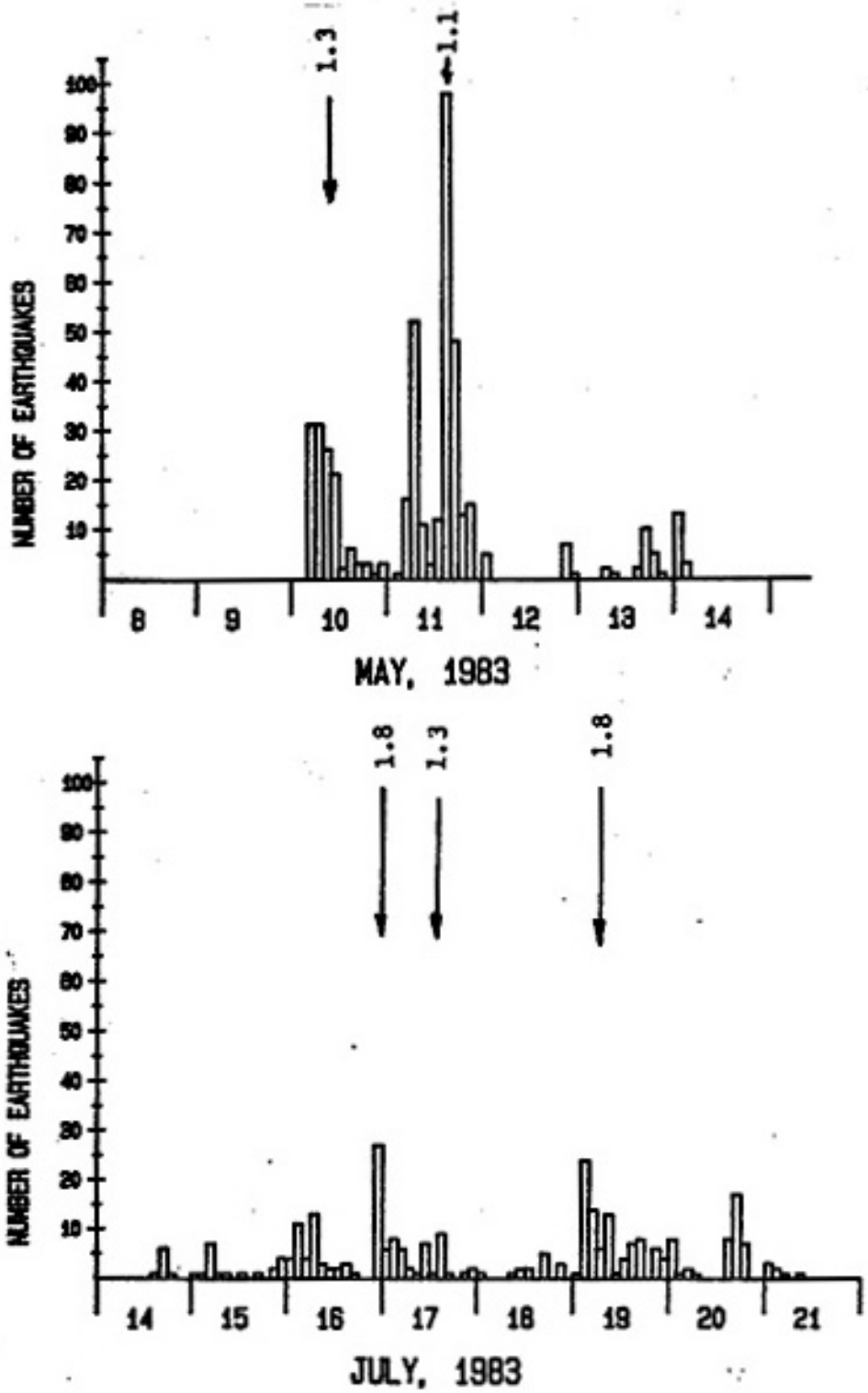

Figure 7. Temporal distribution of earthquakes in May (top) and July (bottom), 1983, swarms. Total number of earthquakes with M_L>-0.8 was 446 for the May swarm and 296 for the July swarm. Arrows indicate the time of occurrence of the strongest shocks.

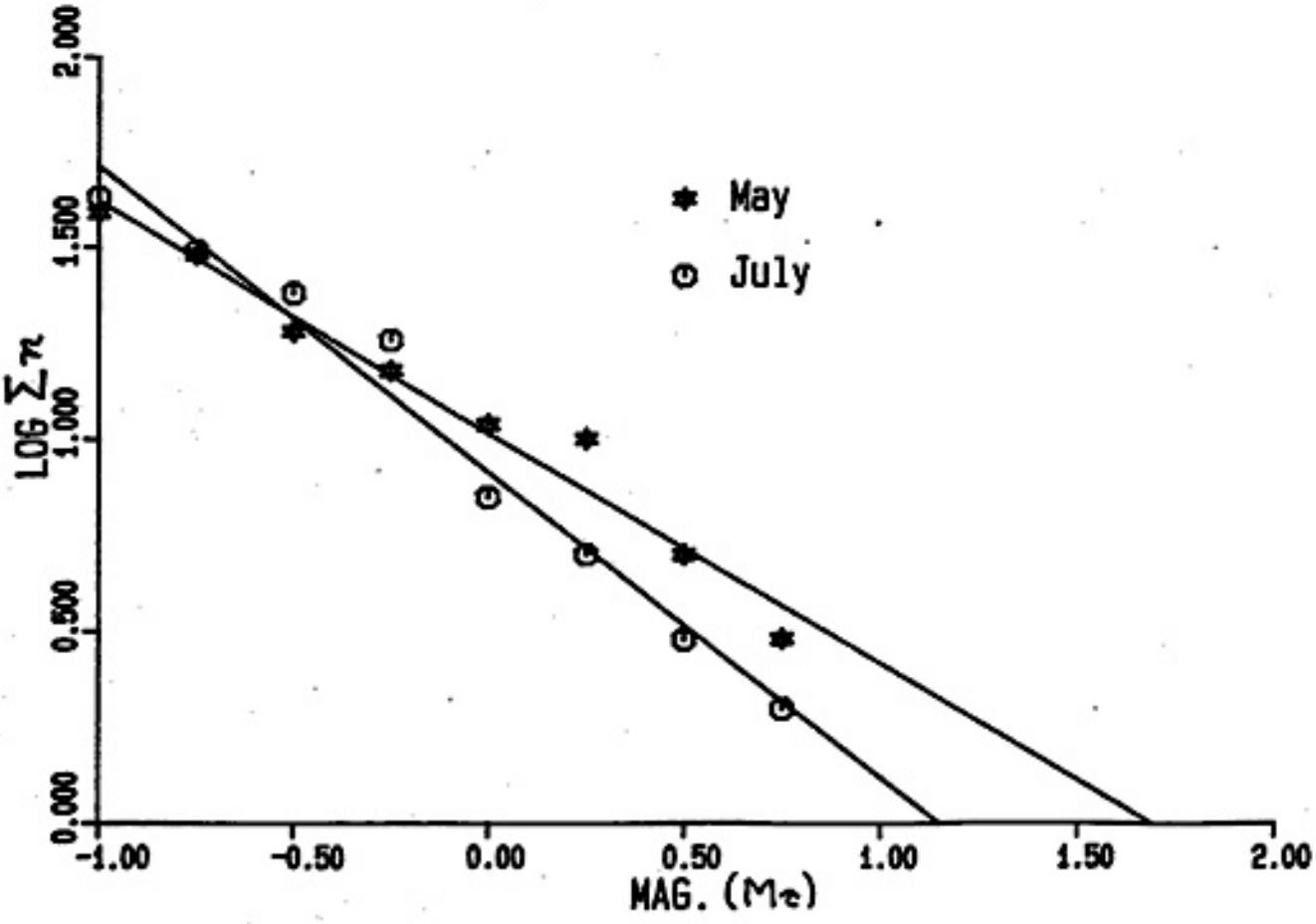

Figure 8. Plot of cumulative number of shocks versus duration magnitude. The cumulative number of events $\geq$-1.0 is plotted at M_t=-1.0 etc. Thus events with M_t <-1.0 have not been plotted. For the May data, linear regression indicates $\log \Sigma n = 1.017 - 0.603(\pm 0.043) M_t$. For the July data, linear regression indicates $\log \Sigma n = 0.910 - 0.802(\pm 0.050) M_t$.

detected. However,to overcome the possible problems related to the calculation of magnitudes for the smaller events, a somewhat arbitrary scheme was employed. The magnitude calculated from the LANL formula for a duration of ten seconds is -0.84. For a duration of five seconds it is -1.68. The majority of the smaller events on the WTX record had durations less than ten seconds (many as low as three seconds). Hence, the duration magnitude scheme would indicate most events were less than M_L=-0.85. The 1.5mm (peak to peak) minimum amplitude used in the count criteria (on the WTX record) on the other hand, indicates a minimum amplitude-based magnitude of -0.80.

The problems with the durations of the smaller events probably result from a poor signal-to-noise ratio leading to a consistent underestimation of the duration. As a compromise (while still using the LANL formula) the magnitude of any event with a duration less than ten seconds was set to -1.0. The above argument not withstanding, it is probable that due to the sensitivity and proximity of station WTX all events stronger than M_L=-1.0 were detected.

A linear regression of the two data sets was performed; in each case the data points at M_t<-1.0 and $\log\Sigma n$=0 were neglected in the regression. So, all seven points for each swarm shown in Figure 8 were used in the regression. The slope values (i.e. the b-values) differ somewhat between the two swarms. For the May data the regression indicated $\log\Sigma n$=1.017-0.603($\pm$0.043)M_t, and for the July data,

$\log \Sigma n = 0.910 - 0.802(\pm 0.050) M_\ell$. This difference appears to be statistically significant at almost the 2σ level. The reason for this difference is unclear at this time. Several other interesting features of the two swarms are also apparent from Figure 8. The total number of events in the two swarms is quite different, yet the number of events larger than $M_\ell = -1.0$ was just about the same. Further, the largest shock predicted by Figure 8 for the May swarm is larger than that predicted for the July swarm ($M_\ell = 1.69$ versus $M_\ell = 1.15$). In contrast, the duration magnitude of the largest July event ($M_\ell = 1.79$) was larger than that of the largest May event ($M_\ell = 1.38$).

The b-value is sometimes taken to have tectonic significance. It is difficult however, to compare the b-value between studies by different workers as b will depend on the method used to calculate the magnitude (Majer and McEvilly, 1979). Typical b-values in the literature fall between -0.8 and -1.2 (Molnar, 1979). In a similar study to this, using duration magnitudes, Jarpe (1984) found a b-value of -0.81 for an earthquake swarm 30 km north of Socorro. Jaksha (1983) found a b-value of -0.87 for the geographical area of the Socorro magma body (using duration magnitudes). The July, 1983, swarm data (b=-0.802) appears to be consistent with these other results for the Socorro area. The reason for the lower b-value of the May data (b=-0.603) is unclear however.

EARTHQUAKE LOCATIONS

The first step in any earthquake study is the (hopefully precise) location of the events. The positions of the hypocenters relative to the stations will usually determine the precision of location efforts. The swarms of May and July, 1983, were nearly ideally located to facilitate good quality locations using the NMT-USGS seismograph network. The Socorro Peak area has one nearby station, WTX, and is well circled by the other network stations. The array of stations around Socorro allows for good epicentral control while the station close to the epicentral region signifcantly reduces errors in depth estimates.

The revised HYPO71 (Lee and Lahr, 1975) linear inversion earthquake location program was utilized for microearthquake locations in this study. A homogeneous, isotropic half-space model was used with a P-wave velocity of 5.85 km/second (Ward, 1980) and an S-wave velocity of 3.38 km/second. The S-wave velocity was determined by assuming a Poisson's ratio of 0.25, which has been found to be an appropriate value for the Socorro area from previous studies (Caravella, 1976; Fender, 1978; and Frishman, 1979).

The HYPO71 program assigns an assessment of solution quality (A through D) based upon a complicated set of parameters (summarized in Table 3). The overall solution

Table 3. Summary of HYPO71 Criteria for Solution Quality

QS	RMS (sec)	ERH (km)	ERZ (km)
A	<0.15	<1.0	<2.0
B	<0.30	<2.5	<5.0
C	<0.50	<5.0	>5.0
D	>0.50	>5.0	>5.0

QD	NO.	GAP	DMIN (km)
A	>6	<90	< DEPTH or 5
B	>6	<135	<2x DEPTH or 10
C	>6	<180	< 50
D	<6	>180	> 50

where:

DMIN=distance from epicenter to closest station

NO.=number of station readings used in solution

R_i=time residual for i^{th} station

RMS= $\sqrt{R_i^2/NO.}$

SDX and SDY=standard errors of latitude and longitude of epicenter

ERH= $\sqrt{SDX^2 + SDY^2}$ =standard error of epicenter in km

ERZ= standard error of focal depth in km

GAP= largest angular distance between any two stations

quality depends on the combination of QS and QD. If one factor is C and the other A, the overall solution quality is B. Typical values for the variables for the 1983 Socorro Mountain swarms are presented in Appendix 3. In light of these criteria, two factors were most strongly considered when deciding which earthquakes to locate. First, the analog records of the array were searched and only those events that were clearly recorded by at least two of the three northern stations (BMT, LAZ and LPM) were considered. If this criteria was not satisfied the angular gap usually exceeded 90 degrees. Second, to reduce the RMS value only those events with clearly readable phases were used (i.e. favorable signal-to-noise ratio). Using the above standards, 18 events from the May swarm and 42 events from the July swarm were selected for location.

Because the digital event recorder was operational for a substantial period of time at the closest station (WTX), very high quality readings of the S-P time interval could be made. For the May digital data (n=13 readings) the average S-P time interval was 1.012 ± 0.007 seconds. For the July digital data (n=55 readings) the average S-P time interval was 1.025 ± 0.016 seconds. Because the average S-P time interval is not statistically different at even the 10% level, an average value for both swarms was found ($\overline{S-P} = 1.023 \pm 0.013$ seconds). This value was then utilized to determine an S-phase arrival time at station WTX (where the S-phase arrival was usually not readable on the analog

records). These readings were then weighted (in the solution procedure) more heavily than is customary for S readings (Wieder, 1981). The net effect of this procedure was to reduce the uncertainty in hypocentral depth calculations.

Prior to this study, the HYPO71 program utilized station corrections based upon the results of Ward (1980). The magnitude and sign of these corrections essentially accounts for the thickness and type of material beneath each station. The corrections were derived from a large number of events originating from a variety of locations within the Socorro area. Because of the constant S-P time interval at station WTX, all microearthquakes were believed to be originating from essentially the same place. This allowed a separate test of the applicability of the station corrections for travel paths originating beneath Socorro Peak to be made. Twelve of the strongest events from the July swarm were chosen and P-wave arrival times were read. These events were then located using HYPO71 with the corrections from Ward. The resulting cumulative RMS residuals for each station were then applied as "corrections" to the former station corrections. The twelve strong events in effect became "master" events for the subsequent location of the other swarm events. This procedure allowed for a set of station corrections to be used which were optimized for events that originated in the Socorro Peak area. These corrections are listed in Appendix

1.

For the 18 events located from the May swarm, three C quality, four B quality and 11 A quality solutions were obtained. For the 42 events located from the July swarm, one C quality, 18 B quality and 23 A quality solutions were obtained. A summary of the location results of all 60 events is contained in Appendix 3. To minimize uncertainties, the data base for further location analysis was reduced to only A quality solutions with $M_c \geq 0.0$. Eleven events from the May swarm and twelve from the July swarm satisfied this criteria. The locations, errors, magnitudes and times of occurrence for these 23 events are summarized in Table 4. In general, the epicenters are clustered roughly two kilometers southwest of station WTX and trend north-south (Figure 9). The epicenters are clustered within an area roughly 2.5 km (north-south) by 1.6 km (east-west).

It appears that the differences in location between the main group of shocks and those further to the south is statistically significant. The average standard error in epicenters, roughly corresponding to two standard deviations, (Lahr, personal communication, 1984) is only 0.46 km, whereas there is a distance of $\sim$2.5 km between the extreme northern and southern locations. Epicenters do not appear to have migrated with time (Figure 10). Further, there does not appear to be a statistically different average epicentral location between the May and July swarms

Table 4. Summary of Location Data for Highest Quality Events in 1983 Socorro Mountain Swarms

Ev No.	Date	O.T.	Lat	Long	Depth	Mag	Gap	RMS	ERH	ERZ	Q	SQD
1	5/10	0657	3.56	57.49	8.76	0.05	70	0.04	0.3	0.2	A	A/A
2	5/10	0838	3.48	57.51	8.77	1.33	86	0.04	0.3	0.3	A	A/A
3	5/10	1105	3.64	57.32	9.16	0.99	84	0.06	0.4	0.3	A	A/A
4	5/10	1142	3.32	57.49	9.18	0.14	72	0.12	0.6	0.5	A	A/A
5	5/10	1637	3.71	57.42	9.75	0.21	70	0.07	0.4	0.3	A	A/A
6	5/11	0616	3.38	57.41	8.53	0.36	71	0.09	0.4	0.4	A	A/A
7	5/11	1359	3.58	57.46	7.02	0.52	70	0.05	0.3	0.3	A	A/A
8	5/11	1430	2.66	57.48	8.65	0.64	75	0.15	0.9	0.8	A	A/A
9	5/11	1433	3.64	57.31	7.55	0.34	70	0.07	0.4	0.3	A	A/A
10	5/11	1525	3.10	57.33	8.94	1.05	73	0.07	0.3	0.3	A	A/A
11	5/14	0108	3.71	57.90	9.14	0.09	69	0.14	0.4	0.5	A	A/A
12	7/14	1109	2.89	57.57	8.14	0.50	89	0.09	0.5	0.4	A	A/A
13	7/14	1139	2.54	57.35	10.05	0.15	75	0.11	0.8	0.6	A	A/A
14	7/16	0859	3.07	57.70	8.62	0.79	72	0.14	0.8	0.7	A	A/A
15	7/16	1739	3.51	57.61	9.31	0.16	71	0.09	0.5	0.4	A	A/A
16	7/16	2206	3.51	57.51	8.92	1.77	71	0.09	0.5	0.4	A	A/A
17	7/16	2248	3.44	57.11	9.11	0.15	71	0.07	0.4	0.3	A	A/A
18	7/17	1132	3.66	57.39	9.08	1.27	74	0.03	0.2	0.2	A	A/A
19	7/17	2245	3.24	57.05	8.92	0.29	72	0.06	0.6	0.4	A	A/A
20	7/19	0340	3.40	57.60	8.18	1.79	71	0.03	0.2	0.1	A	A/A
21	7/19	0440	3.43	57.48	8.55	0.45	71	0.07	0.4	0.3	A	A/A
22	7/19	0912	3.34	57.76	8.44	0.52	71	0.10	0.6	0.5	A	A/A
23	7/20	1657	3.65	57.42	9.42	0.49	70	0.05	0.3	0.2	A	A/A

Latitudes are expressed as minutes north of 34°, longitudes as minutes west of 106°.

Explanations of other quantities and units are contained in Table 3.

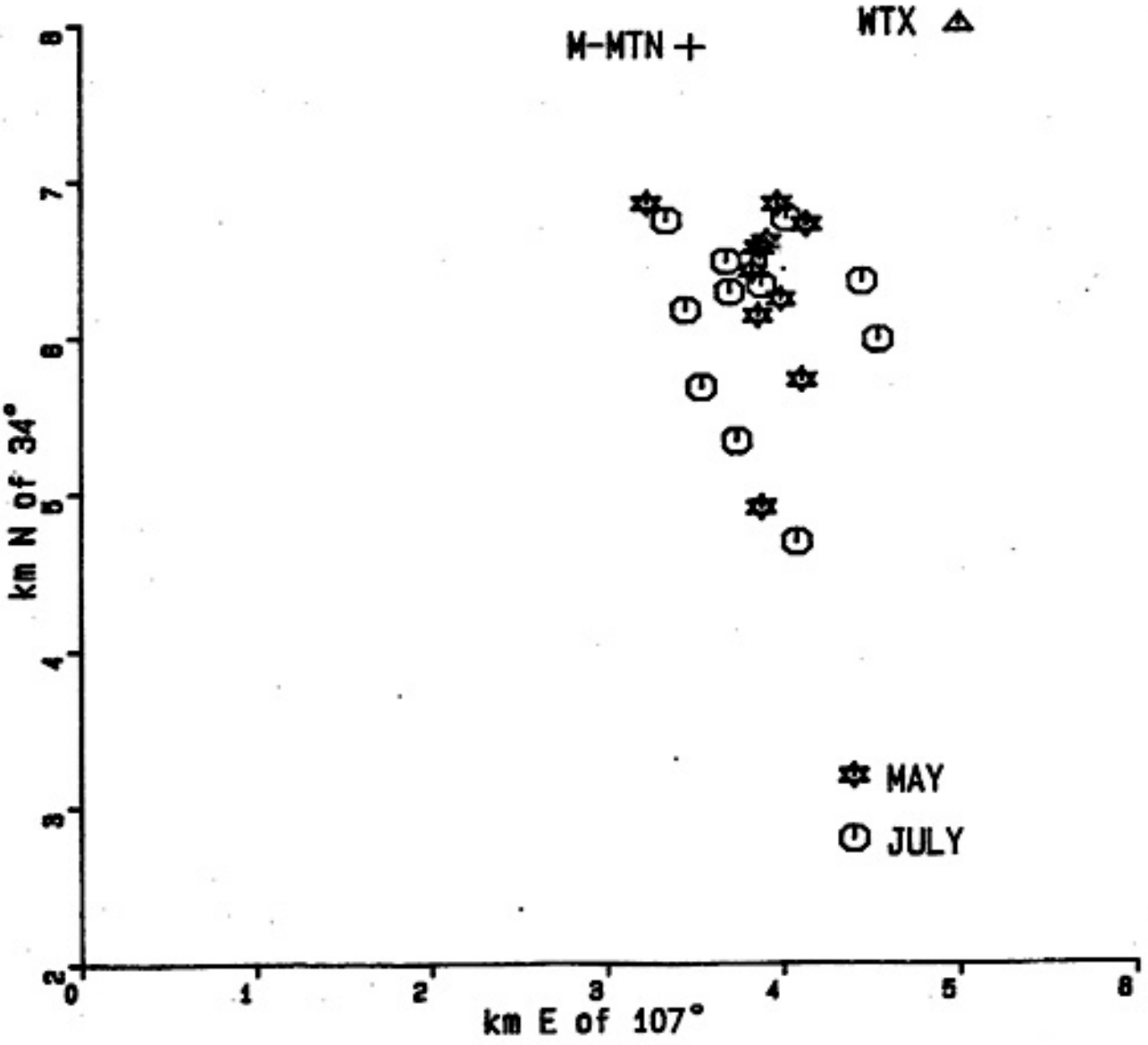

Figure 9. Epicentral locations for the 23 best located events in the May and July, 1983, Socorro Mountain swarms. The overall average ERH for these events was 0.46 km.

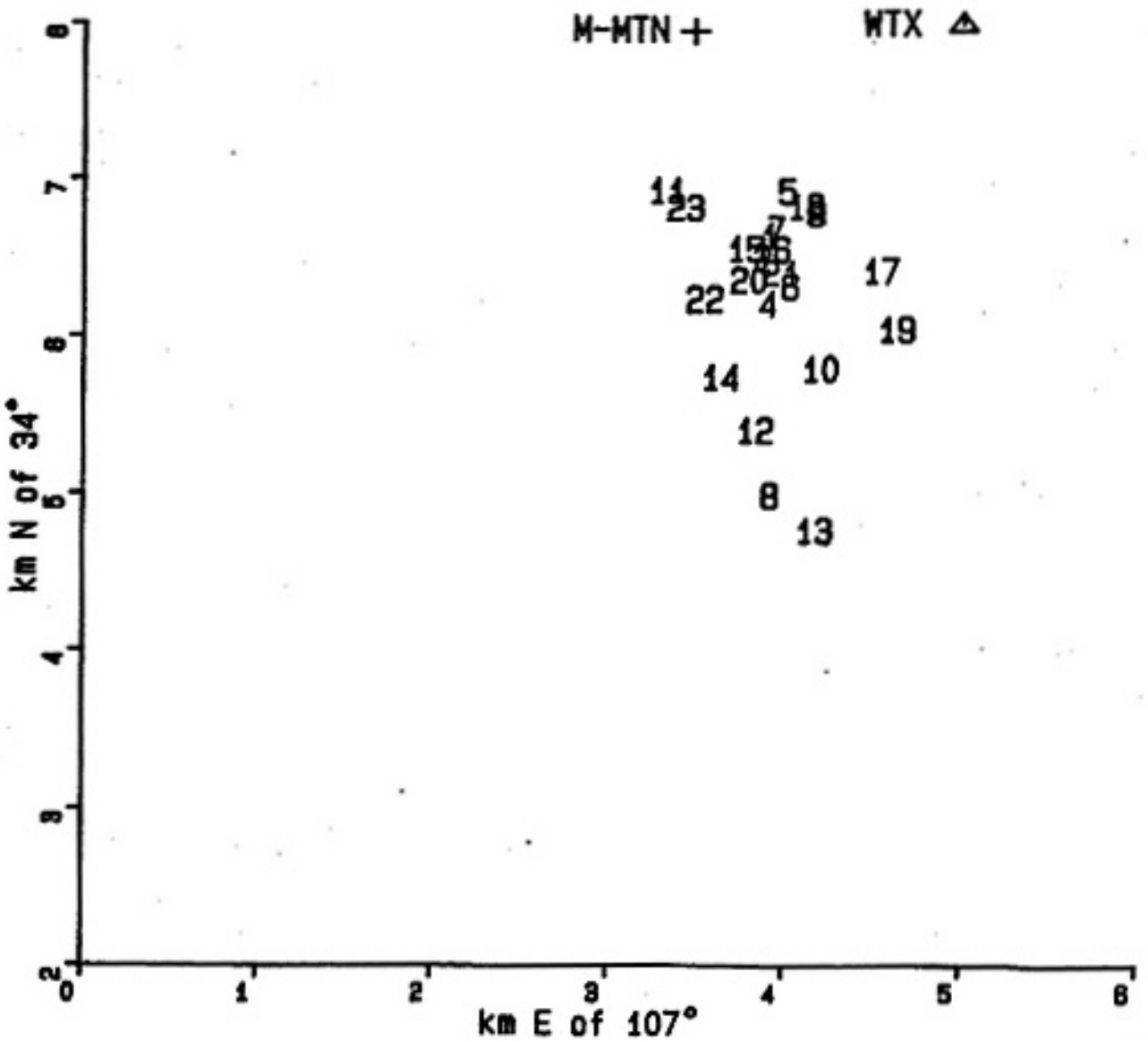

Figure 10. Variation in earthquake epicenters with time for the 23 best located events. Refer to Table 4 for key to event numbers.

(Figure 11).

Depths of focus for both swarms are summarized in Figure 12. The average focal depth for the May swarm is 8.86±0.55 km. The average focal depth for the July swarm is 8.90±0.55 km. Again there is no statistical difference between the May and July swarms. The focal region for the majority of the shocks appears to occupy a small volume of crust (roughly 4.4 km^3). In particular the focal region appears to be tightly constrained in depth inasmuch as 80 percent of the events fall between 8.33 and 9.43 km. This relatively tight constraint on focal depth is not a quirk of the location program. The essentially constant S-P intervals observed at station WTX (from the digital data) indicate that focal depths must be narrowly confined. This observation (small changes in depth within swarms) is similar to that noted in other Socorro area swarms (Sanford et al., 1983d).

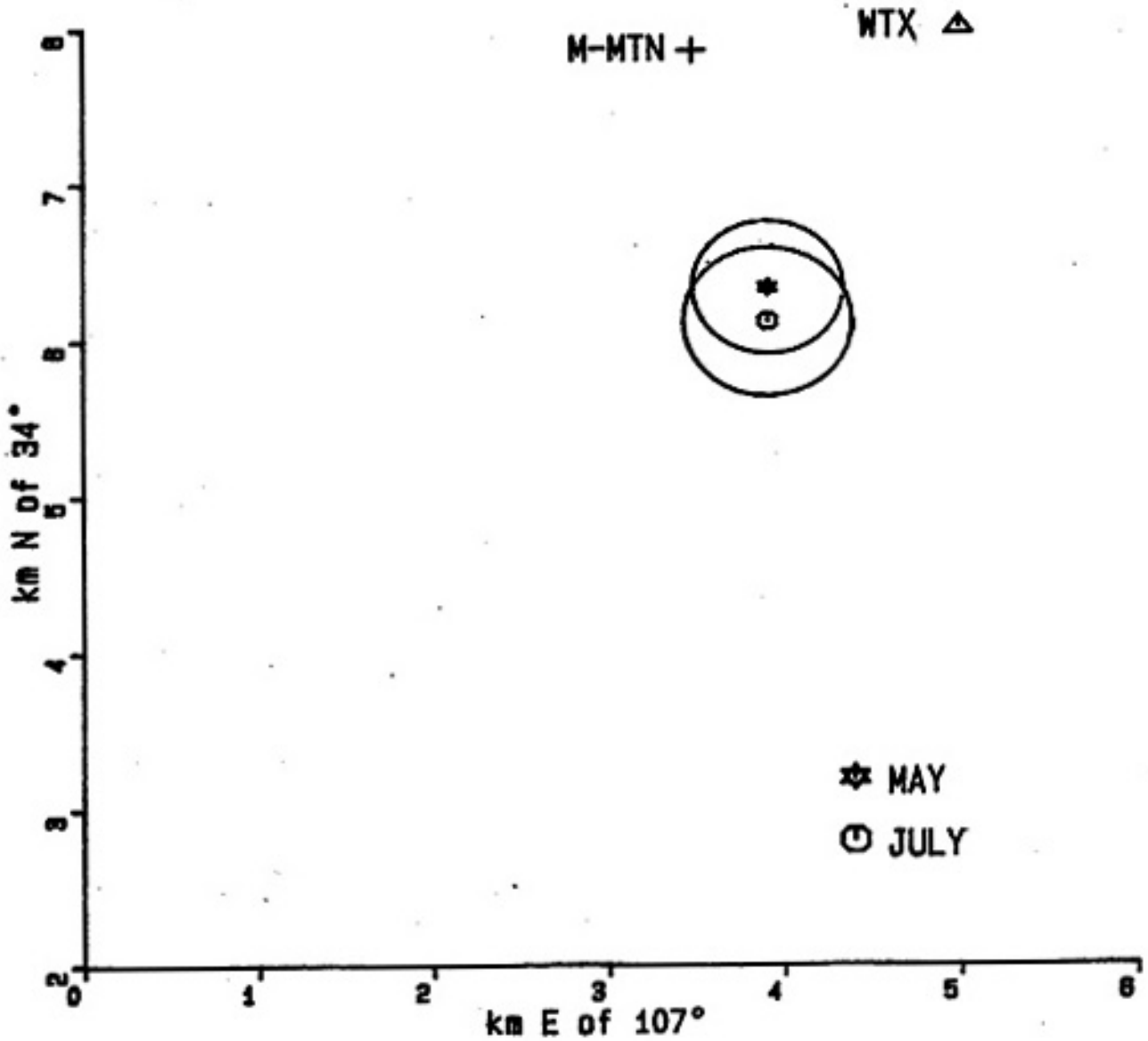

Figure 11. Average epicentral locations from the 23 best-located events in the May and July, 1983, Socorro Mountain swarms. Circles represent the average ERH for each data set.

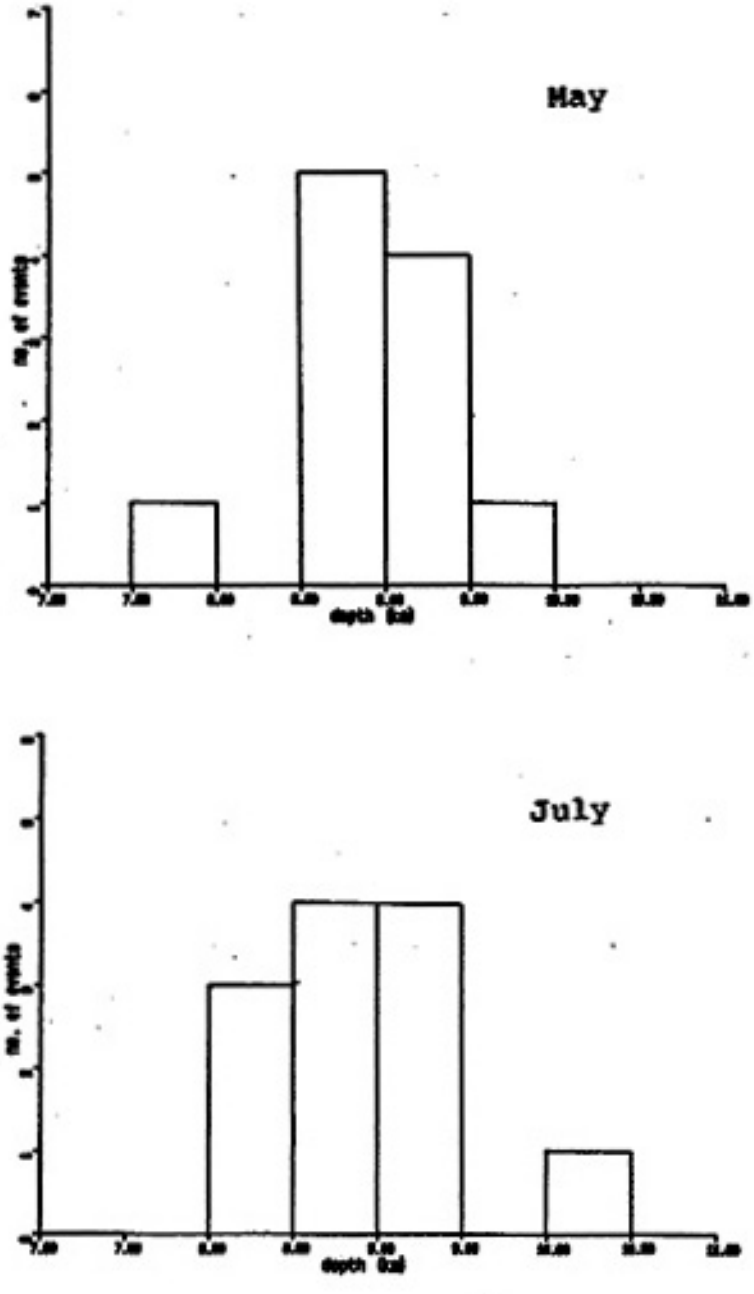

Figure 12. Distribution of focal depths for stronger "A" quality solutions from May and July, 1983, swarms. The average error in focal depths was 0.38 km.

WAVEFORM DUPLICATION

The availability of high quality digital data allowed detailed comparisons of waveforms to be made. In previous studies in the Socorro area, comparisons of digital data have shown a striking similarity between waveforms of microearthquakes within swarms (Sanford et al., 1983c; Sanford, in prep.). The data in this study also exhibited close similarity of waveforms (Figures 13 and 14). When cross-correlating entire waveforms (eight second windows) several pairs of events had correlation coefficients greater than 0.94. This is quite remarkable as the strengths of the events and time of occurrence varied substantially. A listing of the cross-correlation program utilized in this study is contained in Appendix 4. Although some remarkably high correlation coefficients were found when comparing the entire waveform of separate events, this result was not universal. To study the duplication phenomena further, the P and S-phases were analyzed separately. It should be noted that because the digital event recorder was operational only during the last portion of the May swarm, the analysis of the digital data is somewhat biased towards the July data set.

To analyze the P-phase in detail, only the first 0.6 seconds (60 points) of the waveform was examined. Figure 15 is a sequence of normalized P-phase waveforms from the May swarm. All the events have been cross-correlated with the

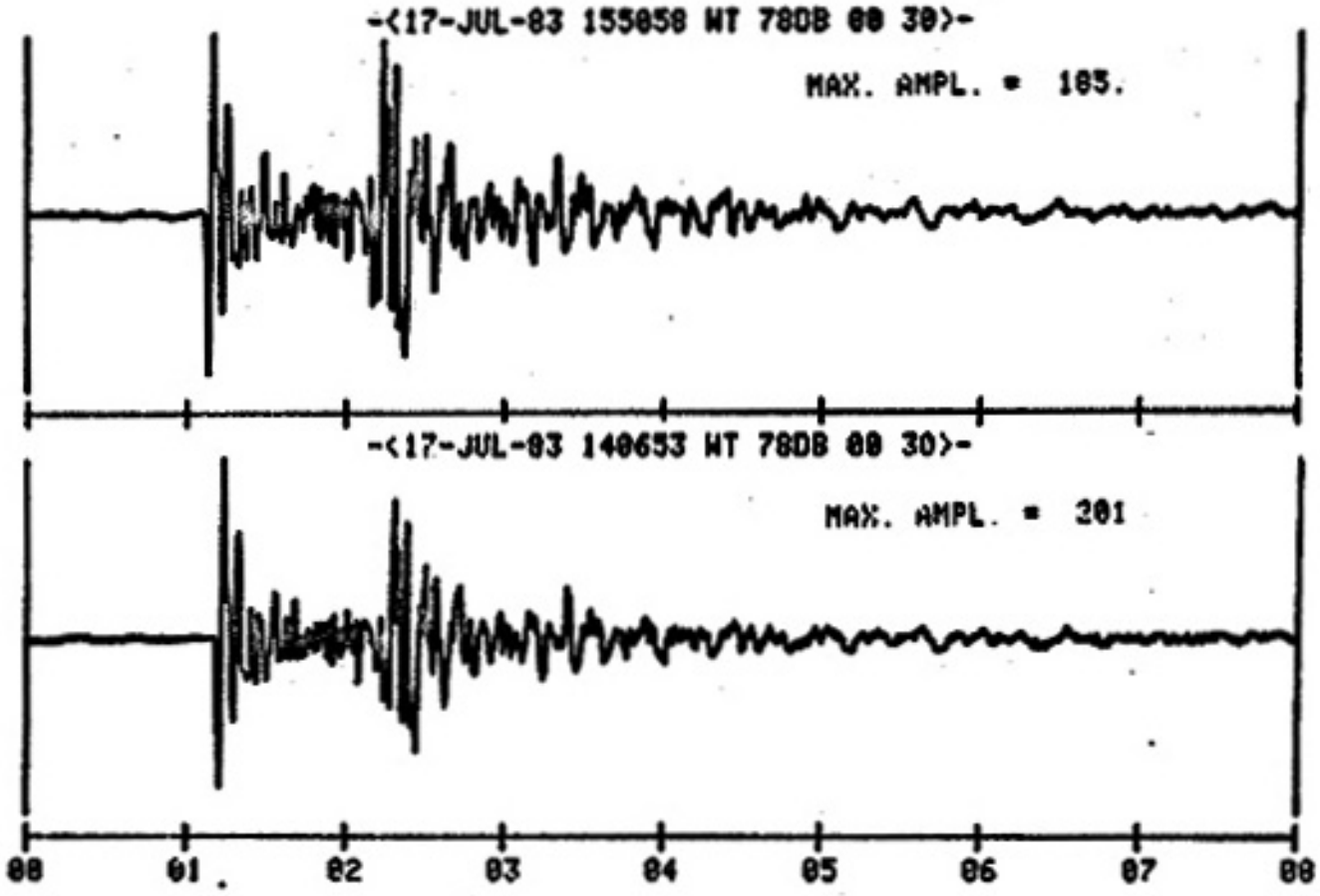

Figure 13. Example of duplication between entire waveforms (8 second window), cross correlation coefficient=0.96.

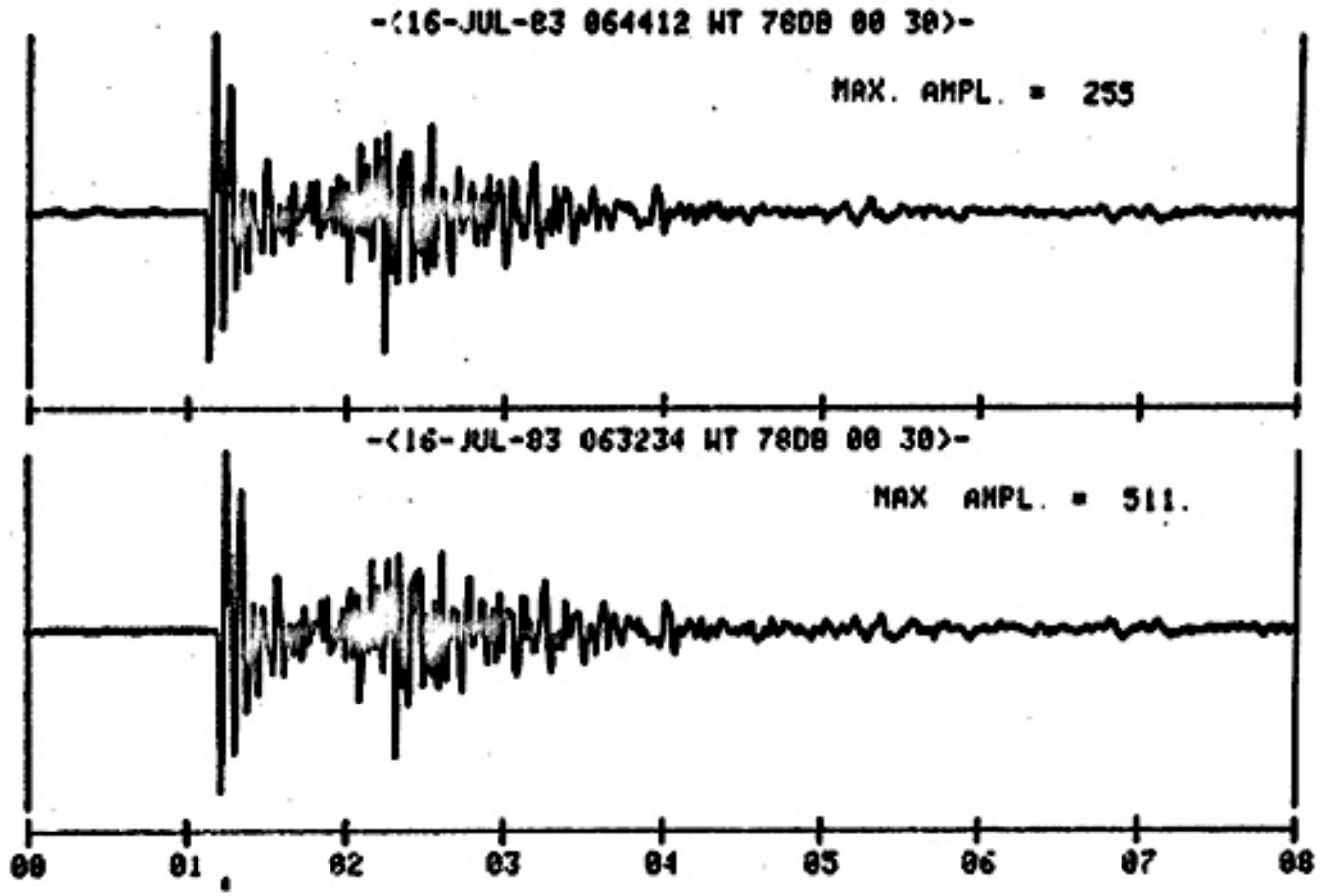

Figure 14. Example of duplication between entire waveforms (8 second window), cross correlation coefficient=0.94.

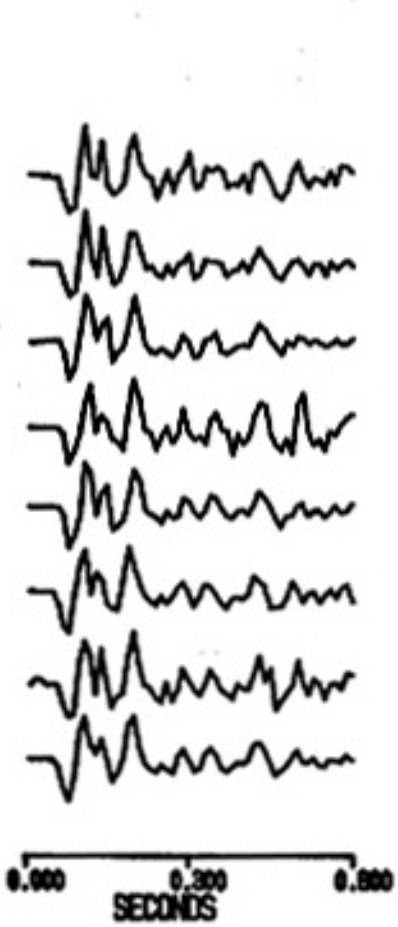

Figure 15. Sequence of normalized P-phase waveforms from the May, 1983, swarm illustrating waveform similarity. A correlation coefficient of 1.0 indicates event used as master.

strongest event shown (the bottom trace). The resulting cross-correlation coefficients range from 0.79 to 0.90. These events span a range of magnitudes from -0.8 to 0.70. This group of traces exhibits remarkable similarity considering the events were recorded in the presence of noise (which will have a larger relative effect on the weaker events).

A series of normalized waveforms from the July swarm is plotted in Figure 16. These events span an even larger magnitude range (-0.6 to 1.8) and, with one exception, over this range the correlation coefficients are all greater than 0.89 (with respect to the event at 03:30:26 on July 16). Notice, however, the decrease in correlation coefficient for the strongest event in the panel, M_L=1.8 at 22:06:13 on July 16. This waveform has the same general character as the other events in the panel but the fundamental frequency is lower. Nearly all the P-phase digital data for microearthquakes less than or equal to 1.2 in magnitude could be well represented by a single characteristic waveform. The average correlation coefficient for these events was 0.91. In contrast, the two events with magnitudes greater than 1.2 showed a decrease in correlation coefficient to less than 0.68 when cross-correlated with the smaller events.

To evaluate the duplication of the S-phase, 0.9 second (90 point) windows were examined. Figure 17 shows the normalized S-phases of the same events plotted in Figure

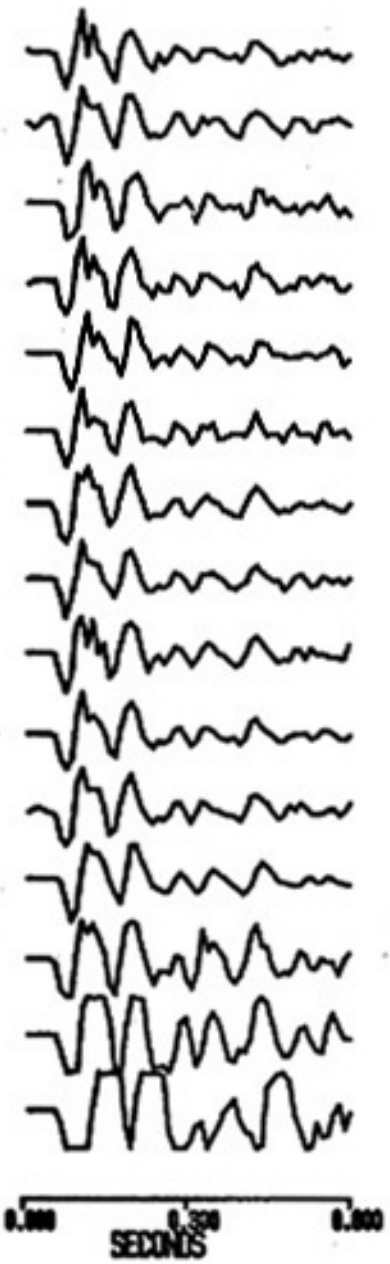

	Dig Amp	M	Corr Coeff
16-JUL-83 220910	51.	-0.6	0.91
17-JUL-83 145309	87.	-0.36	0.92
17-JUL-83 113545	116.	-0.24	0.93
16-JUL-83 043637	192.	-0.02	0.97
20-JUL-83 041107	256.	0.11	0.94
16-JUL-83 043554	364.	0.26	0.95
17-JUL-83 024240	527.	0.42	0.93
17-JUL-83 142709	607.	0.48	0.96
16-JUL-83 173952	771.	0.57	0.94
16-JUL-83 033026	972.	0.69	1.00
16-JUL-83 031037	1472.	0.87	0.97
20-JUL-83 004155	1786.	0.95	0.95
16-JUL-83 085950	2047.	1.08	0.90
17-JUL-83 113258	2047.	1.3	0.89
16-JUL-83 220613	2047.	1.8	0.88

Figure 16. Sequence of normalized P-phase waveforms from the July, 1983, swarm illustrating waveform similarity over a large magnitude range.

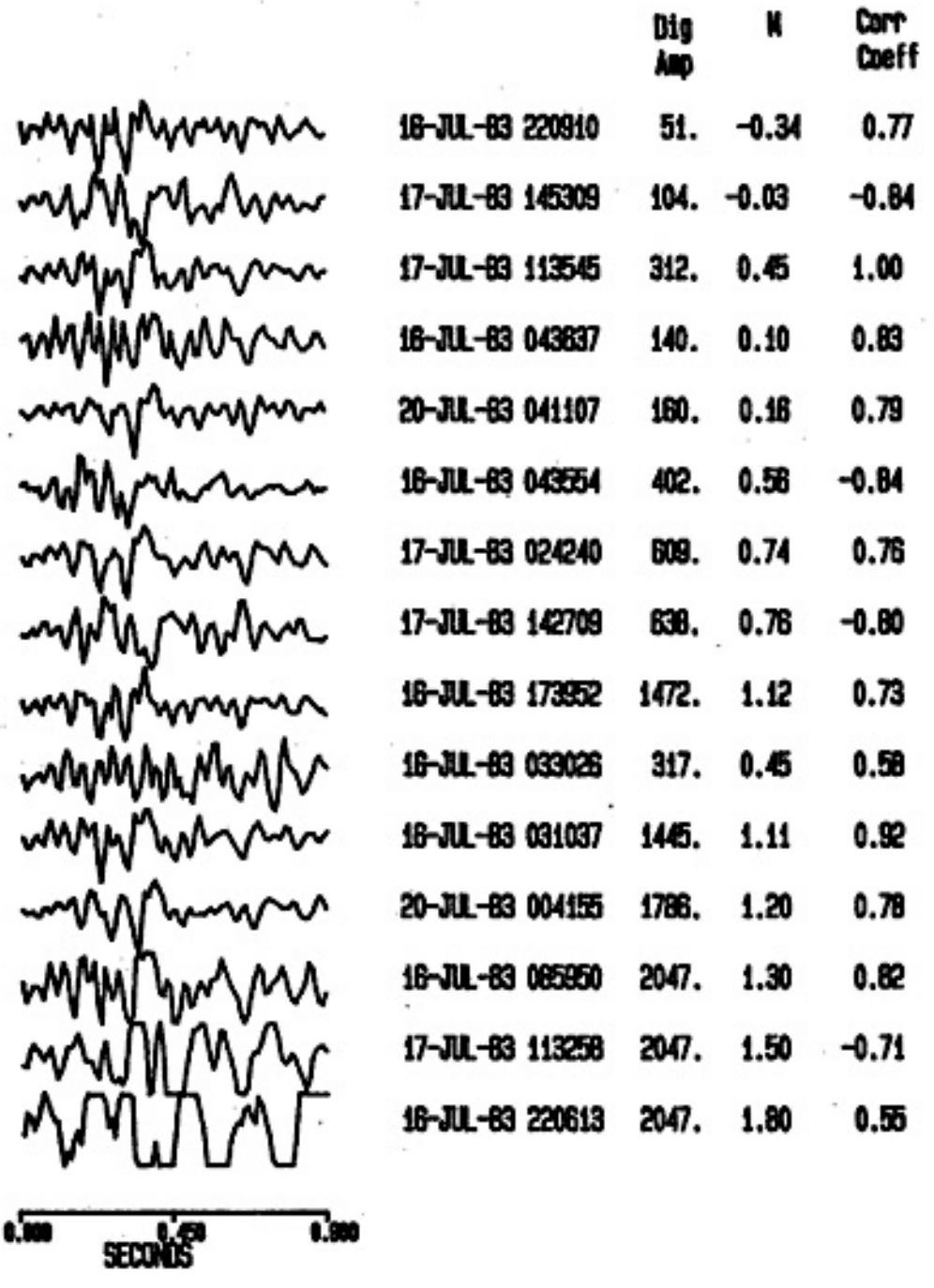

Figure 17. Comparison of normalized S-phase waveforms corresponding to P-phase windows in Figure 16. Negative correlation coefficients indicate phase reversal.

16. As can be seen, some events in this panel have high correlation coefficients and some have fairly low correlation values. The choice of master event in this panel was not the same as in Figure 16. The master was chosen to be that event giving the highest average correlation coefficient with all the events in the panel. In general the correlation coefficients here are lower than those for the same events on the P-phase panel. Again notice that the largest event on the panel (M_L=1.8) shows a low correlation coefficient (0.55). By searching through all the S-phase data available, groups of events could be found that were quite similar in character (Figure 18), but in general, the similarity between S-phase waveforms was not as great as with the P-phases. The reason for this somewhat unusual behavior is not clear at this time.

For certain events (e.g. in Figure 17) the correlation coefficient was negative. This occurs when the two waveforms being correlated are 180 degrees out of phase. This phase reversal occurred fairly frequently for the S-phase data but not at all for the P-phase data.

This duplication (except for amplitude) of waveforms over a large range of magnitude ($-0.8<M_L<1.2$) and hence seismic moment indicates the smaller events are the impulse response of the path and instrument (Frankel and Kanamori, 1983). The small number of events above M_L=1.3 prevents a precise determination of where duplication ends.

The first arrival of the direct P-phase travels the

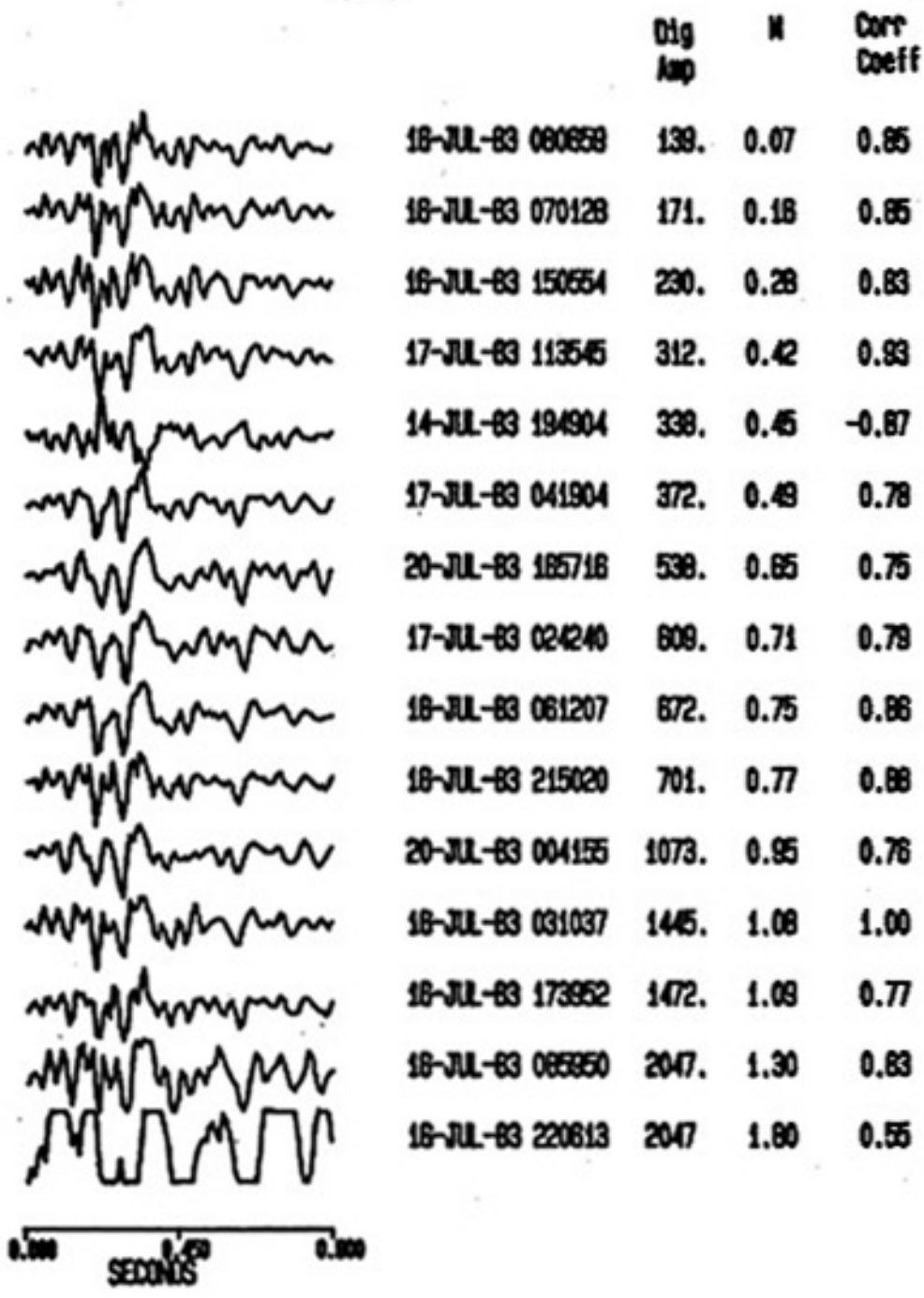

Figure 18. Sequence of normalized S-phase waveforms from the July, 1983, swarm illustrating duplication over a large magnitude range.

minimum time path. Hence the first cycle of motion in the direct P-phase should have the minimum amount of complexity due to multipathing and reverberations. To study path, instrumentation and source properties, an examination of this initial portion of the P-phase was conducted.

The time between the direct P-wave onset and the first zero crossing ($\tau_{1/2}$) was measured for both the May and July data sets. For the May digital data (16 events) the average $\tau_{1/2}$ was nearly constant (0.038±0.003 seconds) over the entire range of event strengths ($-0.8<M_L<0.7$). The July data (77 events) was also nearly constant ($\tau_{1/2}$=0.038±0.005 seconds) up to a magnitude of 1.2. However, the largest event, M_L=1.8, again failed to group with the other data as $\tau_{1/2}$ was 0.069 seconds. This is more than three standard deviations from the mean for the shocks with magnitudes less than 1.2.

If the hypothesis postulated in the previous section is true, the smaller events are merely the impulse response of the path and instruments. Therefore any value of $\tau_{1/2}$ which is statistically significantly larger than the average for the smaller events has some source information contained in the waveform.

Thus by using two different approaches, correlation coefficients and measurement of $\tau_{1/2}$, the magnitude at which source information begins to appear in the waveform is constrained to lie between M_L=1.3 and 1.8 for the swarm-WTX travel path. Unfortunately the lack of more data above

magnitude 1.2 prevents a more precise estimate of the end of duplication and the beginning of the arrival of source information. Obviously this particular value will hold only for this travel path; slightly different values have been determined in other Socorro area studies (Sanford, in preparation).

FAULT PLANE SOLUTIONS

In focal mechanism studies the source is assumed to be surrounded by an imaginary sphere, the focal sphere. To determine the focal mechanism, the focal sphere can be projected onto a plane, the stereonet. Because this study was concerned with local events, the upper hemisphere was utilized as the plane of projection. A detailed discussion of the use of the stereonet in fault plane solutions may be found in Wieder (1981). The first motion (compression or dilatation) is plotted as a point on the stereonet with the coordinates, azimuth and angle of incidence, determined by the HYPO71 solution. For this study a homogeneous, isotropic half-space was used, hence the raypaths from source to receiver were straight lines.

To reduce the possible errors in attempting to read first motion directions of weak events, the composite fault plane solutions presented here utilized only the strongest shocks in each of the two swarms. Nine events from the May swarm and ten from the July swarm were studied. Table 2 contains a listing of the 19 events. Table 5 contains a listing of the direction of first motion observed at each station. Only those readings that were clear were utilized.

For the data from the May swarm there was only one reading that reversed first motion direction, up rather than down at station SB. The P-phase onset at stations LPM and

Table 5. Summary of First Motions by Station Used in Fault Plane Studies

May Data, Events #1-9:

Station	Usable Readings	1st Motion	Character
WTX	9	9 down	impulsive
BAR	9	9 up	impulsive
CAR	9	9 up	impulsive
SB	7	6 down; 1 up	impulsive
SMC	9	9 up	impulsive
BMT	9	9 up	somewhat emergent
LPM	4	4 up	emergent
LAZ	6	6 up	emergent
MLM	3	3 up	emergent and weak

July Data, Events #10-19:

WTX	11	11 down	impulsive
SNM	11	11 down	impulsive
BAR	11	11 up	impulsive
CAR	11	11 up	impulsive
SB	11	11 down	somewhat emergent
SMC	8	8 up	somewhat emergent
BMT	7	6 up; 1 down	emergent
LPM	9	8 up; 1 down	somewhat emergent
LAZ	4	2 up; 2 down	emergent

LAZ was generally more emergent in character and thus had fewer clear readings than the other stations. For the July data, station LAZ shows a clear reversal of first motion direction during the swarm. Station BMT also shows an emergent character to the P-wave onset. This data indicates that one P-nodal plane must pass near these stations (LAZ, BMT and SB).

In addition to the first motions, an additional constraint may be placed upon the location of nodal planes by considering the amplitude ratio of the S and P-phases. Table 6 summarizes the measured ratios of the direct S to direct P-phase for the local network of stations for the 19 strongest shocks of the May and July swarms. The ratios show a large variation in value with the standard deviation usually being a significant fraction of the mean. In general, stations LAZ, BMT, SMC and LPM have large values for the S/P amplitude ratios. There were no statistically significant differences in S/P amplitude ratios between the May and July swarm data.

Based upon the above data, composite fault plane solutions were obtained for both the May and July swarms (shown in Figure 19). Due to the S/P amplitude ratios at BMT and LAZ and the reversal of first motions at LAZ, one P-nodal plane appears to be well constrained to strike N15°E. The orientation of the complementary plane is somewhat less constrained. The position of the second plane was chosen based upon the pole of the first plane and the S/P amplitude

Table 6. S/P Amplitude Ratios for Local Stations

May Data, Events 1 Through 9:

Station	S/P Amplitude Ratio	Std.Deviation (±)
WTX	2.42	1.44
BAR	2.47	1.17
CAR	2.54	0.75
SB	1.45	0.99
SMC	3.48	0.41
BMT	3.58	2.58
LPM	4.64	1.68
LAZ	4.56	2.18
MLM	1.35	0.13

July Data, Events 10 Through 19:

Station	S/P Amplitude Ratio	Std. Deviation (±)
WTX	1.41	0.52
BAR	1.20	0.31
CAR	2.35	0.57
SB	1.17	0.36
SMC	3.90	1.49
BMT	3.96	1.56
LPM	3.24	0.91
LAZ	5.05	1.00

(Note: all amplitudes were measured from analog records)

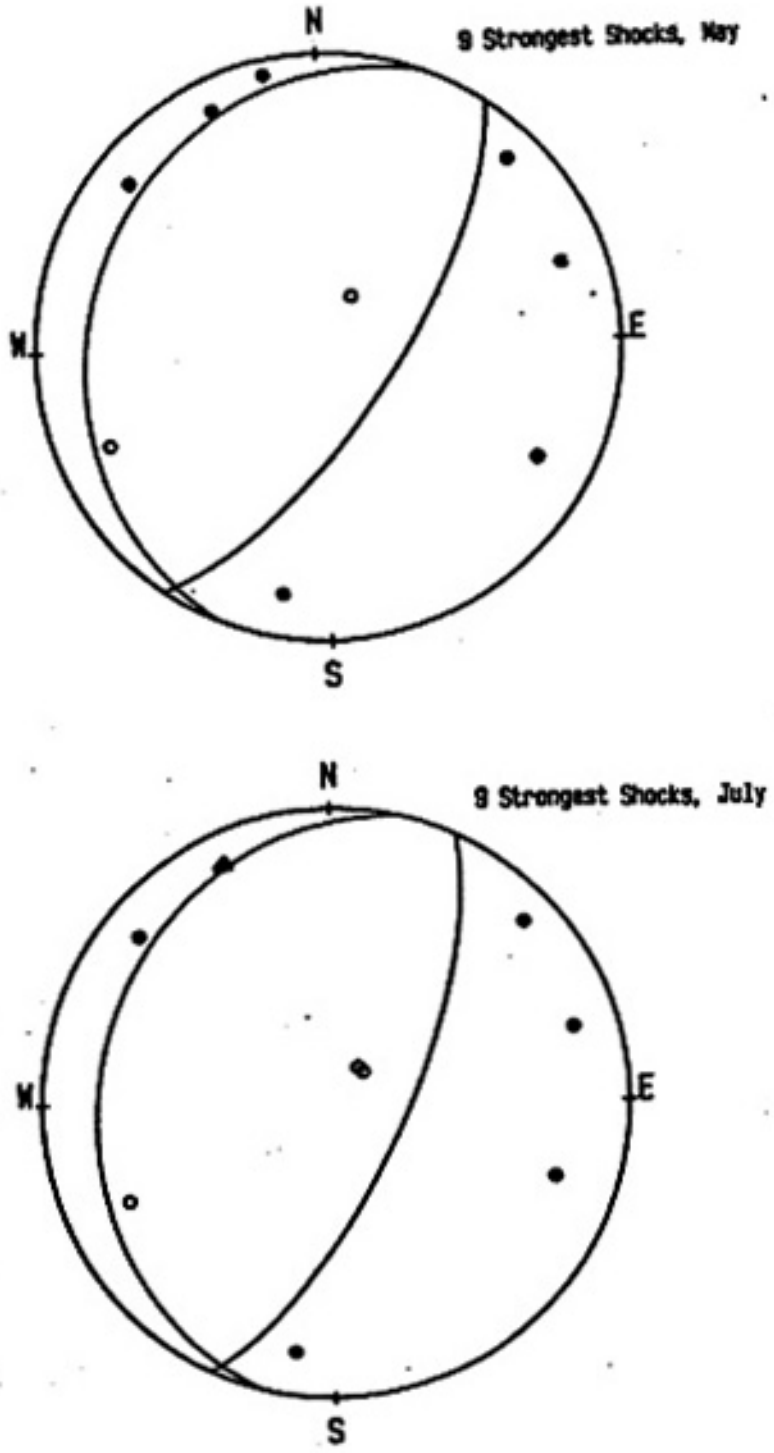

Figure 19. Fault plane solutions (upper focal sphere) from the May and July, 1983, swarms. Compressions are dark circles, dilatations are open circles. The triangle indicates reversal of first motions.

ratios at stations LPM, WTX and SMC. The resulting solutions for the May and July swarms are quite similar. The focal mechanism appears to be nearly pure normal dip-slip.

An earlier comprehensive study of focal mechanisims in the Socorro area was conducted by Wieder (1981). Wieder subdivided the general Socorro region into 12 smaller areas. His areas 9 and 5 are in fairly close proximity to the area of this study. Wieder's results for his area 5 show dominantly dip-slip motion with nodal planes striking N7°W and N21°E. The nodal planes both dip at 47 degrees. For area 9, Wieder finds azimuths of N48°W and N7°E with dips of 40 and 66 degrees respectively. Wieder prefers the eastward-dipping planes in both these areas. Although the azimuths found in this study agree fairly well with Wieder's study, the dips differ quite a bit. For the 1983 swarm data there appears to be either a plane dipping steeply (~70°) westward or a plane dipping at a shallow angle (~20°) to the east. These planes may be interpreted as either straight or curving features that extend to the surface (possible geometries are illustrated in Figure 20). Upon projecting the possible fault planes to the surface, there does not appear to be any correlation with mapped surface faults having the correct sense of movement.

In an attempt to eliminate one of the possible planes, the focal positions of the 23 best located events (see Figure 9) were projected onto a vertical plane normal to the

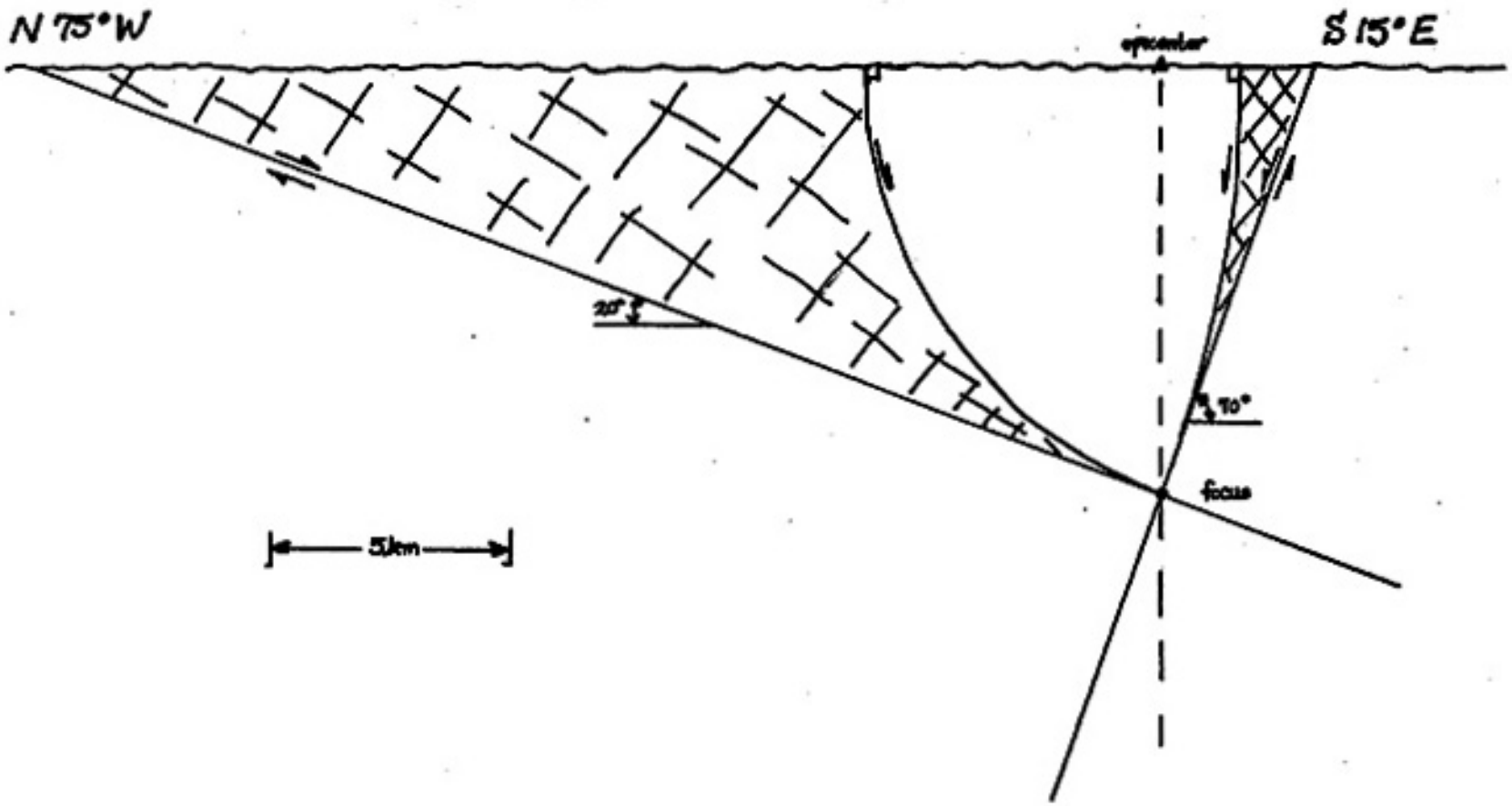

Figure 20. Illustration of possible fault geometries based upon assumption of planar or curving fault surfaces. Hatchured areas indicate possible zones of faulting.

average strike of the possible fault planes (i.e., onto a plane with azimuth=105 degrees). This procedure, shown in Figure 21, suggests that the westward-dipping plane is somewhat more likely to be the true fault plane. The steep, westward-dipping fault plane would also seem to be a more logical choice based upon other physical considerations. Consider the body forces associated with these fault planes. If the low-angle normal fault were chosen, the effect of gravity as a driving force would be negligible compared to the effect of gravity as a normal force across the plane due to lithostatic load. Thus for the steeply-dipping plane, gravity will be assisting in failure while for the shallow dipping plane, gravity will be retarding slippage.

The digital data at station WTX were also examined and S/P amplitude ratios catalogued. The ratios at WTX are generally low, $\overline{S/P}=1.61\pm0.87$, but highly variable, $0.20< S/P <6.6$. As mentioned previously the S-phase at station WTX is apparently reversing direction of first motion. These factors would indicate that considerable complexity in the fault process is associated with at least some of the smaller events. This complexity presents an area for further study.

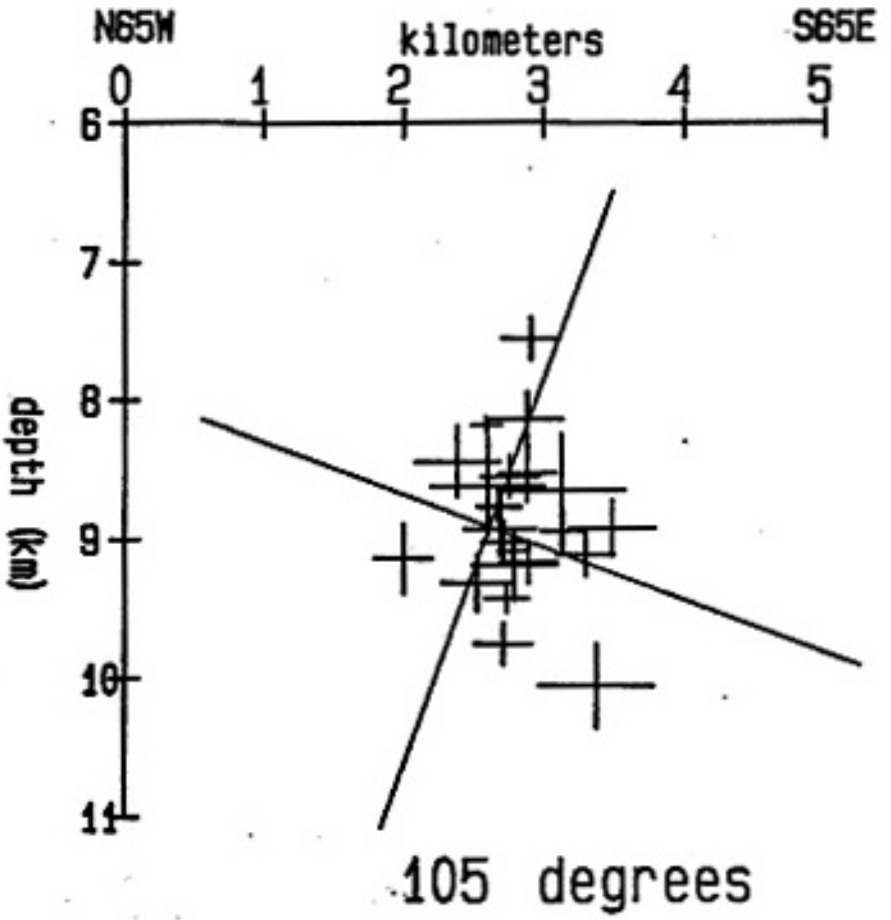

Figure 21. Cross section illustrating the projection of hypocenters onto a plane normal to the strike of the inferred fault planes. Events used are the 23 best located events (see Table 4).

SPECTRA

To extract all possible information from the digitally recorded seismograms, spectral characteristics of some of the WTX digital records were studied. All of the WTX digital data was acquired at 100 samples per second. The DR-100 amplifier filter was low-pass with the low setting at out and the high setting at 30 Hz. To study the frequency content of the incoming seismic waves, the response of the filter and geophone was removed via a straightforward deconvolution procedure. An illustration of the effect of seismometer and filter response on the spectra is shown in Figure 22. The P and S-phases were studied individually with 64 point (0.64 second) windows.

A total of 19 events, six from May and 13 from July, were studied. These events were chosen to represent unsaturated events with a variety of S/P amplitude ratios that covered the entire time period of the swarms. In general the corrected spectra is best represented by a function of the form

$$Amp = e^{-kf} \qquad (3)$$

where k is a decay parameter. Examples of P and S-phase corrected spectra are shown in Figure 23. For events below the threshold of duplication this represents the path response.

Clear peaks in the uncorrected spectra occur roughly between 9 and 13 Hz for the events examined in this study.

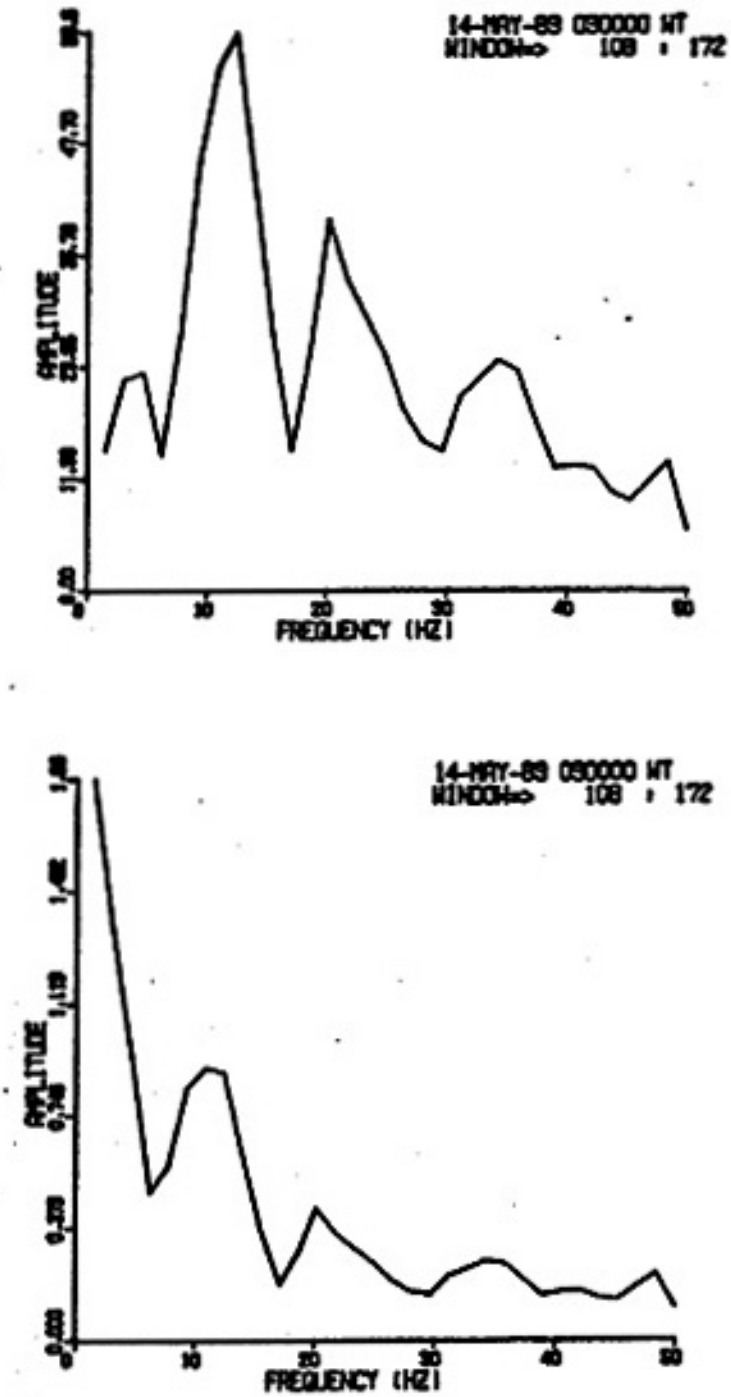

Figure 22. Illustration of the deconvolution of instrument and filter effects from raw P-phase spectra (top). Both spectra plotted with three point moving average filter.

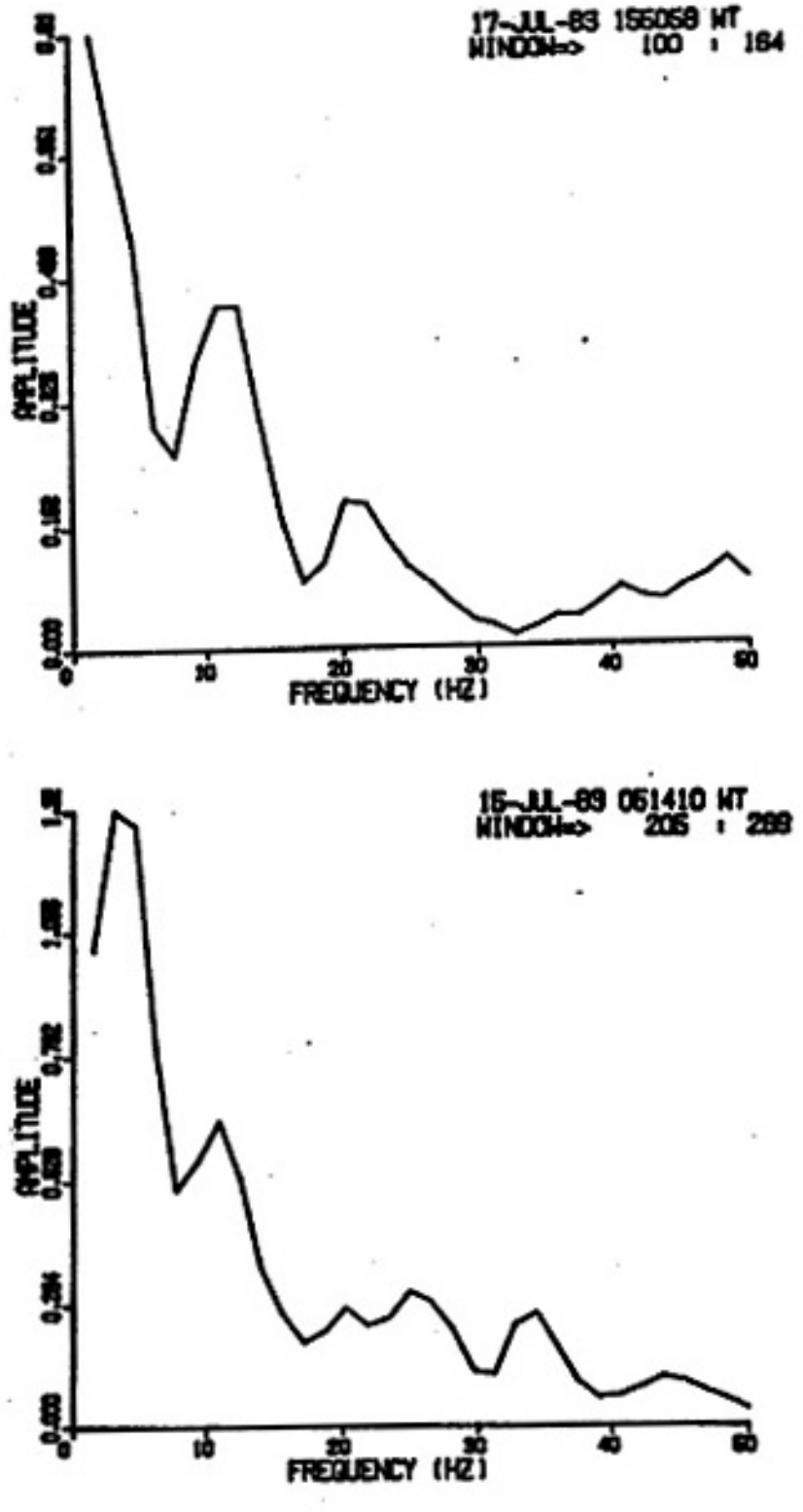

Figure 23. Examples of P-phase (top) and S-phase (bottom) spectra corrected for instrument and filter response. Both spectra plotted using a three point moving average filter.

In general even though the events vary widely in strength, the spectral characteristics do not vary much. This is certainly expected in view of the waveform duplication discussed previously.

Below the threshold of duplication, it is assumed that the shape of the raw spectra is due to a combination of instrument effects and attenuation along the path (see Figures 23 and 24). The instrumentation effect is approximated by

$$\text{Amp}=2\cdot\pi\cdot f \tag{4}$$

The path attenuation is approximated by:

$$\text{Amp}=e^{-kf} \tag{5}$$

where $k=\frac{\pi r}{Qv}$

Q=seismic quality factor,
v=average propagation velocity,
r=distance from focus to station,
and f=frequency.

The raw spectra (see Figure 23, top) show rather pronounced peaks separated by a constant frequency interval. This behavior often indicates a near surface reverberation phenomena. In order to define a single spectral peak, the data was smoothed using a nine point moving average filter. The amplitude of the uncorrected spectra is

$$\text{Amp}=2\cdot\pi\cdot f\cdot e^{-kf} \tag{6}$$

and therefore,

$$\frac{d\text{Amp}}{df}=2\pi e^{-kf_m}+2\pi f_m\left(\frac{\pi r}{Qv}\right)e^{-kf_m}=0$$

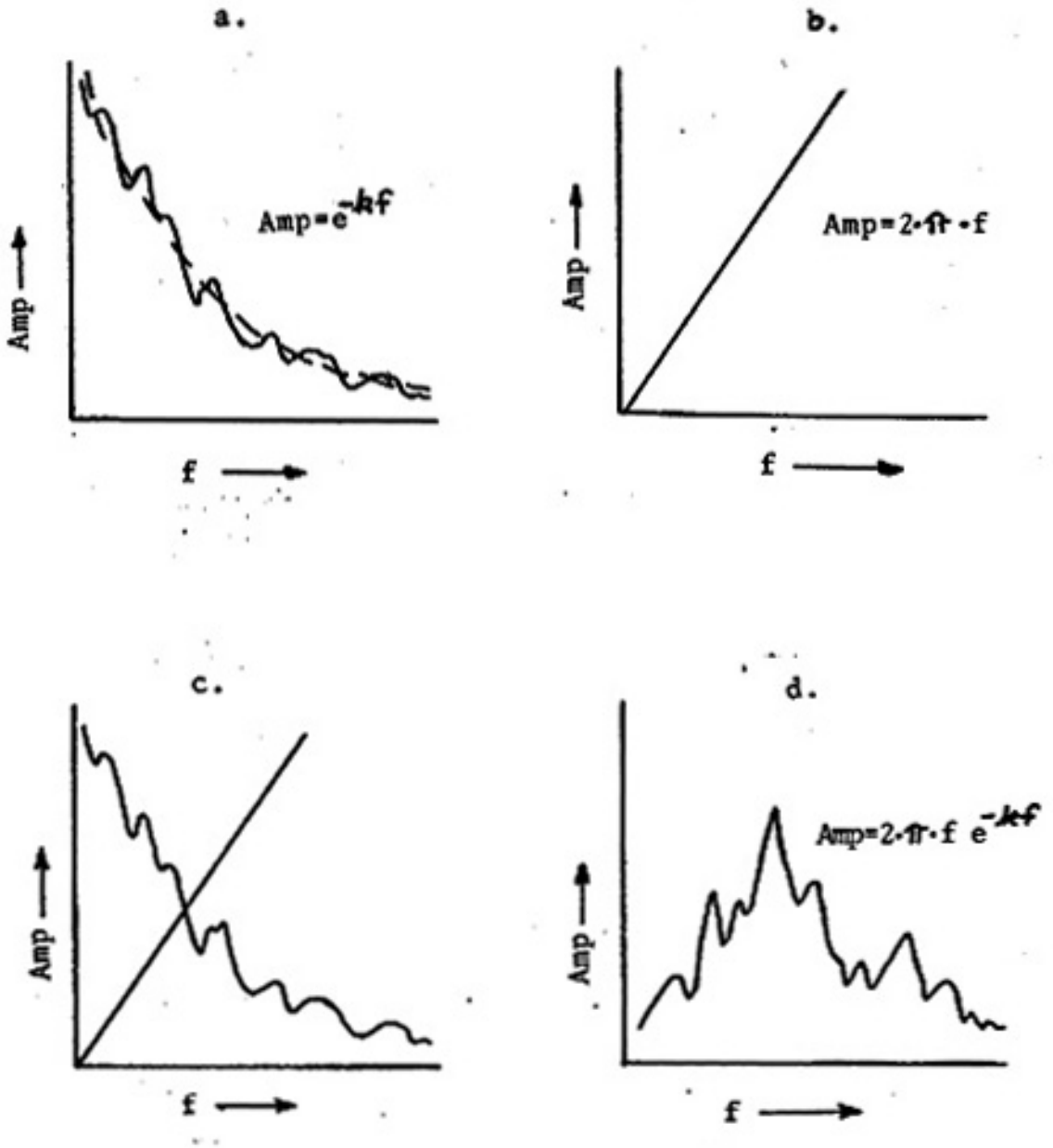

Figure 24. Schematic illustration of the interaction of path attenuation curve (a.) with instrument effects (b.). Since this interaction is a time domain convolution (c.) the interaction results in the observed raw spectra (d.).

where f_m is the spectral maximum. An estimate of Q may be found from

$$Q = \frac{f_m \pi r}{v} \qquad (7)$$

Examples of P and S-phase windows and corresponding uncorrected spectra are shown in Figures 25 and 26. Spectral peaks are summarized in Table 7. The P-phase appears to have a single well-defined peak at 9.4 Hz. This leads to an estimate of Q_p of $42<Q_p<48$ (accounting for the discrete frequency interval). The S-phase shows more variability in spectral peak but 9.4 Hz still appears to be the dominant peak. Hence an estimate of Q_s is then $73<Q_s<86$. Thus it would appear, for this travel path, that Q_s is slightly larger than Q_p. Although not supported by estimates of statistical uncertainty, these values are useful for general comparison. Carpenter (in prep.) found Q_s values ~100 for this path using a different technique.

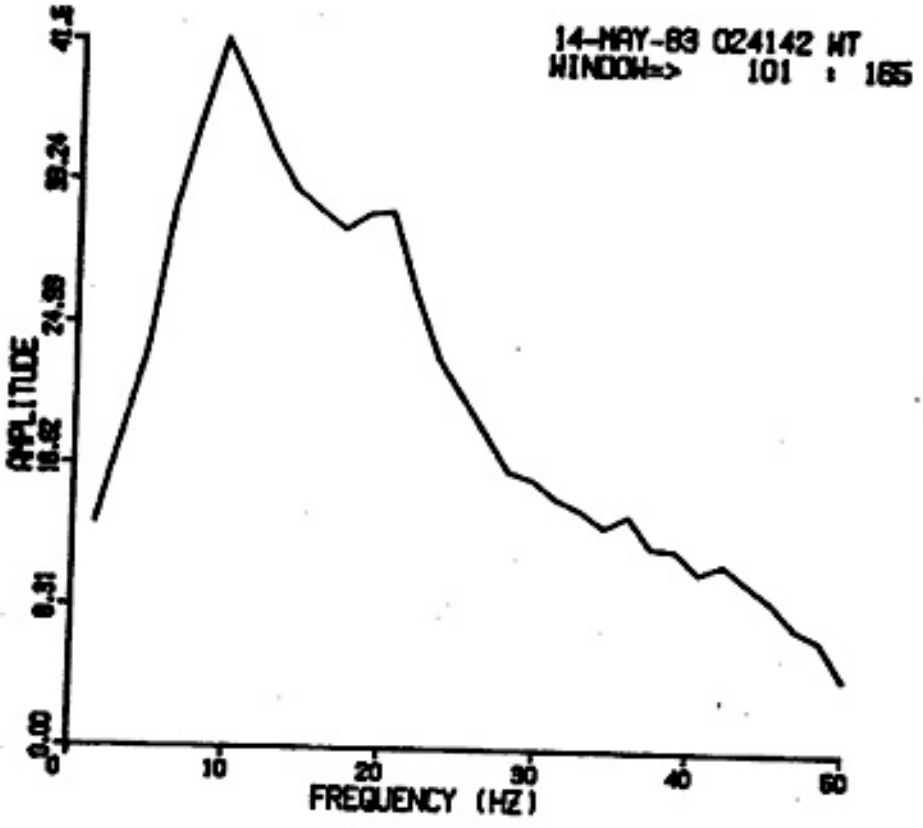

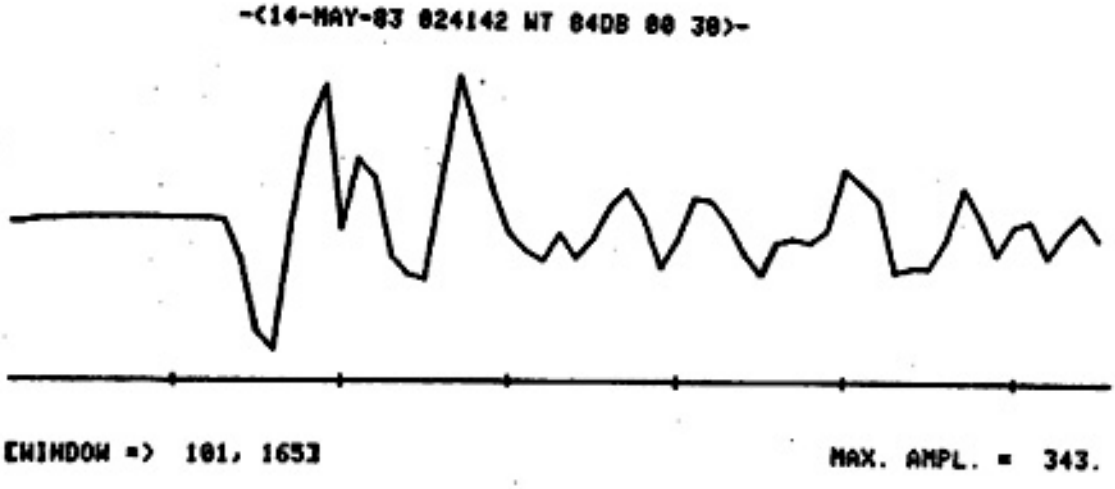

Figure 25. Example of P-phase window (0.64 second) and corresponding uncorrected spectra. Spectra has been smoothed with a nine-point moving average filter.

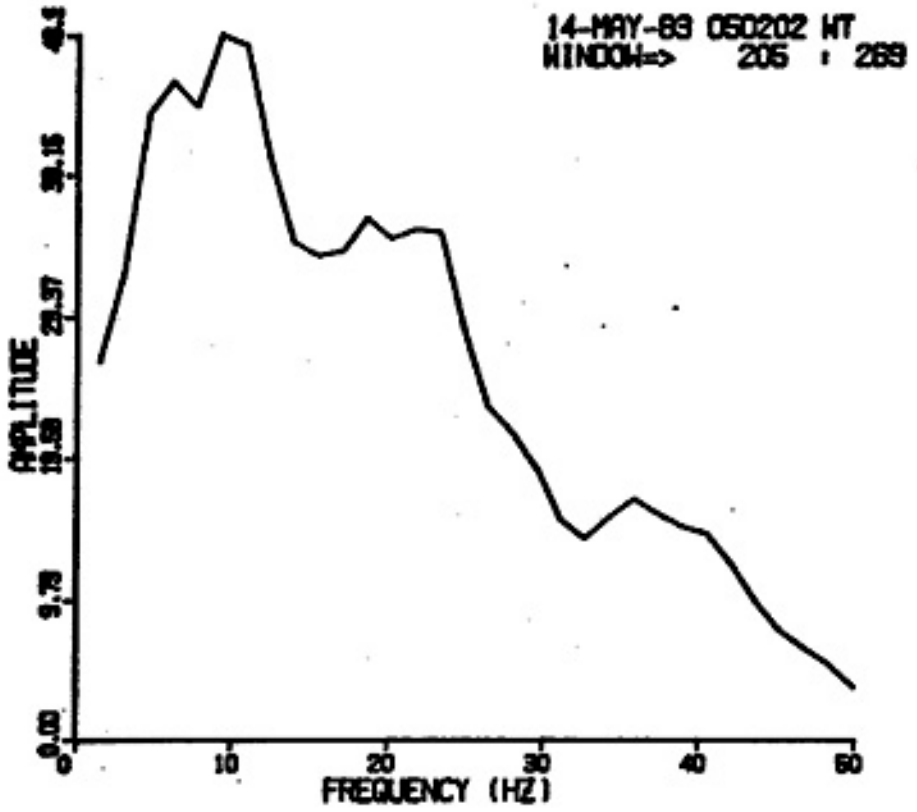

Figure 26. Example of S-phase window (0.64 second) and corresponding uncorrected spectra. Spectra has been smoothed with a nine-point moving average filter.

Table 7. Summary of Smoothed Spectral Peaks from Uncorrected Spectra with Nine Point Moving Average Filter Applied.

Event	P-phase	S-phase
May 14, 010216	9.4	9.4
May 14, 024142	9.4	9.4, 10.9
May 14, 030000	9.4	9.4
May 14, 050202	9.4	9.4, 10.9
May 14, 084938	9.4	9.4
May 14, 144318	9.4	9.4
July 15, 051410	9.4	9.4
July 16, 031037	9.4	9.4
July 16, 043637	9.4, 10.9	20.3
July 16, 173952	9.4	9.4, 10.9
July 16, 230054	9.4	16.7
July 17, 024404	9.4	20.3
July 17, 121303	9.4	20.3
July 17, 155058	9.4	9.4
July 18, 110937	9.4	9.4
July 20, 004155	9.4	9.4
July 20, 185217	9.4	9.4, 10.9
July 22, 070252	9.4	9.4, 10.9

Note: if two values appear the spectra was flat between the two values.

SOURCE CHARACTERISTICS

The waveform recorded by the seismic system (A(t)) may be expressed as the convolution of the source function (S(t)) with the response of the path (the Green's function, G(t)) and the instrument response (I(t)), thus

$$A(t)=S(t)*G(t)*I(t). \quad (8)$$

The duplication of events noted previously suggests the source function is very 'delta-like' and the observed waveform is merely the impulse response of path and instrument, i.e.

$$A_o(t)=G(t)*I(t). \quad (9)$$

This may be described somewhat differently by considering the spectral corner frequencies dictated by path and source. As the source-time function becomes more delta-like, the resulting source spectrum becomes broader band. Thus as the source becomes more delta-like, the source corner frequency will eventually fall above the path attenuation curve. Hence at some source size the waveform becomes source independent (summarized in Figure 27).

A logical analysis procedure would be to simply determine the Green's function for a particular path from small (i.e., source independent) events. Then merely deconvolve this Green's function and the instrument response from the waveform of a large event to determine the source properties of the large event. Unfortunately, for this data

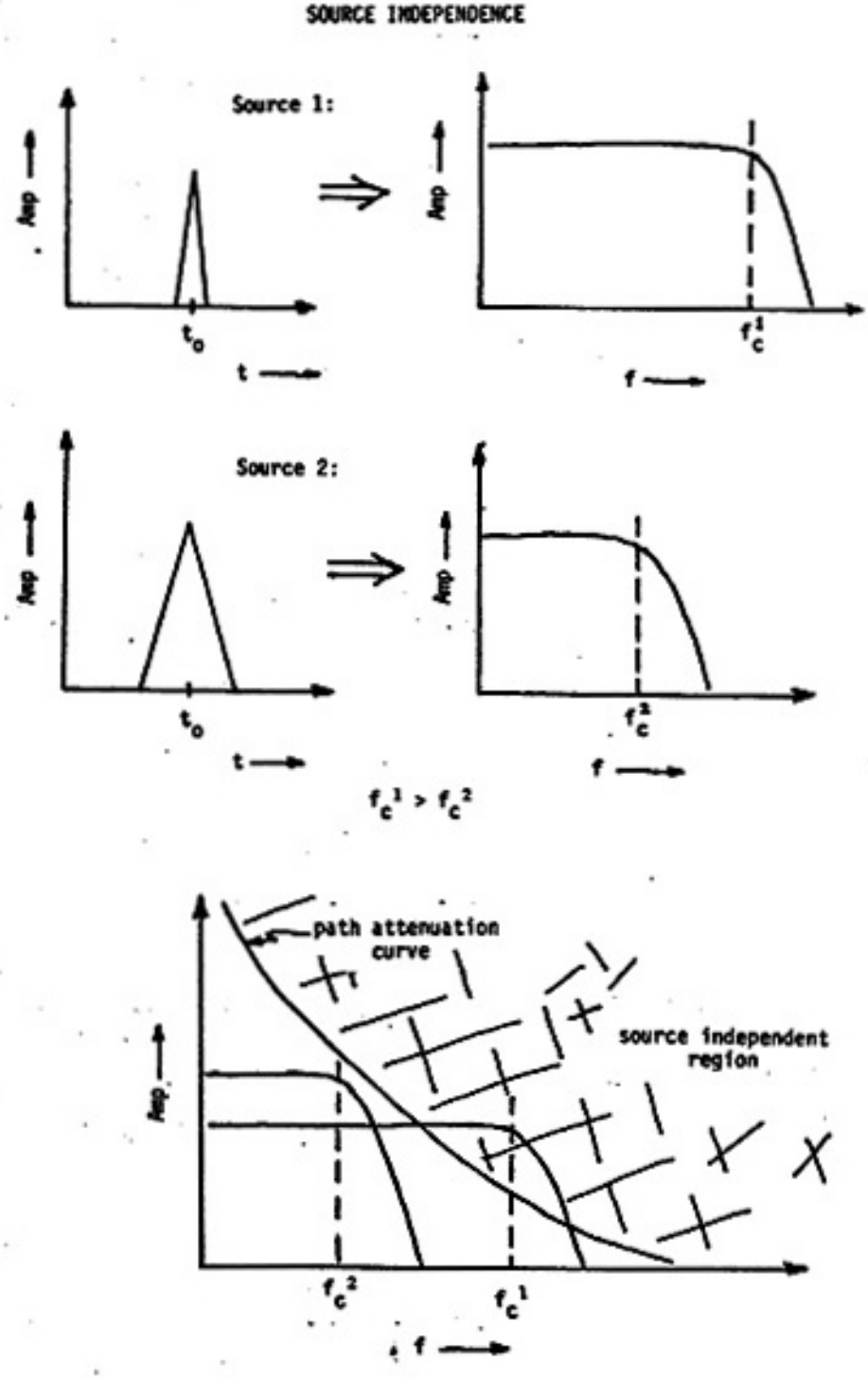

Figure 27. Schematic diagram illustrating the location of corner frequency depends on the "deltaness" of the source function. Source independence depends on the position of corner frequency relative to the path attenuation curve.

set, the events which fall above the duplication threshold, as determined by $\tau_{1/2}$ and cross-correlation, are all clipped. Hence frequency domain analysis would be fruitless.

Frankel and Kanamori (1983) suggest a simple method to approximate this deconvolution. This approximation involves deconvolving the "empirical" Green's function of a smaller event from a large (i.e., above duplication threshold) event by finding the difference in $\tau_{1/2}$ between the two, i.e.

$$\tau_{1/2}^{source} = \tau_{1/2}^{large} - \tau_{1/2}^{small} \quad . \tag{10}$$

This result is an approximate estimate of the pulse width ($\tau_{1/2}^{source}$) of the source time function. Since both waveforms are recorded by the same instrument there should be negligible instrumentation effect.

In Frankel and Kanamori's model, the pulse width of the source time function is converted to an estimate of the source radius. A model with a circular rupture propagating at a constant velocity that stops instantaneously is used (Sato and Hirasawa, 1973). Following Boatwright (1980) the fault radius is then estimated from

$$r = \frac{\tau_{1/2}^{source} \, v}{1 - \frac{v}{c} \sin\theta} \tag{11}$$

where c is wave velocity and θ is the angle between the normal and outgoing ray. The rupture velocity (v) is taken to be a constant 0.9β. For the 1983 Socorro Mountain swarms, the steeply dipping fault plane is assumed to be

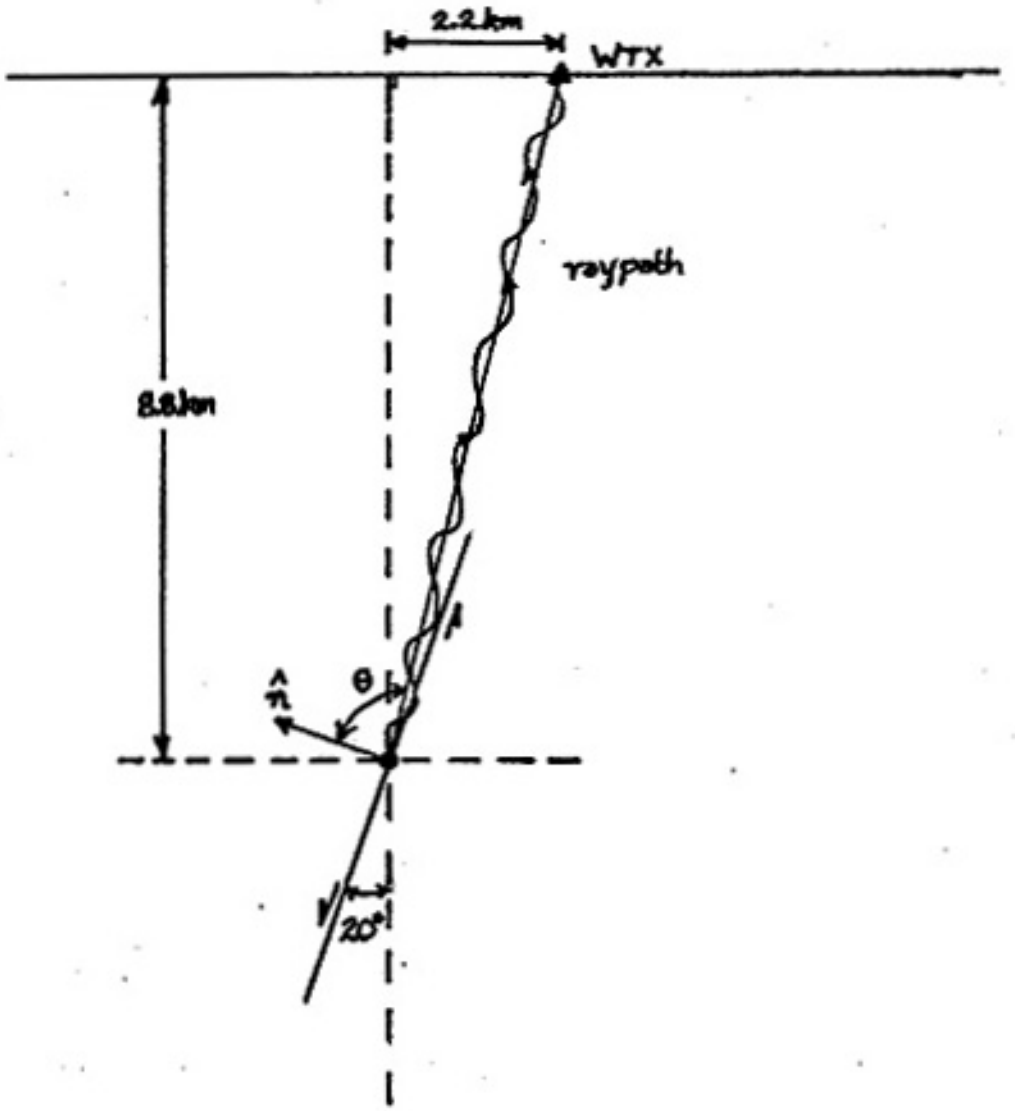

Figure 28. An illustration of the definition of the quantity θ used in equation 11. A constant velocity half-space model is used.

appropriate, then θ is found to be 83° (see Figure 28). The value of c is set to a constant 5.85 km/sec.

The magnitude of the larger shocks was determined from peak amplitudes (see Table 2). Then from the relationship of Archuleta et al. (1982),

$$\log M_0 = 1.05 M_L + 17.76 , \qquad (12)$$

seismic moments could be calculated. Once source radius and seismic moment are known, the stress drop ($\Delta\sigma$) may be found from Brune's (1970) circular fault model

$$\Delta\sigma = \frac{7 M_0}{16 r^3} \qquad (13)$$

Recall, for the May data set, $\bar{\tau}_{1/2}$=0.0380±0.0026 seconds and for the July data: $\bar{\tau}_{1/2}$=0.0382±0.0046 seconds. Only four events (all from July) have both large enough magnitudes and $\tau_{1/2}$'s to analyze with this approach. The results for these events are summarized in Table 8. The stress drops appear to be slightly lower than those reported from California by Frankel and Kanamori but within the scatter of other studies (O'Neill and Healy, 1972; Archuleta et al., 1982; Modiano and Hatzfeld, 1982).

The two largest events (numbers two and four in Table 8) show consistently small values for stress drop. This arises as a consequence of the large source radius calculated for these events. The radius is found from equation (11) and is directly proportional to $\tau_{1/2}^{source}$. However, the rupture velocity is assumed to be constant in equation (11). If for the larger events, v is not a

Table 8. Summary of Source Characteristics for Events Above Duplication Threshold, May and July, 1983 Swarms.

Event	$\tau_{\frac{1}{2}}$(sec)	M_L	r(m)	M_0(dyne-cm)	$\Delta\sigma$(bars)
16-Jul 0859	0.044	1.17	36	$7.65 \cdot 10^{18}$	74
16-Jul 2206	0.069	1.56	184	$2.51 \cdot 10^{19}$	2
17-Jul 1132	0.045	1.24	42	$1.15 \cdot 10^{19}$	71
19-Jul 0340	0.068	1.43	178	$1.83 \cdot 10^{19}$	1.4

Note: $\bar{\tau}_{\frac{1}{2}}^{small} = 0.0380 \pm 0.0026$ seconds

Table 9. Summary of Source Characteristics for Events With $\tau_{\frac{1}{2}}$ More Than One Standard Deviation Above $\bar{\tau}_{\frac{1}{2}}$, May and July, 1983, Swarms.

Event	$\tau_{\frac{1}{2}}$(sec)	M_L	r(m)	M_0(dyne-cm)	$\Delta\sigma$(bars)
14-May 0108	0.043	0.67	30	$2.91 \cdot 10^{18}$	49
16-Jul 0610	0.042	0.13	24	$7.88 \cdot 10^{17}$	26
16-Jul 2220	0.042	-0.12	24	$4.31 \cdot 10^{17}$	14
17-Jul 0242	0.044	0.42	36	$1.59 \cdot 10^{18}$	15
17-Jul 0419	0.043	-0.14	30	$4.10 \cdot 10^{17}$	7
17-Jul 0545	0.042	-0.04	24	$5.22 \cdot 10^{17}$	17
17-Jul 1135	0.042	-0.24	24	$3.22 \cdot 10^{17}$	11

Note: $\bar{\tau}_{\frac{1}{2}}^{small} = 0.0380 \pm 0.0026$ seconds

constant some errors in r and hence $\Delta\sigma$ may occur.

Another approach is to examine any event where $\tau_{1/2}$ is more than one standard deviation from $\overline{\tau}_{1/2}$ regardless of magnitude and determine the stress drop. For the May data this is any event where $\tau_{1/2}$>0.041 seconds and for the July data the critical $\tau_{1/2}$ is 0.042 seconds. There are seven events that meet these criteria (summarized in Table 9). There is little difference in $\tau_{1/2}$ and magnitude for these events hence no significant differences in radius and stress drop are noted.

It would appear possible to bound the values of stress drop for events that contain source information. Since the two smallest events in Table 8 have small $\tau_{1/2}$ values and fairly large magnitudes, these would appear to be the events with the largest stress drop. The other two events in Table 8 have large $\tau_{1/2}$ values and only slightly larger magnitudes. Considering the functional relationship between stress drop, magnitude and $\tau_{1/2}^{source}$, these would appear to have the smallest stress drop of any events. Thus, it would appear that the stress drop for all events in these swarms falls between 1.5 and 75 bars. All values obtained here of course, depend critically on the model used.

SUMMARY AND CONCLUSIONS

During May and July, 1983, two distinct microearthquake swarms occurred near Socorro, New Mexico. Over 700 events were clearly recorded at the closest seismograph station at an epicentral distance of ~3km. Although there is a large amount of uncertainty in the estimates of magnitudes, the largest shocks in both swarms certainly had magnitudes less than two. The temporal disribution of activity was typical of swarms, i.e., sporadically occurring clusters of events. The larger events occurred at intervals of several days throughout both swarms. This sort of swarm activity has previously been correlated with contemporary magma movement in certain areas (Richter, 1958). This particular area has in the past been suggested by other studies as a potential region for the location of upper crustal magma (Chapin et al., 1978).

No significant difference in earthquake locations exists between the two swarms. Epicenters are clustered 2.2km southwest of station WTX at an average focal depth of 8.8 km. The very small changes in S-P time interval on the digital data at station WTX strongly indicates very little migration of hypocenters occurred. The total volume of crust "active" during the two swarms was probably no more than 4 km^3. As is the case with essentially all the earthquake data in the central Rio Grande rift, no events with hypocenters below 10.5 km were noted (Sanford et

al.,1983a). This lack of brittle failure below ~11 km is probably due to increased ductility arising from elevated temperatures in the middle crust.

Composite fault plane solutions obtained for the strongest events in the May and July swarms indicate normal faulting with nearly pure dip-slip motion on possible fault planes striking N15°E. The dip of one plane is low (~20°) and the other high (~70°). The high angle, westward-dipping plane is felt to be the more probable failure plane. These results agree with other fault plane studies (using different data) for this area (Wieder, 1980). The fault plane determined in this study does not appear to correlate in position or sense of motion with any mapped surface faults in the area.

Spectra from the P and S-phase of 19 unsaturated events were compared. The corrected spectra showed peak frequencies between 9 and 13 Hz. Very little energy was apparent above 25 Hz in any of the waveforms studied. An estimate of whole path attenuation (Q) was made. For this path, it appears Q_S is slightly larger than Q_P. The estimate of Q_S obtained (~80) is in reasonable agreement with values obtained by other studies using different techniques.

From high quality digital data at station WTX waveforms were found to be quite similar, except for amplitude, up to a magnitude of 1.2. This duplication is especially pronounced for the P-phase. Cross-correlation of the P-

phase data for different events from these swarm often yields correlation coefficients greater than 0.90. Duplication occurs between S-phase data but it is not as perfect as for the P-phase. This duplication does not extend beyond M_L=1.3 for either the P or S-phase.

The period of the first half cycle of the P-phase ($\tau_{1/2}$) was measured from the digital data and indicated no change in its duration up to magnitudes on the order of 1.2. This duplication of events over a large range of seismic moment indicates the seismograms for events below magnitude 1.2 are the impulse response of the path and instrumentation.

Utilizing the source independence of the smaller events, source characteristics of the larger events were studied. An estimate of the pulse width of the source was obtained by "deconvolving" an empirical Green's function from the waveform of a larger event. This pulse width was then converted to an estimate of source radius. Using the seismic moment for each event (found from the event magnitude) along with the source radius, the stress drop was calculated. The largest events showed large source radii and small stress drops, r>150m and $\Delta\sigma$<3 bars. Whether this behavior is an actual manifestation of the fault process or an artifact of the model used is not completely clear at this time. Because $\Delta\sigma \propto (\tau_{1/2}^{source})^{-3}$ for the model used, it is the very large $\tau_{1/2}$ values which lead to the small values of stress drop.

The data set presented here offers excellent

possibilties for further study. Possible areas of future work include a more detailed comparison of source characteristics from other local data sets and the investigation of source properties using different fault models. A more detailed fault plane study including correction of amplitudes to the focal sphere and analysis of S-nodal planes could also be pursued. The $\tau_{1/2}$ study suggests that this parameter may be useful as a qualitative indicator of whole path Q. For a given event magnitude, the more severe the high frequency attenuation along a given path, the broader the pulse width.

REFERENCES

Ake,J.P., A.R. Sanford and S.P. Jarpe, A magnitude scale for central New Mexico based on signal duration, N. Mex. Inst. of Mining and Technol., Geophys. Open-File Rep. No. 45, Socorro, 1983.

Caravella, F. J., A study of Poisson's ratio in the upper crust of the Socorro, New Mexico area, N. Mex. Inst. of Mining and Technol., Geophys. Open-File Rep. No. 11, Socorro, 1976.

Chamberlin, R. M., Cenozoic stratigraphy and structure of the Socorro Peak volcanic center, central New Mexico, [Ph. D. thesis], New Mexico Bureau of Mines and Mineral Resources Open File Report No. 118, 1980.

Chamberlin, R. M., Cenozoic stratigraphy and structure of the Socorro Peak volcanic center, central New Mexico; a summary, New Mexico Geology, 3, no. 2, p22-24, 1981.

Chapin, C. E., Evolution of the Rio Grande rift-a summary, in Riecker, R. E., ed., Rio Grande Rift:Tectonics and Magmatism, A.G.U., Wash. D.C., 1-5, 1979.

Chapin C. E. and W. R. Seager, Evolution of the Rio Grande rift in the Socorro and Las Cruces area, N. Mex. Geol. Soc. Field Conf. Guideb., 26, 297-321, 1975.

Chapin C. E., R. M. Chamberlin, G. R. Osburn, D. W. White and A. R. Sanford, Exploration framework of the Socorro Geothermal Area, New Mexico, Field Guide to Selected Cauldrons and Mining Districts of the Datil-Mogollon Volcanic Field, New Mexico, New Mexico Geol. Soc. Spec. Pub. 7, 114-129, 1978.

Cordell L., Regional geophysical setting of the Rio Grande rift, Geol. Soc. Amer. Bull., 89, 1073-1090, 1978.

Fender, J. J., A study of Poisson's ratio in the upper crust in the Socorro, New Mexico area, N. Mex. Inst. of Mining and Technol., Geophys. Open-File Rep. No. 25, 1978.

Frankel, A. and H. Kanamori, Determination of rupture duration and stress drop for earthquakes in southern California, Bull. Seism. Soc. Amer., 73, 1527-1551, 1983.

Frishman, M. S., Use of linear inverse techniques to study Poisson's ratio in the upper crust in the Socorro, New Mexico area, N. Mex. Inst. of Mining and Technol., Geophys. Open-File Rep. No. 27, Socorro, 1979.

Jaksha, L., Earthquakes near Albuquerque, New Mexico, 1976-1981, EOS, Trans. Amer. Geophys. U., 64, No. 45, 753, 1983.

Johnston, J. A., Microearthquake frequency attenuation of S-phases in the Rio Grande rift near Socorro, New Mexico, N. Mex. Inst. of Mining and Technol., Geophys. Open-File Rep. No. 24, Socorro, 1978.

Lee, W. H. K. and J. C. Lahr, HYPO71 (revised): A computer program for determining hypocenter, magnitude, and first motion pattern of local earthquakes: U.S. Geological Survey, Open-File Rep. 75- 311, 1975.

Majer, E.L. and T. V. McEvilly, Seismological investigations at The Geysers geothermal field, Geophysics, 44, No. 2, 246-269, 1979.

Modiano, T. and D. Hatzfeld, Experimental study of the spectral content of shallow earthquakes, Bull. Seism. Soc. Amer., 72, No. 5, 1739-1758, 1982.

Molnar, P., Earthquake recurrence intervals and plate tectonics, Bull. Seism. Soc. Amer., 69, No. 1, 115-133, 1979.

Reiter, M. and R. Smith, Subsurface temperature data in the Socorro Peak KGRA, New Mexico, Geothermal Mag., 37-41, 1977.

Richter, C. F., Elementary Seismology, W. H. Freeman and Co., San Fransisco, 1958.

Rinehart, E. J., A. R. Sanford and R. M. Ward, Geographic extent and shape of an extensive magma body at mid-crustal depths in the Rio Grande rift near Socorro, New Mexico, in Rio Grande Rift:Tectonics and Magmatisim, R. E. Riecker, ed., Amer. Geophys. Union, Washington D.C., 237-251, 1979.

Sanford, A.R., R. P. Mott,Jr., P. J. Shuleski, E. J. Rinehart, F. J. Caravella, R. M. Ward and T. C. Wallace, Geophyical evidence for a magma body in the crust in the vicinity of Socorro, N. M., in Heacock, J. G. ed., The Earth's Crust, Amer. Geophys. Union Monograph 20, Wash. D.C., 385-403,

1977.

Sanford A.R., Gravity surveys in central Socorro County, New Mexico, N. Mex. Bur. of Mines and Miner. Resour., Circ. 91, Socorro, 1968.

Sanford A. R., A. J. Budding, J. P. Hoffman, O. S. Alptekin, C. A. Rush and T. R. Toppazada, Seismicity of the Rio Grande rift in New Mexico, N. Mex. Bur. of Mines and Miner. Resour., Circ. 120, Socorro, 1972.

Sanford A. R., L. Jaksha and D. Weider, Seismicity of the Socorro area of the Rio Grande rift, N. Mex. Geol. Soc. Field Conf. Guideb., 34, 127- 132, 1983a.

Sanford, A. R., J. P. Ake, S. P. Jarpe, P. J. Carpenter and L. Jaksha, Source independent spectra up to M=1.2 implied from duplication of P- phase waveforms in a Rio Grande rift microearthquake swarm, N. Mex. Inst. of Mining and Technol., Geophys. Open-File Rep. No. 48, Socorro, 1983b.

Sanford, A. R. and C. R. Holmes, Microearthquakes near Socorro, New Mexico, Jour. of Geophys. Res., 67, No. 11, 4449-4459, 1962.

Sanford, A. R. and J. W. Schlue, Seismic exploration for shallow magma bodies in the vicinity of Socorro, New Mexico, New Mexico Energy Institute at New Mexico State Univ., N.M.E.I., 56, 1980.

Sanford A. R., K. H. Olsen and L. Jaksha, Seismicity of the Rio Grande rift, in Rio Grande Rift: Tectonics and Magmatism, R. E. Riecker, ed., Amer. Geophys. Union, Wash. D.C., 145-168, 1979.

Sanford A. R., P. J. Carpenter and E. J. Rinehart, Characteristics of a microearthquake swarm in the Rio Grande rift near Socorro, New Mexico, N. Mex. Inst. of Mining and Technol., Geophys. Open-File Rep. No. 43, Socorro, 1983c.

Sanford A. R., Magma bodies in the Rio Grande rift in central New Mexico, N. Mex. Geol. Soc. Field Conf. Guideb., 34, 123-125, 1983d.

Shuleski, P. J., Seismic fault motion and SV screening by shallow magma bodies in the vicinity of Socorro, New Mexico, N. Mex. Inst. of Mining and Technol., Geophys. Open-File Rep. No. 8, Socorro, 1976.

Ward, R. M., Determination of three-dimensional velocity anomalies within the upper crust in the vicinity of Socorro, New Mexico using first P arrivals from local earthquakes, [Ph. D. thesis], N. Mex. Inst. of Mining and Technol., Socorro, 1980.

Wieder, D. P., Tectonic significance of microearthquake activity from composite fault plane solutions in the Rio Grande rift near Socorro, New Mexico, N. Mex. Inst. of Mining and Technol., Geophys. Open-File Rep. No. 37, Socorro, 1981.

Appendix 1

This appendix contains a listing of the locations, station corrections and any major "down times" for each of the NMT-USGS seismic network stations.

Appendix Ia. Listing of Locations and Station Corrections for NMT-USGS Network

Station	Lat	Long	Elev (m)	Station Corr. (sec)
BAR	3408.52	10637.68	2120	0.06
BMT	3416.50	10715.61	-	0.14
CAR	3357.15	10644.07	-	0.09
LAZ	3424.12	10708.36	-	-0.01
LPM	3418.77	10638.03	-	-0.33
MLM	3448.85	10718.70	2088	-0.23
POL	3410.70	10658.15	1717	-
SB	3358.51	10710.84	3230	0.28
SMC	3346.72	10701.16	1560	0.20
SNM	3404.21	10656.61	1511	-0.04
WTX	3404.33	10656.75	1555	-0.16

If no station elevation appears in the table, HYPO71 utilized the average elevation of all the stations.

Appendix Ib.

Listed below are any major down times for stations in the NMT-USGS seismic network during the course of the two swarms. If no particular down time is listed for a given station, the the station was down for the entire day.

May Swarm

May 9, all stations operational

May 10, BMT off

May 11, POL off

May 12, POL and WTX off

May 13, POL off

May 14, all stations operational

July Swarm

July 14 WTX off, -1900-2230, MLM and POL off

July 15, MLM and POL off

July 16, MLM and POL off

July 17, MLM and POL off

July 18, MLM and POL off

July 19, MLM and POL off

July 20, MLM and POL off

July 21, MLM and POL off

Appendix II. Response Curves

Appendix IIa. Response Curves For the NMT-USGS Seismograph Stations as of mid-1983.

The raw data used in this appendix was acquired by Larry Jaksha and the response calculations were performed by Scott Phelps and Larry Jaksha.

Response Curve For Station BAR

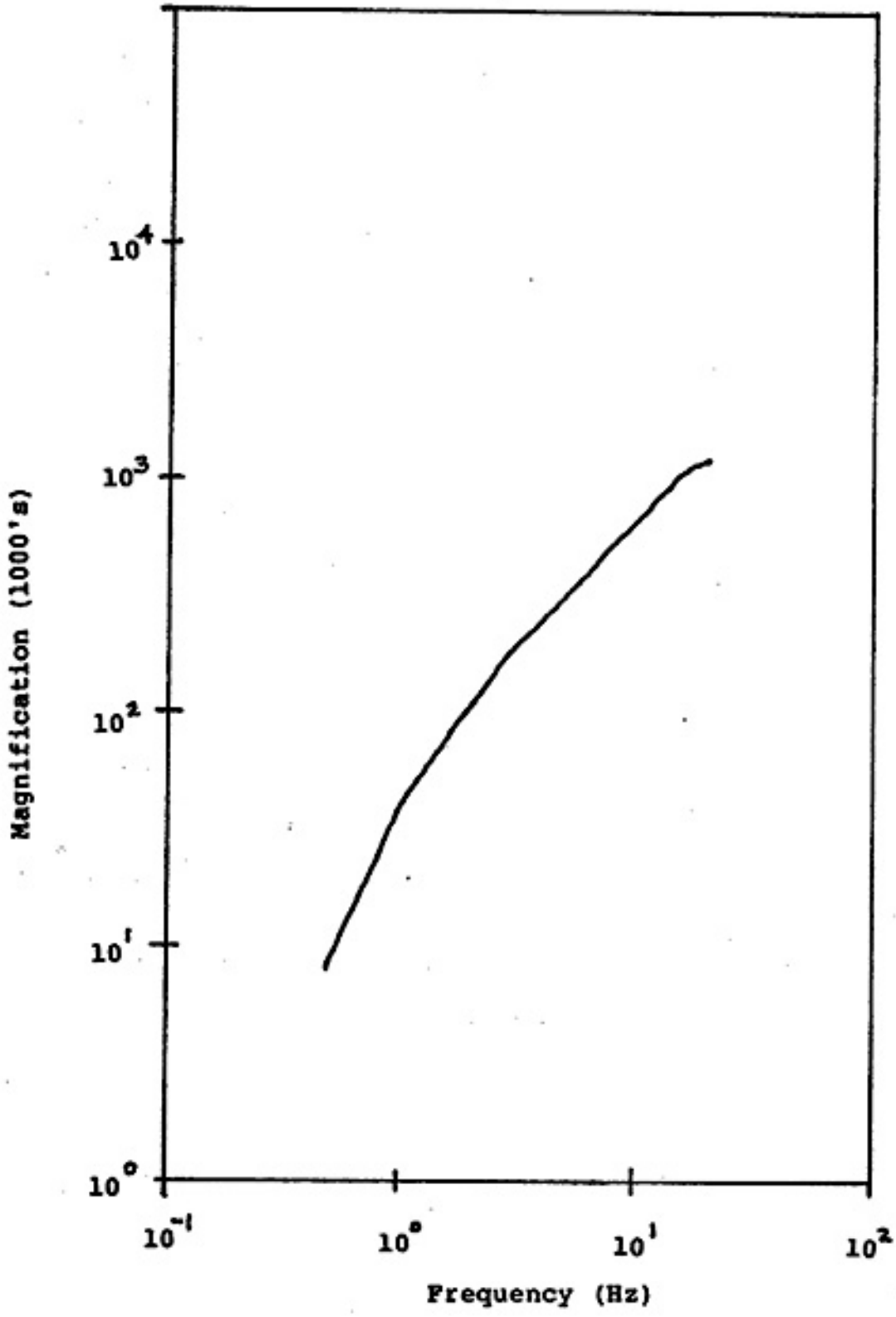

Base Attenuator Setting=12 db

Response Curve For Station BMT

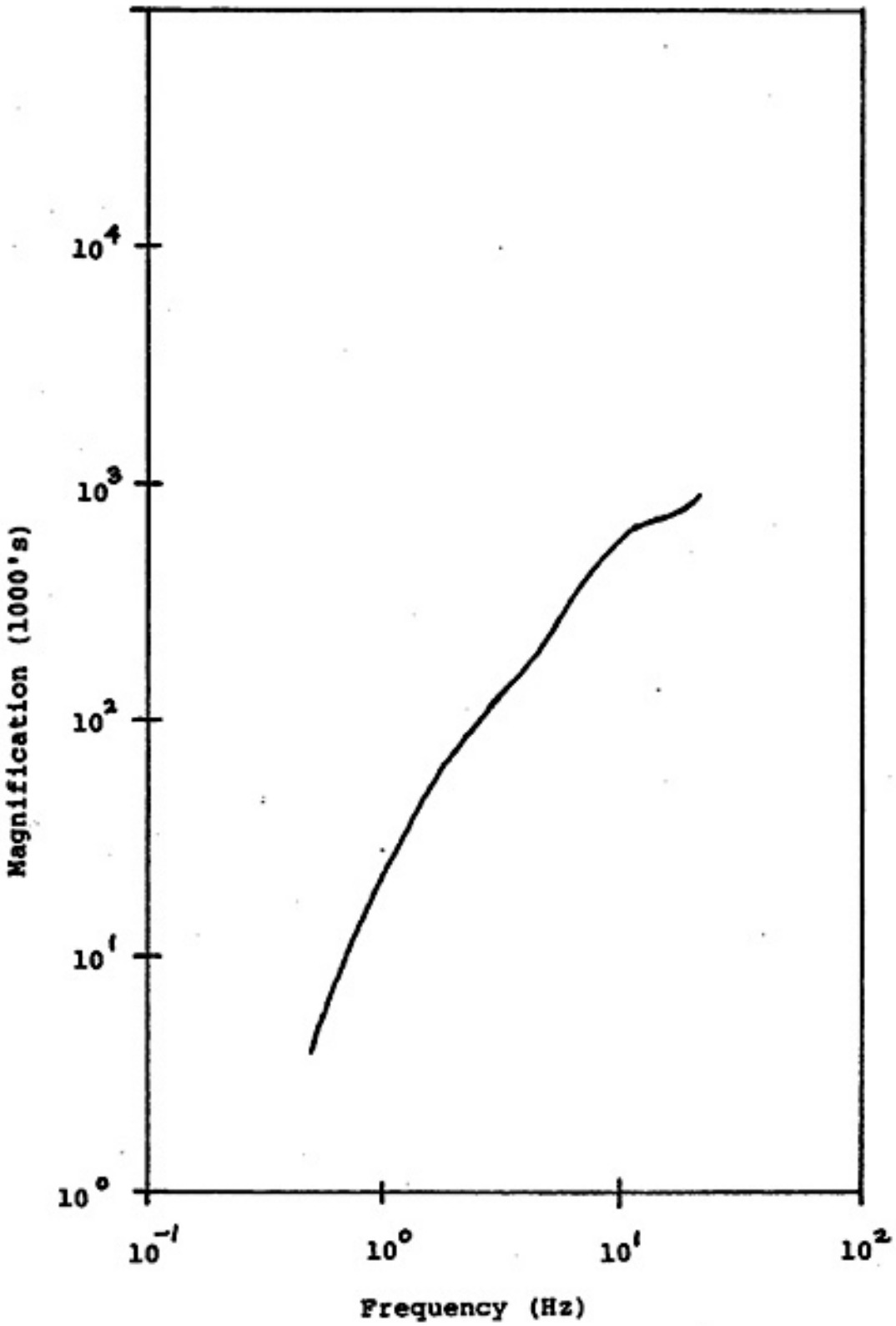

Base Attenuator Setting=18 db

Response Curve For Station CAR

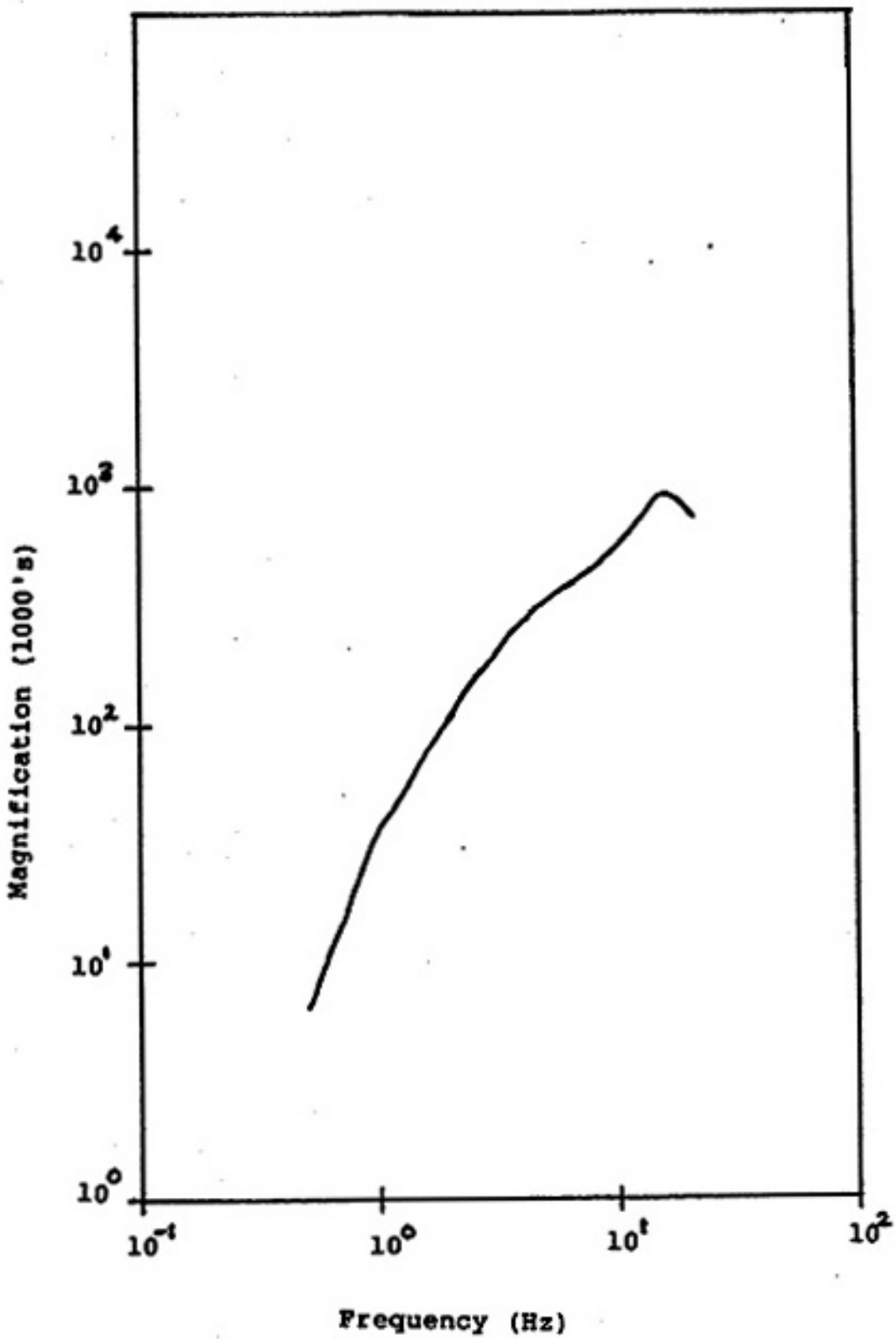

Base Attenuator Setting=24 db

Station LAZ

A complete response curve calculation could not be performed for LAZ. However, the response was determined for a single frequency; at 1 Hz the magnification of LAZ is 53,000 with an attenuator setting of 36 db.

Response Curve For Station LPM

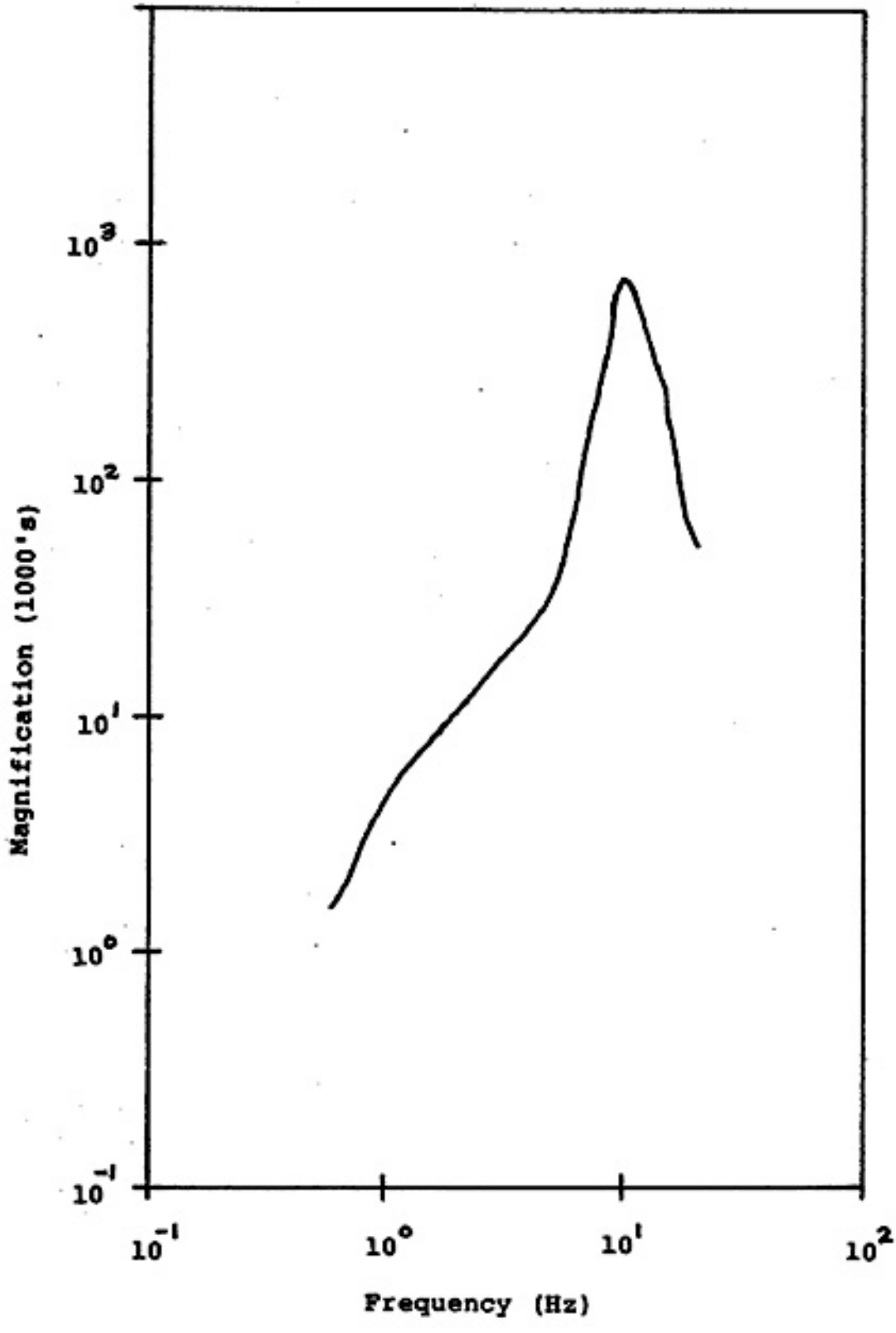

Base Attenuator Setting=24 db

Response Curve For Station SB

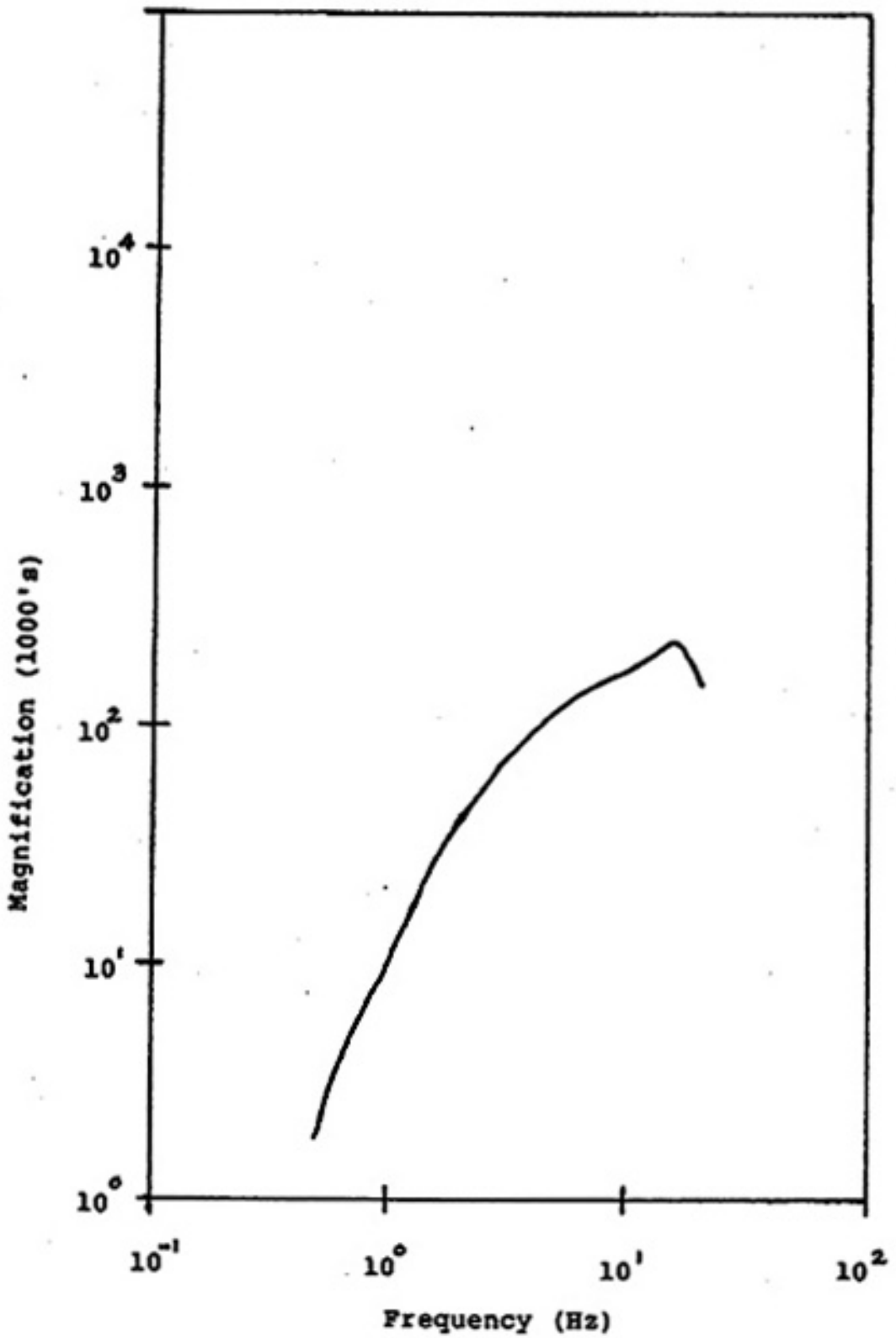

Base Attenuator Setting=30 db

Response Curve For Station SMC

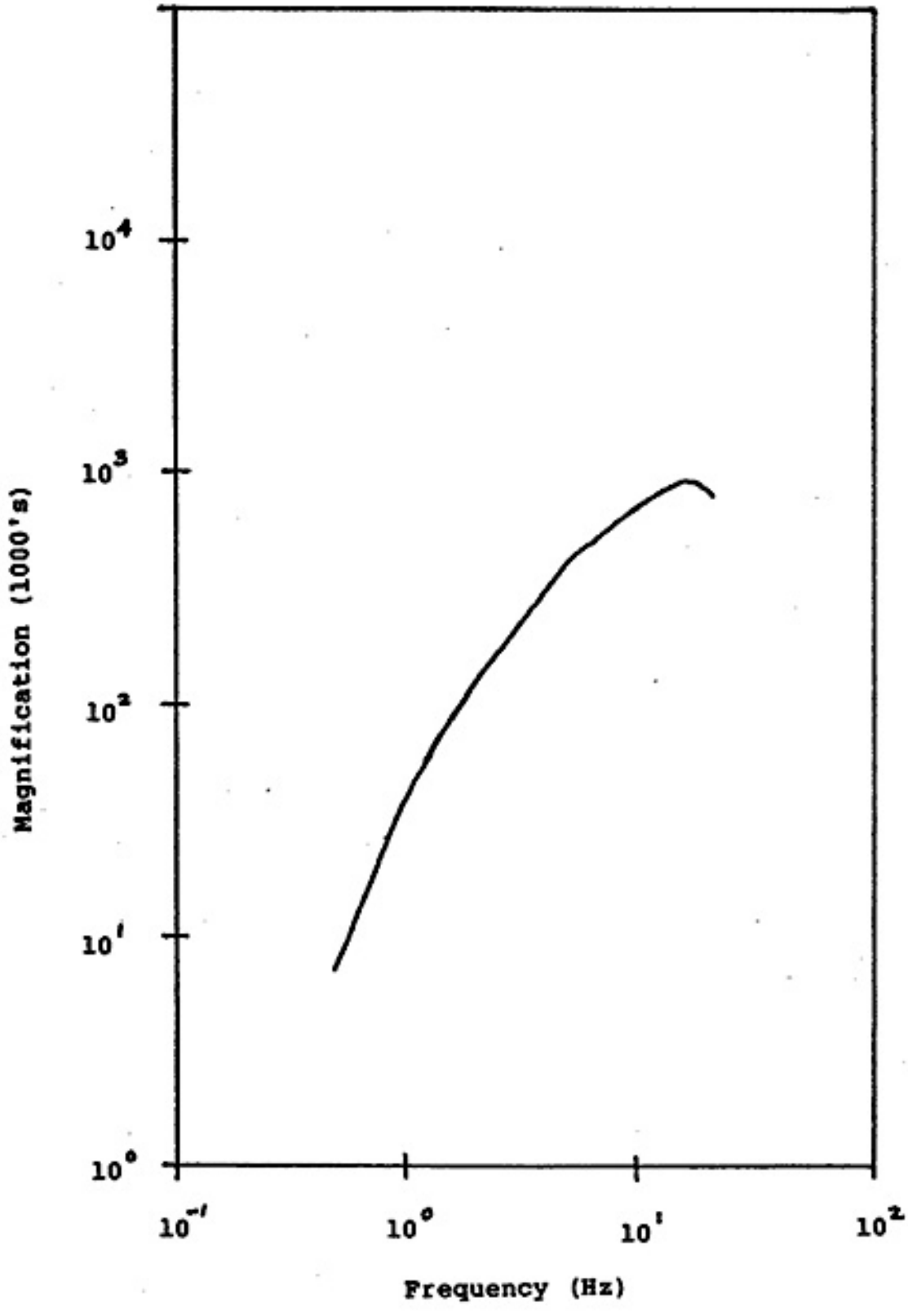

Base Attenuator Setting=18 db

· Response Curve For Station WTX

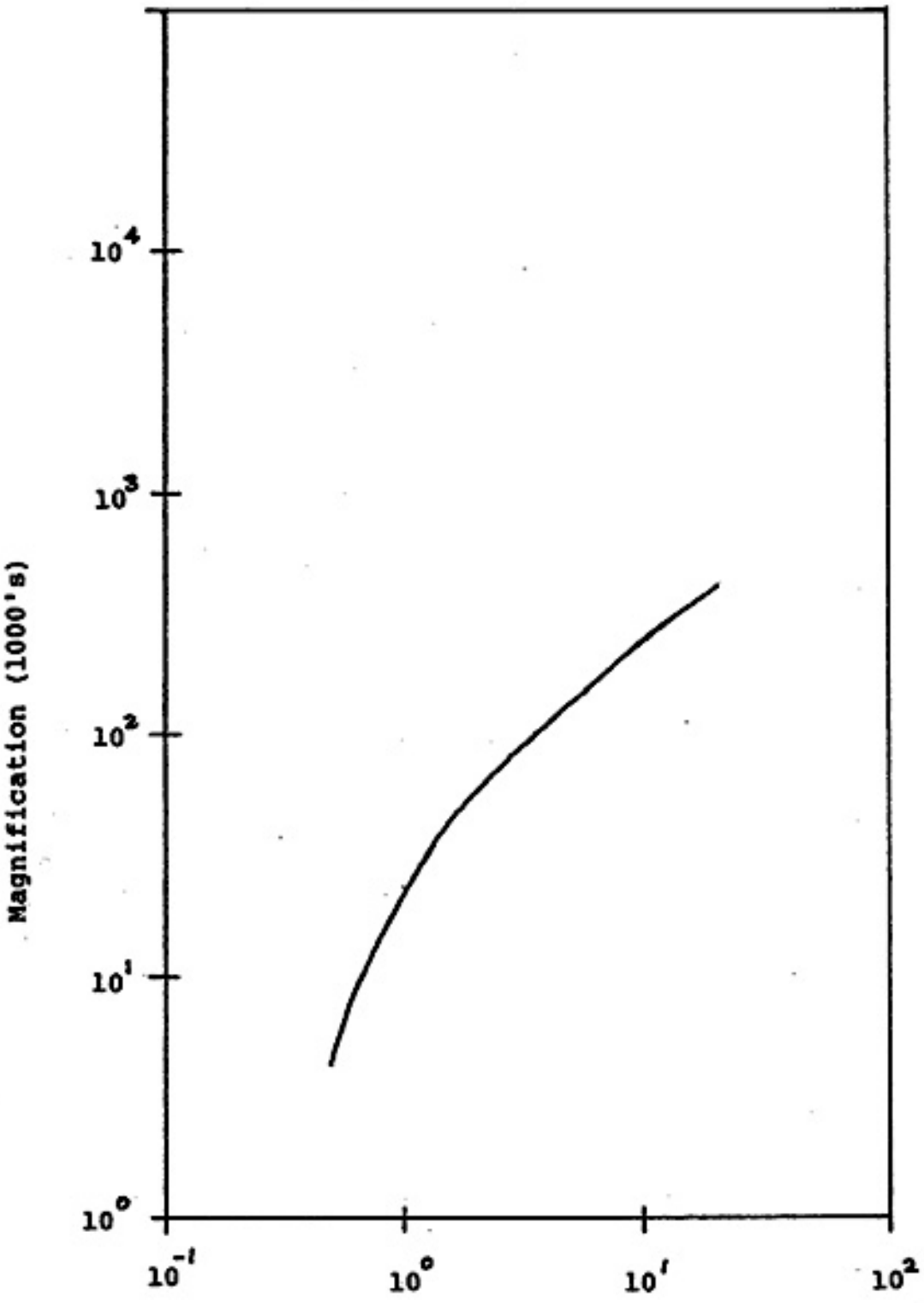

Base Attenuator Setting=18 db

Appendix IIb. Response Curves For the DR-100 Digital Event Recorder

The data utilized in this study was all acquired with filter settings of

low=out

and high=30 Hz.

The different response curves for a particular filter setting are a function of the random application of the digital timing comb to the incoming analog signal. For a complete discussion of this phenomena see Carpenter (1984).

DR-100 Response Curves With Filter Settings

of Low=5 Hz, and High=30 Hz.

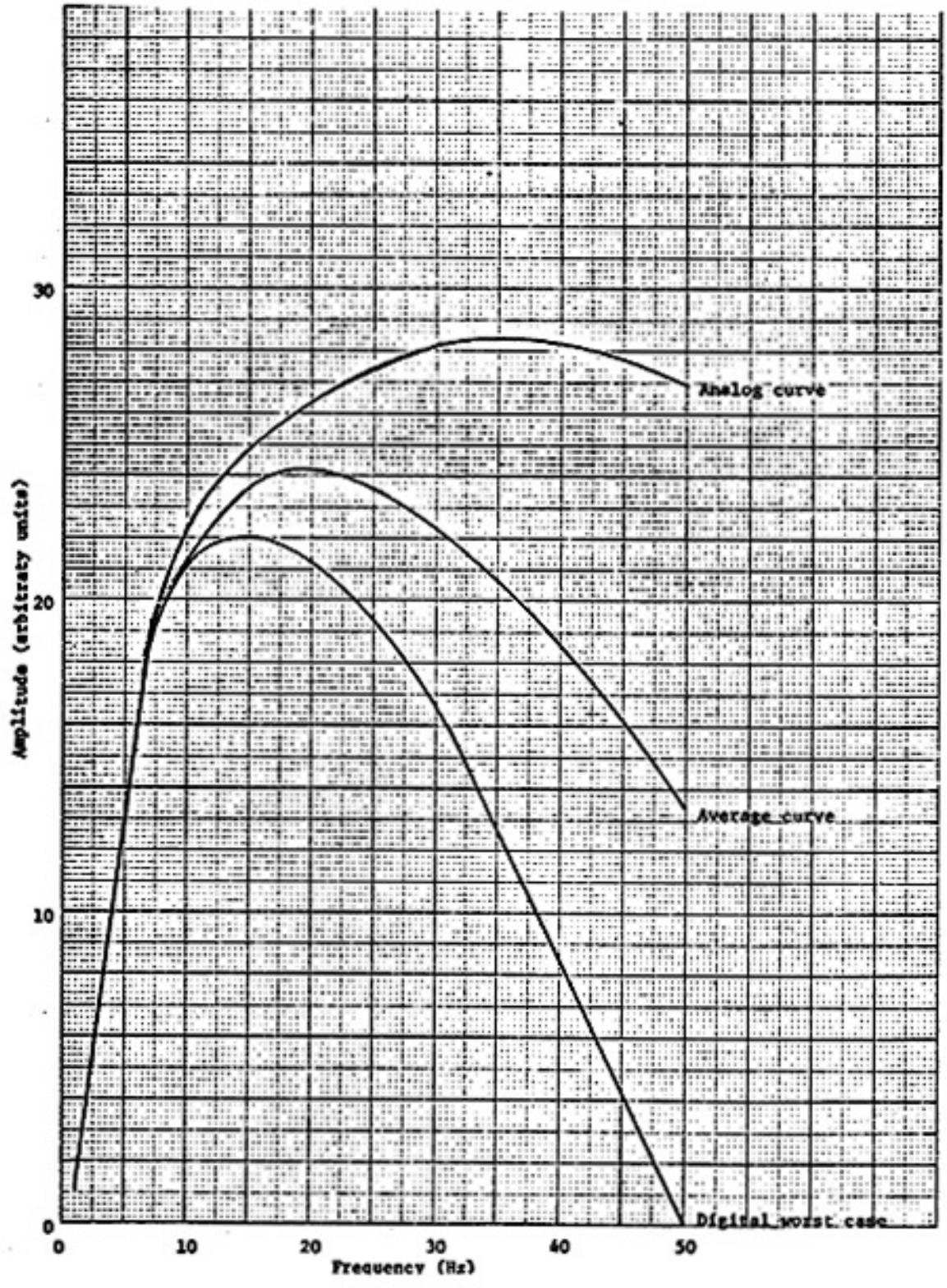

DR-100 Response Curves With Filter Settings

of Low=Out, and High=30 Hz.

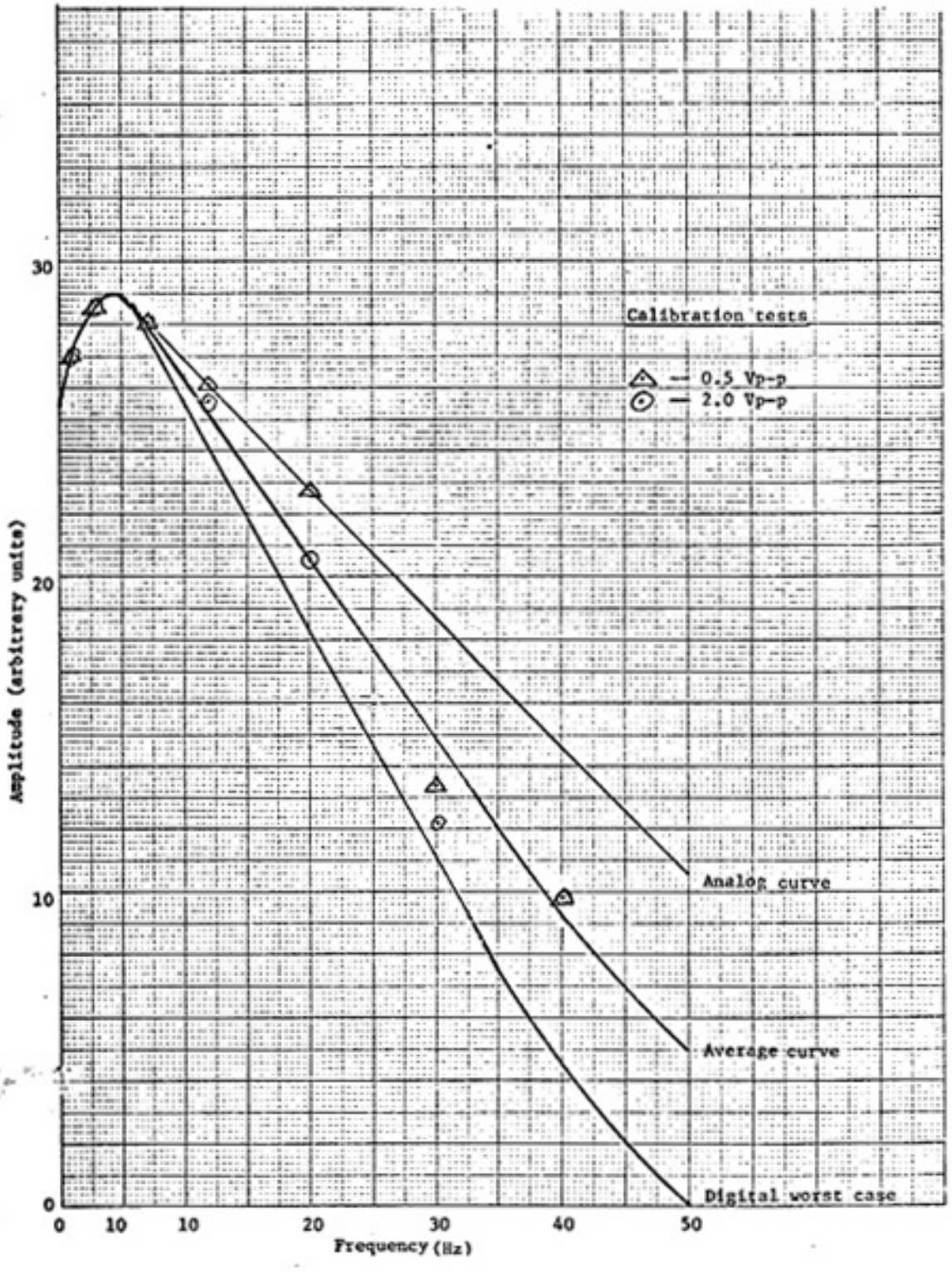

Appendix III.

This appendix contains a summary of the location data for the 60 microearthquakes located in this study. The origin time is given in universal time and the focal depth is given in kilometers below the average elevation of the recording stations. Also see Table 3 for a further explanation of the quantities used.

	Date		Lat-N	Long-W	Depth	Mag	No	Gap	RMS	ERH	ERZ	Q	SQD
1.	5/10/83	0434	34-3.38	106-57.84	9.89	0.19	9	92	0.10	0.6	0.5	B	A;B
2.	5/10/83	0627	34-0.98	106-56.85	7.00	0.39	10	84	0.68	3.8	4.4	C	D;A
3.	5/10/83	0657	34-3.56	106-57.49	8.76	0.05	8	70	0.04	0.3	0.2	A	A;A
4.	5/10/83	0838	34-3.48	106-57.51	8.77	1.33	8	86	0.04	0.3	0.3	A	A;A
5.	5/10/83	1105	34-3.64	106-57.32	9.16	0.99	10	84	0.06	0.4	0.3	A	A;A
6.	5/10/83	1142	34-3.32	106-57.49	9.18	0.14	11	72	0.12	0.6	0.5	A	A;A
7.	5/10/83	1637	34-3.21	106-57.42	9.75	0.21	10	70	0.07	0.4	0.3	A	A;A
8.	5/11/83	0611	34-3.81	106-57.65	9.07	-0.09	8	124	0.10	0.8	0.5	B	A;B
9.	5/11/83	0616	34-3.38	106-57.41	8.53	0.36	11	71	0.09	0.4	0.4	A	A;A
10.	5/11/83	1359	34-3.58	106-57.46	9.02	0.52	9	70	0.05	0.3	0.3	A	A;A
11.	5/11/83	1430	34-2.66	106-57.48	8.65	0.64	9	75	0.15	0.9	0.8	A	A;A
12.	5/11/83	1433	34-3.64	106-57.81	7.55	0.34	9	70	0.07	0.4	0.3	A	A;A
13.	5/11/83	1452	34-2.61	106-57.35	7.53	0.32	7	121	0.08	0.7	0.6	B	A;B
14.	5/11/83	1525	34-3.10	106-57.33	8.94	1.05	12	73	0.07	0.3	0.3	A	A;A
15.	5/11/83	1549	34-3.00	106-57.66	7.00	-0.04	9	142	0.16	1.1	1.1	C	B;C
16.	5/13/83	0813	34-3.39	106-57.85	7.82	-0.69	11	159	0.21	1.1	1.1	C	B;C
17.	5/14/83	0108	34-3.71	106-57.90	9.14	0.09	16	69	0.14	0.4	0.5	A	A;A

	Date		Lat-N	Long-W	Depth	Mag	No	Gap	RMS	ERH	ERZ	Q	SQD
18.	5/14/83	1443	34-3.55	106-58.03	8.51	-0.24	12	126	0.07	0.3	0.3	B	A;B
19.	7/14/83	0552	34-3.82	106-57.71	9.09	-0.41	10	124	0.03	0.2	0.1	B	A;B
20.	7/14/83	1109	34-2.89	106-57.57	8.14	0.50	11	89	0.09	0.5	0.4	A	A;A
21.	7/14/83	1123	34-3.16	106-57.07	10.16	-0.40	10	129	0.18	1.1	0.9	B	B;B
22.	7/14/83	1139	34-2.54	106-57.35	10.05	0.15	9	75	0.11	0.8	0.6	A	A;A
23.	7/14/83	1242	34-4.43	106-57.29	8.67	-0.51	9	119	0.09	0.7	0.5	B	A;B
24.	7/14/83	1351	34-4.31	106-58.34	9.96	-0.34	9	99	0.16	1.1	0.9	B	B;B
25.	7/14/83	1613	34-3.15	106-57.92	8.90	-0.67	10	129	0.14	0.9	0.7	B	A;B
26.	7/14/83	1617	34-4.03	106-58.58	9.68	-0.48	9	122	0.16	1.2	0.8	B	B;B
27.	7/15/83	0514	34-3.87	106-57.64	8.99	-0.45	10	123	0.12	0.8	0.5	B	A;B
28.	7/15/83	0851	34-4.31	106-57.83	9.84	-0.07	12	73	0.13	0.7	0.6	A	A;A
29.	7/16/83	0310	34-3.60	106-57.68	10.81	0.56	8	96	0.08	0.6	0.5	B	A;B
30.	7/16/83	0435	34-3.30	106-57.60	8.76	-0.43	10	128	0.06	0.4	0.3	B	A;B
31.	7/16/83	0612	34-3.58	106-57.92	8.14	0.16	14	122	0.10	0.5	0.3	B	A;B
32.	7/16/83	0859	34-3.07	106-57.70	8.62	0.79	10	72	0.14	0.8	0.7	A	A;A
33.	7/16/83	1739	34-3.51	106-57.61	9.31	0.16	10	71	0.09	0.5	0.4	A	A;A
34.	7/16/83	2150	34-3.02	106-57.81	9.20	-0.37	11	73	0.12	0.6	0.6	A	A;A

	Date		Lat-N	Long-W	Depth	Mag	No	Gap	RMS	ERH	ERZ	Q	SQD
35.	7/16/83	2206	34-3.51	106-57.50	8.92	1.77	10	71	0.09	0.5	0.4	A	A;A
36.	7/16/83	2248	34-3.44	106-57.11	9.11	0.15	12	71	0.07	0.4	0.3	A	A;A
37.	7/16/83	2300	34-2.86	106-57.60	8.36	-0.86	9	132	0.15	1.1	0.9	B	B;B
38.	7/17/83	0101	34-3.45	106-57.31	9.60	-0.27	11	71	0.09	0.5	0.4	A	A;A
39.	7/17/83	0242	34-3.28	106-57.28	8.33	0.19	7	119	0.02	0.2	0.1	B	A;B
40.	7/17/83	1132	34-3.66	106-57.39	9.08	1.27	8	74	0.03	0.2	0.2	A	A;A
41.	7/17/83	1427	34-3.64	106-57.49	8.81	-0.18	12	70	0.11	0.5	0.5	A	A;A
42.	7/17/83	2245	34-3.24	106-57.05	8.92	0.29	8	72	0.06	0.6	0.4	A	A;A
43.	7/18/83	1109	34-4.08	106-57.47	8.58	-0.48	13	98	0.09	0.5	0.3	B	A;B
44.	7/18/83	1756	34-3.52	106-57.23	9.82	0.11	11	126	0.07	0.4	0.3	B	A;B
45.	7/19/83	0327	34-3.51	106-57.96	8.31	-0.08	11	70	0.11	0.7	0.5	A	A;A
46.	7/19/83	0340	34-3.40	106-57.60	8.18	1.79	10	71	0.03	0.2	0.1	A	A;A
47.	7/19/83	0343	34-3.86	106-57.76	8.03	-0.10	12	71	0.10	0.5	0.4	A	A;A
48.	7/19/83	0440	34-3.43	106-57.48	8.55	0.45	10	71	0.07	0.4	0.3	A	A;A
49.	7/19/83	0442	34-3.44	106-57.72	8.13	0.35	9	91	0.05	0.4	0.3	B	A;B
50.	7/19/83	0503	34-3.52	106-57.59	9.03	-0.10	11	71	0.05	0.3	0.2	A	A;A
51.	7/19/83	0654	34-4.19	106-58.25	8.12	0.47	12	72	0.14	0.8	0.5	A	A;A

	Date		Lat-N	Long-W	Depth	Mag	No	Gap	RMS	ERH	ERZ	Q	SQD
52.	7/19/83	0912	34-3.34	106-57.76	8.44	0.52	10	71	0.10	0.6	0.5	A	A;A
53.	7/19/83	1230	34-4.43	106-58.43	8.92	-0.23	10	73	0.13	0.8	0.6	A	A;A
54.	7/20/83	0041	34-3.54	106-57.50	8.90	0.60	9	117	0.03	0.2	0.2	B	A;B
55.	7/20/83	0146	34-3.17	106-57.81	9.29	-0.58	13	72	0.06	0.3	0.3	A	A;A
56.	7/20/83	0411	34-4.25	106-57.36	9.26	-0.75	10	120	0.05	0.3	0.3	B	A;B
57.	7/20/83	1650	34-5.51	106-56.85	7.89	-0.27	11	107	0.31	1.7	1.4	C	C;B
58.	7/20/83	1657	34-3.65	106-57.42	9.42	0.49	10	70	0.05	0.3	0.2	A	A;A
59.	7/20/83	1722	34-3.84	106-57.51	9.21	-0.07	11	71	0.05	0.3	0.2	A	A;A
60.	7/20/83	1853	34-4.31	106-56.71	9.12	-0.64	11	73	0.16	0.9	0.7	B	B;A

Appendix IV.

This appendix contains a listing of several programs used in this study. Each program has at least some internal documentation.

```
C
CC      PROGRAM CCORR-- COMPUTE CROSS-CORRELATION OF TWO SEISMOGRAMS
CC
CC
CC      SYMBOLS USED:
CC
CC              CMP             EVENT RECORDING PARAMETERS
CC              VFNIN           INPUT FILE NAME
CC
CC      NOTE-- THE 1ST SERIES LAGS THE 2ND I. E. IT IS PROGRESSIVELY
CC             SHIFTED TOWARDS THE LEFT
CC
C

        INTEGER ANSWER,RES(2000)
        REAL CMP1*8(3),VFNIN*8,CMP2*8(3)
        REAL WIN*8
        DIMENSION XY(4000),Y1(1500),Y2(1500),C(3000)

 8      FORMAT(A10)
        OPEN(UNIT=1,DEVICE='DSK',ACCESS='SEQIN',FILE='CROS.DAT')
 6      FORMAT (//5X,' INPUT DATA FOR CROSS-CORRELATION'//)
        WRITE (3,6)
C
CC      READ IN 1ST EVENT
C
        READ(1,19) CMP1,IBEG1,IEND1
 19     FORMAT (3A10,2I6)
        DO 30 I=1,1991,10
        READ(1,40) (Y1(J),J=I,I+9)
 40     FORMAT(10F5.0)
        IF(Y1(I) .EQ. 99999.) GO TO 45
        GO TO 30
 45     NPTS1=I-1
        GO TO 56
 30     CONTINUE
 56     IDIFF=IEND1-IBEG1
        WRITE (3,19) CMP1,IBEG1,IEND1
        WRITE (3,40) (Y1(J),J=1,IDIFF)
C
CC      READ IN 2ND EVENT
C
        READ(1,19) CMP2,IBEG2,IEND2
        DO 50 I=1,1991,10
        READ(1,40) (Y2(J),J=I,I+9)
        IF(Y2(I) .EQ. 99999.) GO TO 55
        GO TO 50
 55     NPTS2=I-1
        GO TO 57
 50     CONTINUE

 57     CONTINUE
        IDIFF=IEND2-IBEG2
        WRITE (3,19) CMP2,IBEG2,IEND2
        WRITE (3,40) (Y2(J),J=1,IDIFF)
C
CC      SET UP PARAMETERS FOR CROSS-CORRELATION
C
        IF (NPTS1.EQ.NPTS2) GO TO 94
        IF (NPTS1.GT.NPTS2) GO TO 92
        DO 91 I=NPTS1+1,NPTS2
 91     Y1(I)=0.
        N=NPTS2
        GO TO 95
```

```
   92    DO 93 I=NPTS2+1,NPTS1
   93    Y2(I)=0.
         N=NPTS1
         GO TO 95
   94    N=NPTS1
   95    CONTINUE
C
         NLAGS=2*N-1
         LMAX=N
         LMIN=-1*(N-1)
C
         WRITE (3,6762)
         WRITE (3,6761) N,NLAGS,LMIN,LMAX
 6761    FORMAT (/5X,I5,5X,I5,5X,I5,5X,I5)
 6762    FORMAT(/7X,' N',3X,' NO. OF LAGS',3X,' MIN. LAG', 4X,' MAX LAG')
C
C        COMPUTE CROSS-CORRELATION
C
C
C        COMPUTE NEGATIVE LAG VALUES
C
         DO 210 J=1,N
         TERM=0.
         IT=N-J+1
         DO 200 I=1,J
         TERM1=Y1(I)*Y2(IT)
         TERM=TERM+TERM1
  200    IT=IT+1
  210    C(J)=TERM
C
C        COMPUTE POSITIVE LAG VALUES
C
         DO 220 J=2,N
         TERM=0.
         IT=1
         DO 215 I=J,N
         TERM1=Y1(I)*Y2(IT)
         TERM=TERM+TERM1
  215    IT=IT+1
  220    C(N+J-1)=TERM
C
C        COMPUTE NORMALIZATION FACTOR FOR
C          CROSS-CORRELATION
C
         SMU1=0.
         SMU2=0.
         DO 760 I=1,N
         SUM1=Y1(I)*Y1(I)
         SUM2=Y2(I)*Y2(I)
         SMU1=SMU1+SUM1
  760    SMU2=SMU2+SUM2
         TNORM=SQRT(SMU1*SMU2)
         WRITE (3,775) TNORM
  775    FORMAT (/5X,' NORMALIZATION FACTOR:',F8.2/)
C
C        NORMALIZE CROSS-CORRELATIONS
C
         DO 790 I=1,NLAGS
  790    C(I)=C(I)/TNORM
C
         NLAG1=NLAGS+1
         WRITE(5,1100)
 1100    FORMAT(' DO YOU WANT A PRINTOUT OF CROSS-CORRELATIONS?')
```

```
      READ(5,130) ANS
130   FORMAT(A3)
      IF(ANS .EQ. 'N') GO TO 100
      WRITE(3,1200) CMP1,CMP2
1200  FORMAT(1X,'CROSS-CORRELATION DATA FOR ',3A10,' X ',3A10)
      WRITE(3,1250)
1250  FORMAT(//10X,'LAG',20X,'X-CORR',/,10X,'___',20X,'_____'/)
      DO 225 LAG=1,NLAGS
      WRITE(3,1300) LAG,C(LAG)
1300  FORMAT(10X,I3,18X,F8.2)
225   CONTINUE
100   CONTINUE
      WRITE(5,1400)
1400  FORMAT(' DO YOU WANT TO COMPUTE RESIDUALS?')
      READ(5,130) ANS
      IF(ANS .EQ. 'N') GO TO 300
      CMAX=0.
      DO 250 I=1,NLAGS
      IF(C(I).LE.CMAX) GO TO 250
      CMAX=C(I)
      LAG=I
250   CONTINUE
      DO 275 I=LAG,LMAX
      RES(I)=Y1(I)-Y2(I-LAG+1)
275   CONTINUE
300   CONTINUE
      CALL SECC(CMP1,CMP2,C,NLAG1,IBEG1,IBEG2,IEND1,IEND2,
     * N,LMAX,LMIN)

      STOP
      END

      SUBROUTINE SECC(CMP1,CMP2,C,NLAG1,IBEG1,IBEG2,IEND1,IEND2,
     * N,LMAX,LMIN)

C
C     SECC-- DISPLAY OF CROSS-CORRELATION
C
C
C     SYMBOLS USED:
C
C           CMP1,CMP2       EVENT RECORDING PARAMETERS
C           VFNIN           INPUT FILE NAME
C           IBEG1,IBEG2     BEGINNING OF WINDOW
C           IEND1,IEND2     END OF WINDOW
C           X,Y             SCREEN COORDINATES
C
      INTEGER ANSWER,N2,IVAR,LINE,VALARY(1)
      REAL CMP1*8(3),CMP2*8(3),C(3000)
      REAL WIN*8
C
C     READ IN DATA FROM DATA FILE
C
C
C     INITIALIZE TERMINAL FOR PLOTTING
C
      CALL INITAL(23)
C
C     RESET ORIGIN TO (.5",.5")
C
      CALL PLOT(.5,.5,-3)
C
C     READ IN RANGE OF LAGS FOR PLOTTING
C
```

```
      RLMAX=LMAX
      RLMIN=LMIN
      WRITE (3,9600) RLMAX,RLMIN
 9600 FORMAT(3X,' RLMAX:',F5.0,' RLMIN:',F5.0)
C
C     FIND MAXIMUM CROSS-CORRELATION AMPLITUDE AND SCALE PLOT
C
150   YMAX=0.
      YMIN=0.
      DO 190 J=1,NLAG1
      IF(C(J).LT.YMIN) YMIN=C(J)
      IF(C(J).GT.YMAX) YMAX=C(J)
190   CONTINUE
C     YMIN=YMIN-0.5
C
C     PLOT CORRELATION VALUES
C
      NPT=0
      RNLAG1=NLAG1
      DO 300 I=1,NLAG1
      LAG=I-1
      RLAG=LAG
      IF (RLAG.LT.RLMIN.OR.RLAG.GT.RNLAG1) GO TO 300
      NPT=NPT+1
      X=(RLAG/(RLMAX-RLMIN))*5.
      Y=((C(I)-YMIN)/(YMAX-YMIN))*5.
      IF(NPT.EQ.1) CALL PLOT(X,Y,3)
      CALL PLOT(X,Y,2)
 300  CONTINUE

C
C     PLOT AND LABEL AXES

C
 320  CALL NEWPEN(1)
      RLINC=(RLMAX-RLMIN)/5.
      YINC=(YMAX-YMIN)/5.
      XBASE=0.
      CALL AXIS(XBASE,0.,'LAG NUMBER',-10,5.,0.,RLMIN,RLINC,2)
      CALL AXIS(XBASE,0.,'X-CORR AMPL',11,5.,90.,YMIN,YINC,2)
C
C     ADD TITLE AND PERTINENT INFORMATION FOR EACH PLOT
C
      XBASE=XBASE+2.5
      CALL SYMBOL(XBASE,5.,.09,CMP1,0.,30)
      CALL SYMBOL(XBASE,4.6,.09,CMP2,0.,30)
      WIN='WINDOW=>'
      CALL SYMBOL(XBASE,4.8,0.09,WIN,0.,8)
      CALL SYMBOL(XBASE,4.4,0.09,WIN,0.,8)
      BEGIN1=FLOAT(IBEG1)
      END1=FLOAT(IEND1)
      BEGIN2=FLOAT(IBEG2)
      END2=FLOAT(IEND2)

      XBASE=XBASE+.80

      CALL NUMBER(XBASE,4.8,.09,BEGIN1,0.,-1)
      CALL NUMBER(XBASE,4.4,.09,BEGIN2,0.,-1)
      COLON=':'
      XBASE=XBASE+.25
      CALL SYMBOL (XBASE,4.8,.09,COLON,0.,1)
      CALL SYMBOL (XBASE,4.4,.09,COLON,0.,1)
      XBASE=XBASE+.20
      CALL NUMBER(XBASE,4.8,.09,END1,0.,-1)
```

```
      CALL NUMBER(XBASE,4.4,.09,END2,0.,-1)
220   CALL RSTR(0)
      RETURN
      END
```

```
C
C       PROGRAM SERAW-- AMPLITUDE/VELOCITY SPECTRUM PLOT ROUTINE
C
C
C       SYMBOLS USED:
C
C               CMPVAR          EVENT RECORDING PARAMETERS
C               VFNIN           INPUT FILE NAME
C               IBEGIN          BEGINNING OF WINDOW
C               IEND            END OF WINDOW
C               IVAR            VARIANCE OF TIME SERIES
C               XYMV1           MEAN OF TIME SERIES
C               XYMV2           ST. DEV. OF TIME SERIES
C               N2              NUMBER OF SAMPLES IN WINDOW/2
C               FREQ            FREQUENCY
C               AS              AMPLITUDE SPECTRA VALUES
C               YMAX            MAX. AMPL. SPECTRA VALUE
C               YMIN            MIN. AMPL. SPECTRA VALUE
C               X,Y             SCREEN COORDINATES
C
      INTEGER ANSWER,IBEGIN,IEND,N2,IVAR,LINE,VALARY(102)
      REAL CMPVAR*8(3),FREQ(2000),AS(4000),VFNIN*8,XYMV1,
     1XYMV2,YMAX,WIN*8,EVENT*8(3)

      NPLOT=0
      PI=3.14159
C
C     READ IN DATA FROM DATA FILE
C
      TYPE 5
5     FORMAT('-','DESIGNATE AMPLITUDE SPECTRA INPUT FILE NAME:  '$)
      READ(5,8) VFNIN
8     FORMAT(A10)
      OPEN(UNIT=1,DEVICE='DSK',ACCESS='SEQIN',FILE=VFNIN)
C
C     INITIALIZE TERMINAL FOR PLOTTING
C
      CALL INITAL(23)
C
C     RESET ORIGIN TO (.5",.5")
C
      CALL PLOT(.5,.5,-3)
C
C     READ IN EVENT PARAMETERS AND SPECTRAL VALUES
C
      TYPE 6
 6    FORMAT(' WHICH EVENT DO YOU WANT TO SEE?  '$)
      READ(5,9) EVENT
 9    FORMAT(3A10)
10    READ(1,20,END=51) CMPVAR,IBEGIN,IEND,IVAR,XYMV1,XYMV2,N2,
     1FIL1,FIL2,DIST,VS
      N2P1=N2+1
20    FORMAT(3A10/I4,2(1X,I4)/F7.4,1X,F15.4,1X,I4,4F7.2)
      DO 30 J=1,N2P1
      READ(1,40) FREQ(J),AS(J)
 30   CONTINUE
40    FORMAT(5X,F5.2,1X,E15.4)
      READ(1,50) LINE
50    FORMAT(A5)
      IF(EVENT(1).EQ.CMPVAR(1).AND.EVENT(2).EQ.CMPVAR(2)) GO TO 55
      GO TO 10
 51   STOP '*** EVENT NOT FOUND ***'
55    WRITE(5,1000)
 1000 FORMAT(' ENTER MIN. AND MAX. FREQ. FOR PLOT')
```

```
      READ(5,*) FMIN, FMAX
      WRITE(5,1350)
1350  FORMAT(' DO YOU WANT TO DIVIDE SPECTRUM BY 2*PI*FREQ? ')
      READ(5,2010) ANS
      IF(ANS .EQ. 'N') GO TO 130
      DO 127 I=2,N2P1
      AS(I)=AS(I)/(2.*PI*FREQ(I))
127   CONTINUE
130   WRITE(5,1070)
1070  FORMAT(' DO YOU WANT FILTER RESPONSE REMOVED?')
      READ(5,2010) ANS
      IF(ANS .EQ. 'N') GO TO 151
      IF(FIL1 .EQ. 0.) GO TO 150
      CALL DECON(AS,FIL1,FREQ,N2)
150   IF(FIL2 .EQ. 0.) GO TO 151
      CALL DECON(AS,FIL2,FREQ,N2)
151   WRITE(5,1090)
1090  FORMAT(' NUMBER OF POINTS FOR MOVING AVERAGE FILTER?')
      READ(5,*) NPF
C
C     SMOOTH SPECTRAL ESTIMATES USING MOVING AVERAGE FILTER (IF DESIRED)
C
      CALL SMOOTH(NPF,AS,N2P1)
C     DO 113 I=2,N2P1
C113  AS(I)=AS(I)*EXP(-PI*10*FREQ(I)/(50.*3.4))*2.*PI*FREQ(I)
      DO 189 I=2,N2P1
      WRITE(3,3011) FREQ(I),AS(I)
189   CONTINUE
3011  FORMAT(1X,'FREQUENCY =',F7.2,3X,'AMPLITUDE =',F7.2)
C
C     FIND MAXIMUM SPECTRAL AMPLITUDE TO SCALE PLOT
C
      YMAX=0.
      YMIN=0.
      DO 190 J=2,N2P1
      IF(FREQ(J) .LT. FMIN .OR. FREQ(J) .GT. FMAX) GO TO 190
C     IF(AS(J) .LT. YMIN) YMIN=AS(J)
      IF(AS(J) .GT. YMAX) YMAX=AS(J)
190   CONTINUE
C
C     PLOT SPECTRAL VALUES
C
      NPT=0.
      DO 300 I=2,N2P1
      IF(FREQ(I) .LT. FMIN .OR. FREQ(I) .GT. FMAX) GO TO 300
      NPT=NPT+1
      X=(FREQ(I)-FMIN)/(FMAX-FMIN)*5.
      Y=(AS(I)-YMIN)/(YMAX-YMIN)*5.
      IF(NPT .EQ. 1) CALL PLOT(X,Y,1)
      CALL PLOT(X,Y,2)
C     CALL SYMBOL(X,Y,.01,1,0.,-1)
300   CONTINUE
C
C     PLOT AND LABEL AXES
C
      FINC=(FMAX-FMIN)/5.
      YINC=(YMAX-YMIN)/5.
      XBASE=NPLOT*20.
      CALL AXIS(XBASE,0.,'FREQUENCY (HZ)',-14,5.,0.,FMIN,FINC,2)
      CALL AXIS(XBASE,0.,'AMPLITUDE',9,5.,90.,YMIN,YINC,2)
      XBASE=XBASE+3.
      CALL SYMBOL(XBASE,5.,.14,CMPVAR,0.,20)
      WIN='WINDOW=>'
```

```
      CALL SYMBOL(XBASE,4.8,0.14,WIN,0.,8)
C     CALL SYMBOL(XBASE,4.6,0.14,'MEAN OF SERIES = ',0.,17)
      BEGIN=FLOAT(IBEGIN)
      END=FLOAT(IEND)
      XBASE=XBASE+1.25
      CALL NUMBER(XBASE,4.8,.14,BEGIN,0.,-1)
      COLON=':'
      XBASE=XBASE+.50
      CALL SYMBOL(XBASE,4.8,.14,COLON,0.,1)
      XBASE=XBASE+.25
      CALL NUMBER(XBASE,4.8,.14,END,0.,-1)
C     CALL NUMBER(XBASE,4.6,0.14,XYMV1,0.,2)
      GO TO 220
C
CC    SKIP COMPUTATION OF CHI-SQUARED CONFIDENCE INTERVALS
CC    FOR SPECTRAL ESTIMATES
C
210   WRITE(5,2000)
 2000 FORMAT(' DO YOU WANT TO SEE CONFIDENCE INTERVALS?')
      READ(5,2010) ANS
 2010 FORMAT(A1)
      IF(ANS .EQ. 'N') GO TO 220
      DT=.01
C
CC    IF CONFIDENCE INTERVALS DESIRED, COMPUTE AND PLOT ON LOG GRAPH OF SPECTRUM
C
C     CALL SPERR(N2,DT,CI1,CI2,NPF,BW)
      CI1=ALOG(CI1)
      CI2=ALOG(CI2)
      YMAX=-10.
      YMIN=10.
      NPLOT=NPLOT+1
      CALL PLOT(8.,0.,-3)
      DO 400 I=2,N2P1
C     AS(I)=ALOG(AS(I))
      IF(AS(I) .LT. YMIN) YMIN=AS(I)
      IF(AS(I) .GT. YMAX) YMAX=AS(I)
 400  CONTINUE
C
CC    PLOT LOG SPECTRA
C
      NPT=0.
      DO 600 I=2,N2P1
      IF(FREQ(I) .LT. FMIN .OR. FREQ(I) .GT. FMAX) GO TO 600
      NPT=NPT+1
      X=(FREQ(I)-FMIN)/(FMAX-FMIN)*5.
      Y=(AS(I)-YMIN)/(YMAX-YMIN)*5.
      IF(NPT .EQ. 1) CALL PLOT(X,Y,3)
      CALL PLOT(X,Y,2)
 600  CONTINUE
C
CC    PLOT AND LABEL AXES
C
      FINC=(FMAX-FMIN)/5.
      YINC=(YMAX-YMIN)/5.
      XBASE=0.
      CALL AXIS(XBASE,0.,'FREQUENCY (HZ)',-14,5.,0.,FMIN,FINC,2)
      CALL AXIS(XBASE,0.,'LOGE VELOCITY',13,5.,90.,YMIN,YINC,2)
C
CC    LABEL PLOT WITH PERTINENT INFORMATION
C
      XBASE=3.
      CALL SYMBOL(XBASE,5.,.14,'CI=',0.,3)
      CALL SYMBOL(XBASE,4.8,.14,'BW=',0.,4)
```

```
      XBASE=XBASE+0.5
      CALL NUMBER(XBASE,5.,.14,CI1,0.,2)
      CALL NUMBER(XBASE,4.8,.14,BW,0.,3)
      XBASE=XBASE+0.75
      CALL SYMBOL(XBASE,5.,.14,',',0.,1)
      CALL SYMBOL(XBASE,4.8,.14,'HZ',0.,2)
      XBASE=XBASE+.25
      CALL NUMBER(XBASE,5.,.14,CI2,0.,2)
C
C     PLOT OUT ERROR BARS FOR SPECTRAL ESTIMATES AND BANDWIDTH
C
      CALL PLOT(1.5,1.,-3)
      CI1=CI1/(YMAX-YMIN)*5.
      CI2=CI2/(YMAX-YMIN)*5.

      CALL PLOT(0.,0.,3)
      CALL PLOT(0.,CI1,2)
      CALL TICX(0.,CI1)

      CALL PLOT(0.,0.,3)
      CALL PLOT(0.,CI2,2)
      CALL TICX(0.,CI2)

      BW=BW/(FMAX-FMIN)*2.5

      CALL PLOT(0.,0.,3)
      CALL PLOT(BW,0.,2)
      CALL TICY(BW,0.)

      BW=-BW

      CALL PLOT(0.,0.,3)
      CALL PLOT(BW,0.,2)
      CALL TICY(BW,0.)

220   CALL RSTR(0)
      STOP
      END

      SUBROUTINE TICX(X,Y)
      X1=X-.0625
      X2=X+.0625
      CALL PLOT(X1,Y,3)
      CALL PLOT(X2,Y,2)
      RETURN
      END

      SUBROUTINE TICY(X,Y)
      Y1=Y-.0625
      Y2=Y+.0625
      CALL PLOT(X,Y1,3)
      CALL PLOT(X,Y2,2)
      RETURN
      END
```

```
C
C  WSHAP-- TAPERS DIGITAL DATA FOR SPECIFIC WINDOW FORMS
C
C
C       ANS=2: COSINE-TAPERED RECTANGULAR
C       ANS=3: HAMMING
C
        SUBROUTINE WSHAP(ANS,X,WIDTH)
        INTEGER WIDTH
        REAL X(2000)
        PI=3.14159
        IF(ANS .GT. 3.) GO TO 250
        IF(ANS .NE. 2.) GO TO 150
        DO 100 I=1,WIDTH
        FRAC=FLOAT(I-1)/FLOAT(WIDTH)
        IF(FRAC.LE.0.1.OR.FRAC.GE.0.9) X(I)=(1.-COS(PI*10.*FRAC))/
     12.*X(I)
 100    CONTINUE
        GO TO 250
 150    DO 200 I=1,WIDTH
        FRAC=FLOAT(I-35)/FLOAT(WIDTH)
        X(I)=(.46+0.54*COS(PI*FRAC))*X(I)
 200    CONTINUE
 250    RETURN
        END
```

```
      SUBROUTINE SMOOTH(NPF,Y,N2P1)
C
CCC   SMOOTH SPECTRAL ESTIMATES USING MOVING AVERAGE FILTER
CCCCC
CCC           NPF             NUMBER OF POINTS TO BE AVERAGED
CCC           Y               AMPLITUDE OF POINTS
C
      REAL Y(2000)
      NP=(NPF-1)/2
      DO 100 I=1,N2P1
      SUM=0.
      DO 120 J=I-NP,I+NP,1
      IF(J .LT. 1 .OR. J .GT. N2P1) GO TO 120
      SUM=Y(J)+SUM
  120 CONTINUE
      Y(I)=SUM/FLOAT(NPF)
  100 CONTINUE
      RETURN
      END
```